Republic of Iraq
Ministry of Higher Education and Scientific Research
University of Baghdad
College of Education for Pure Science
Ibn-AL-Haitham

Electrical Properties & Microstructure Of ZnO - Based Varistor Ceramics Doped With Rare Earth

A Thesis

Submitted to University of Baghdad / College of Education for Pure Science (Ibn-AL-Haitham) in partial Fulfillment of the Requirements for the Degree of Philosophy Doctorate of Science In Physics

By

Adil Ismaeel Khadim

Supervisors

Asst. Prof. Dr. Aysar. J. Ibraheem
Asst. Prof. Dr. Abdul Hameed.R.Mahdi

2015

Dedication

To my teacher and inspirer, Prophet Muhammad, peace be upon him, to each science student aware of the request and benefit reform, my mother and to my father soul.

Adil

ACKNOWLEDGEMENT

In the name of God the Most Gracious the Most Merciful
Praise be to God in the start and finish.

I would like to express sincere appreciation and gratitude to Asst. Prof. Dr. Aysar. J. Ibraheem and Asst. Prof. Dr. Abdul Hameed.R.Mahdi for supervision, guidance, and suggestions. My special thanks to (Dr.Samir Atta, Dr. Tariq Al-Dhahir, Dr. Mudhir Shihab, Mr.Ayad Ahmad, Dr.Hameed Majeed, Mr. Firas Khadim, and Mr. Samir Ghanim, in department of Physics).
Sincere thanks are due to (Dr. Khalid Waleed, Dr. Ismaeel Yaseen, Dr.Husam Saleem, Dr. Tagreed Hashim and Dr. Maha Abdulsattar, in department of Chemistry).

Sincere thanks to Assistant Professor Dr. Khalid Fahad Ali the dean of the college of education for pure science, Ibn Al-Haitham.

My sincere thanks and gratitude to my family and my aunt Maida Jassim, and my classmate Zainab Tariq.

I would like to apologize for those whom I forgot to mention them.

Finally, I would like to thank all those who put obstacles and hurdles in my way, where they raised my resolve and my determination to complete the work.

Adil

ABSTRACT

ZnO is a ceramic material which tends to intrinsically form as an n-type semiconductor material, which plays an important role in a wide range of industrial processes and commercial products.

One of most important usages is a Surge protection device which used to protect power and electronic equipment from the destructive transient overvoltage which arises from lightning or other large-magnitude surge, this device is called metal oxide varistor (MOV).

Varistors are voltage dependent, non-ohmic devices whose electrical characteristics are almost similar to back-to-back Zener diodes.

Improvement ZnO varistor performance accomplished by doping it by some metal oxides, Bi_2O_3, Sb_2O_3, Co_3O_4, Cr_2O_3, and MnO_2, where they were testing their effect alone first, and second was added rare earth oxides (M_2O_3) with oxides mentioned above and test their effect on varistor, where (M = Dy, La, Y) and molar concentrations (10^{-3}, $5*10^{-3}$, $10*10^{-3}$)

The preparation process starts from mixing ZnO with additives, calcination at 600℃ in a furnace to remove the gases and the humidity from the powders.

Then the calcined powders uniaxially pressed into discs (pellets) of $15\,mm$ in diameter and $2\,mm$ in thickness under a pressure equals to $25MP$.

After pressing the green pellets sintered under different temperatures (1050, 1100, 1150℃) and a fixed time to accomplish the final shapes and reach the desired properties of the samples.

Then the densities of the samples were measured by using Archimedes Principle with mercury liquid to calculate the relative density and the porosity of each sample, and to study the effect of the sintering temperature and REO concentration, which already be obvious the effect of them.

The microstructure test of the material prepared gave a clear vision for the diffusion and grain growth, although the results of

XRD test showed that the crystal structure is an orthorhombic, and the values of (a, b, c) and the size of a the unit cell has been increased with increase the sintering temperature and ratios of the concentration of oxides added and kind.

Micro and nano grains within the present research showed a significant effect on the studied electrical characteristics, which designed a tool in the laboratory for it and to measure the nonlinear coefficient, the amount breakdown voltage, leakage current, the potential gradient, the energy absorption capability, and the voltage per grain boundary.

It was found that the nonlinear coefficient increases with the increasing of REO concentration added and increasing sintering temperature and then starts decreased after degree (1100℃) due to volatilization and evaporation of bismuth oxide and spinel phase ($Zn_7Sb_2O_{12}$).

The amount of breakdown voltage, potential gradient, energy absorption capability decreased with rising the sintering temperature, while the leakage current has been increased with increasing the sintering temperature, as well as the voltage per grain boundary has been increased with increasing of the sintering temperature.

CONTENTS

No.	Subject	Page
	CHAPTER ONE INTRODUCTION	
1.1	Introduction	1
1.2	ZnO Properties And Device Applications	1
1.3	Crystal Structures	2
1.4	Electrical Properties Of ZnO Pure	4
1.5	Varistors	5
1.6	Literature Review	8
1.7	The Aim Of The Work	15
	CHAPTER TWO (THEORY)	
2.1	Introduction	16
2.2	Transient Voltage Surge Suppressers	18
2.3	Types of Transient Voltage Surge Suppressers	18
2.3.1	Spark plug	19
2.3.2	Zener diode	19
2.3.3	Varistor Device	19
2.4	Varistor	19
2.5	Physics of ZnO Varistors	21
2.6	Microstructure Of ZnO Varistors	21
2.6.1	ZnO grains	24
2.6.2	Spinel Phase	25
2.6.3	Bi_2O_3-rich Phases	25
2.6.3.1	Crystalline Bi_2O_3 phase	26
2.6.3.2	Amorphous Bi_2O_3 Phase	26
2.6.3.3	Pyrochlore Phase	27
2.6.4	Grain Boundary	27
2.6.4.1	ZnO-ZnO Single Grain Boundaries	22
2.6.4.2	Triple And Multiple Grain Junctions	28
2.6.5	Porosity	28
2.7	Sintering	28
2.7.1	Solid Phase Sintering	29
2.7.2	Liquid Phase Sintering	30
2.8	Development Of Microstructure	32
2.9	Varistor Electrical Regions	35
2.10	Varistor Electrical Properties	38

No.	Subject	Page
2.10.1	Non Linear Coefficient	38
2.10.2	Potential Barriers At Grain Boundaries	41
2.10.3	Breakdown Voltage	41
2.10.4	The Leakage Current	41
2.10.5	Energy Absorption Capability	42
2.10.6	The Average Grain Size	43
2.10.7	Clamping Ratio	43
2.11	Conductivity Mechanism	44
2.12	Roles Of Doping	44
2.12.1	Effect Of Bi_2O_3	45
2.12.2	Effect Of Sb_2O_3	46
2.13	Grain Growth Inhibition	47
2.14	Effect of MnO_2, Co_3O_4, and Cr_2O_3	48
2.15	Rare Earth Oxides	48
2.16	XRD Testing	49
	CHAPTER THREE SAMPLES PREPARATION	
3.1	Weighing	51
3.2	Mixing	52
3.3	Calcination	53
3.4	Remilling and Binder Adding	53
3.5	Pressing	53
3.6	Sintering	54
3.7	Presintering	55
3.8	XRD Testing	56
3.9	Measurement Of Density	56
3.10	Polishing	57
3.11	SEM Testing	57
3.12	Electroding	58
3.13	Electrical Testing	58
	CHAPTER FOUR RESULTS AND DISCUTION	
4.1	XRD Results	61
4.2.	Grain Size	64
4.3.	Microstructure	66
4.4.	The Density	69
4.5	Electrical Properties	75
4.5.1	I–V Properties Curve	75
4.5.2	Non-Linear Coefficient ($\boldsymbol{\varphi}$)	77

No.	Subject	Page
4.5.3	Breakdown Voltage	81
4.5.4	Leakage Current	84
4.5.5	Energy Absorption Capability	87
4.5.6	Clamping Ratio	91
4.5.7	Potential Gradient	94
4.5.8	Voltage Per Grain Boundary (V_{gb})	97
	CHAPTER FIVE CONCLUSION AND SUGGESTIONS FOR FUTURE WORK	
5.1	Conclusion	99
5.2	Suggestions For Future Work	100
	REFERENCES	101

LIST OF FIGURES

No.	Figure	Page
1.1	ZnO crystal structures: (a) cubic rocksalt (*B*1), (b) cubic zinc blende (*B*3), and (c) hexagonal wurtzite (*B*4).	4
2.1	(a) Over voltages transitory. (b): safe level voltages.	17
2.2	Transient voltage surge suppresser (TVSS).	18
2.3	The microstructure of ZnO varistor phases.	24
2.4	ZnO varistor microstructure description	24
2.5	Equivalent circuit of ZnO varistor	24
2.6	Triple grain junction, crystalline Bi_2O_3, amorphous bismuth rich film, and ZnO grains.	26
2.7	The distribution of charges at the neighborhood of the grain boundaries (the shaded region) represents the depletion region.	27
2.8	Solid phase sintering.	29
2.9	Liquid phase sintering.	30
2.10	The three stages of sintering process.(a) bound growth starting (initial stage).(b) shrinkage of pores volume (intermediate stage).(c) Formation of grains boundaries (final stage)	32
2.11	temperature composition for (a) ZnO–Bi_2O_3, (b) ZnO–Bi_2O_3–Sb_2O_3 and (c) ZnO–Bi_2O_3–Sb_2O_4 (L =liquid, G = gas).	33
2.12	Electrical circuit proportional to varistor component	34
2.13	Influence of varistor (a) at conventional working, (b) at high voltage working.	35
2.14	Current voltage graph of typical metal oxide varistors	36
2.15	Grain boundary double schottky barrier in ZnO varistor. The localized Interface state is indicated by IS.	40
2.16	Diffraction of X-rays from a set of planes	50
3.1	Powder calcination	53
3.2	The results of the pressing process samples	54
3.3	The samples produced after sintering process	55
3.4	The samples produced after presintering process	55
3.5	Homemade instrument with PHYWE High voltage power supply	60
4.1	XRD of five samples of varistor, (a) ZnO pure, (b) ZnO with other oxides (without REO) where and (c) the samples doped with REO, where, • Bi_2O_3, Δ Sb_2O_3, ♦ $Zn_7Sb_2O_{12}$, ∗ Dy_2O_3, ◊La_2O_3, and ⊕Y_2O_3 phases (from up to down respectively)	64

LIST OF FIGURES

No.	Figure	Page
4.2	The grain size against sintering temperature, of samples doped with REO, where Dy, La, Y represents the samples doped with Dy_2O_3, La_2O_3, and Y_2O_3 respectively	66
4.3	SEM images of sizes ($5\mu m * 5\mu m$), of the samples doped with Dy_2O_3, La_2O_3, and Y_2O_3, at sintering temperature (1150℃), where (a, b, c) at concentration (10^{-3}), while (d,e,f) at concentration ($5 * 10^{-3}$)	69
4.4	Density against temperature, at rare earth oxides concentrations (10^{-3}, $5 * 10^{-3}$ and $10 * 10^{-3}$ mole %), respectively	71
4.5	Relative porosity against temperature, at rare earth oxides concentrations (10^{-3}, $5 * 10^{-3}$ and $10 * 10^{-3}$ mole %), respectively	72
4.6	Density against rare earth oxides concentrations, at sintering temperature (1050, 1100, and 1150℃), respectively	73
4.7	Relative porosity against rare earth oxides concentrations, at sintering temperature (1050, 1100, and 1150℃), respectively	74
4.8	I–V characteristic curve of samples (from up to down), pure ZnO , ZnO with other oxides (without rare earth oxides), and finally doped with rare earth oxides, Dy_2O_3, La_2O_3, and Y_2O_3 respectively	77
4.9	Non-linear coefficient with respect to sintering temperature, (a) pure ZnO, ZnO + other oxides (without REO), and doped with REO at 10^{-3}, (b) $5*10^{-3}$, and (c) $10*10^{-3}$	79
4.10	Non-linear coefficient with respect to REO concentration at fixed sintering temperature, where (a) at 1050℃, (b) 1100℃, and (c) 1150℃, respectively	80
4.11	Breakdown voltage with respect to sintering temperature, (a) ZnO + other oxides (without REO), ZnO + other oxides+ REO at 10^{-3}, (b) $5*10^{-3}$, and (c) $10*10^{-3}$	83
4.12	Breakdown voltage with respect to REO concentration at fixed sintering temperature, where (a) at 1050℃, (b) 1100℃, and (c) 1150℃, respectively	84
4.13	Leakage current with respect to sintering temperature, (a) ZnO + other oxides (without REO), ZnO + other oxides+ REO at 10^{-3}, (b) $5*10^{-3}$, and (c) $10*10^{-3}$.	86

LIST OF FIGURES

No.	Figure	Page
4.14	Leakage current with respect to REO concentration at fixed sintering temperature, where (a) at 1050℃, (b) 1100℃, and (c) 1150℃.	87
4.15	Energy absorption capability with respect to sintering temperature, (a) ZnO + other oxides (without REO), ZnO + other oxides+ REO at 10^{-3}, (b) $5*10^{-3}$, and (c) $10*10^{-3}$	89
4.16	Energy absorption capability with respect to REO concentration at fixed sintering temperature, where (a) at 1050℃, (b) 1100℃, and (c) 1150℃, respectively	90
4.17	Clamping ratio with respect to sintering temperature, (a) ZnO + other oxides (without REO), ZnO + other oxides+ REO at 10^{-3}, (b) $5*10^{-3}$, and (c) $10*10^{-3}$	93
4.18	Clamping ratio with respect to REO concentration at fixed sintering temperature, where (a) at 1050℃, (b) 1100℃, and (c) 1150℃.	94
4.19	Potential gradient with respect to sintering temperature, (a) ZnO + other oxides (without REO), ZnO + other oxides + REO at 10^{-3}, (b) $5*10^{-3}$, and (c) $10*10^{-3}$	96
4.20	Potential gradient with respect to REO concentration at fixed sintering temperature, where (a) at 1050℃, (b) 1100℃, and (c) 1150℃.	97
4.21	Voltage per grain boundary with respect to sintering temperature, pure ZnO, ZnO+ other oxides (without REO), ZnO + other oxides at REO (10^{-3})	98

LIST OF TABLES

No.	Table	Page
4.1	The values of grain size measured by using Scherer's method and SEM images	65
4.2	The crystal system parameters of samples doped with oxides . (where S.T and R.C mean sintering temperature and rare earth oxides concentration respectively).	67
4.3	The values of the density ($gm/cm^{3)}$ and Porosity	70
4.4	Non-linear coefficient values with respect to sintering temperature at fixed rare earth oxide concentration	78
4.5	Breakdown voltage (Volt) with respect to sintering temperature at fixed rare earth oxide concentration	81-82
4.6	The leakage current with respect to sintering temperature at different rare earth oxide concentrations	84-85
4.7	Energy absorption capability with respect to sintering temperature at different REO concentrations	88
4.8	Clamping ratio of ZnO varistors samples with respect to sintering temperature at different rare earth oxide concentrations	91-92
4.9	Potential gradient (V/mm) with respect to sintering temperature at fixed rare earth oxide concentrations	94-95
4.10	Voltage per grain boundary with respect to sintering temperature at rare earth oxide concentrations (10^{-3})	97

LIST OF SYMBOLS

SYMBOLS	MEANING
CHAPTER TWO	
φ	Non linear coefficient
J	Current density
E	Potential gradien
K	Constant
I	Current
V	Voltage
c	Constant
R	Ohmic resistance
R_D	Differential resistance
V_b	Breakdown voltage
I_L	Leakage current
I_{L0}	Leakage current at (t=0)
K_T	Degradation rate coefficient
β	Non linear coefficient inverse
d	Average grain size
L	Random line length
M	Magnification
N	Number of the grain boundaries intercepted by the lines
λ	Wave length
θ	Bragg angle
V_{gb}	Voltage per grain boundary
β	Full width at half maximum
D	Thickness of the varistor
C_r	Clamping ratio
n	Integer
CHAPTER THREE	
ρ	Density
m	Mass
v	Volume
P	Porosity
ρ_s	Practical density
ρ_{th}	Theoretical density
Dy_2O_33	$ZnO+ Bi_2O_3+ Sb_2O_3+ Co_3O_4+ Cr_2O_3+ NiO + MnO_2+ Dy_2O_3$(Sintering temperature 1150℃ , Concentration 10^{-3})

LIST OF SYMBOLS

SYMBOLS	MEANING
$La_2O_3$3	ZnO+ Bi_2O_3+ Sb_2O_3+ Co_3O_4+ Cr_2O_3+ NiO + MnO_2+ La_2O_3(Sintering temperature 1150℃ , Concentration 10^{-3})
$Y_2O_3$3	ZnO+ Bi_2O_3+ Sb_2O_3+ Co_3O_4+ Cr_2O_3+ NiO + MnO_2+ Y_2O_3(Sintering temperature 1150℃ , Concentration 10^{-3})
$Dy_2O_3$2	ZnO+ Bi_2O_3+ Sb_2O_3+ Co_3O_4+ Cr_2O_3+ NiO + MnO_2+ Dy_2O_3(Sintering temperature 1100℃ , Concentration 10^{-3})
$La_2O_3$2	ZnO+ Bi_2O_3+ Sb_2O_3+ Co_3O_4+ Cr_2O_3+ NiO + MnO_2+ La_2O_3(Sintering temperature 1100℃ , Concentration 10^{-3})
$Y_2O_3$2	ZnO+ Bi_2O_3+ Sb_2O_3+ Co_3O_4+ Cr_2O_3+ NiO + MnO_2+ Y_2O_3((Sintering temperature 1100℃ , Concentration 10^{-3})
$Dy_2O_3$1	ZnO+ Bi_2O_3+ Sb_2O_3+ Co_3O_4+ Cr_2O_3+ NiO + MnO_2+ Dy_2O_3(Sintering temperature 1050℃ , Concentration 10^{-3})
$La_2O_3$1	ZnO+ Bi_2O_3+ Sb_2O_3+ Co_3O_4+ Cr_2O_3+ NiO + MnO_2+ La_2O_3(Sintering temperature 1050℃ , Concentration 10^{-3})
$Y_2O_3$1	ZnO+ Bi_2O_3+ Sb_2O_3+ Co_3O_4+ Cr_2O_3+ NiO + MnO_2+ Y_2O_3 (Sintering temperature 1150℃ , Concentration 10^{-3})
ZnO	ZnO pure sample
$Bi_2O_3$2	ZnO+ Bi_2O_3+ Sb_2O_3+ Co_3O_4+ Cr_2O_3+ NiO + MnO_2 (Sintering temperature 1100℃)
$Bi_2O_3$1	ZnO+ Bi_2O_3+ Sb_2O_3+ Co_3O_4+ Cr_2O_3+ NiO + MnO_2 (Sintering temperature 1050℃)

1.1. INTROUCTION

Zinc oxide (ZnO), known by the synonyms "Chinese white, zinc white, flowers of zinc, and philosopher's wool", is a versatile, non-toxic compound which has an important part in a wide range in the processes of industrial and commercial products. ZnO is also an important chemical in rubber production due to its efficient activation of the vulcanization process and for imparting improved heat conductivity and anti-aging properties to finished products [1]. ZnO semiconductor is II-VI compound which shows n-type conductivity as a result of either oxygen vacancy and/or zinc interstitials in the crystal structure , it is a very important material to hope for devices of semiconductors [1,2].

1.2. ZnO Properties And Device Applications

In the following a list of ZnO properties that prefer it from other semiconductors and to make it in the foremost semiconductors for applications includes [2]:

Direct band gap. The band gap is 3.44 eV at low temperatures and 3.37 eV at room temperature. For comparison, the respective values for wurtzite GaN are 3.50 eV and 3.44 eV, which in essential enables optoelectronic applications in the blue and UV regions of the spectrum. This enables applications in optoelectronics in these regions, including photodetectors, laser and light-emitting diodes [3-5].

Large exciton binding energy. The free-exciton binding energy about $60\,meV$ in ZnO, compared with, $25\,meV$ in GaN. Large exciton binding energy demonstrates that the efficient excitonic emission in ZnO can persevere at room temperature and higher. Since strength of excitons is typically much larger than that of direct electron–hole transitions in direct gap semiconductors; then the large exciton binding energy renders ZnO a promising material for optical devices that are based on excitonic effects [1,2].

Large piezoelectric constants. "In piezoelectric materials, an applied voltage generates a deformation in the crystal and vice versa". These materials are generally used as actuators, transducers, and sensors. The low symmetry of the

wurtzite crystal structure combined with a large electromechanical coupling in ZnO gives a superior pyroelectric and piezoelectric features [2,3].

Among the semiconductors, ZnO has the highest piezoelectric constants with electromechanical coupling larger than that in GaN and AlN .This feature to be on top of a technologically important material for a wide range applications such as piezotransducers that need a great electromechanical coupling magnitude [1].

Strong non-linear resistance. Commercially available ZnO varistors are made of semiconducting polycrystalline films with highly nonohmic current voltage particularities [6].

While this feature has often been attributed to grain boundaries, the microscopic mechanisms are still not fully understood and the effects of additives and microstructures, as well as their relation to degradation mechanisms, are still under debate [2].

1.3. Crystal Structures

The prospect of using ZnO as a complement in optoelectronics has driven many research groups worldwide to focus on its semiconductor properties, trying to control the unintentional n-type conductivity and to achieve p-type conductivity. The availability of large single crystals is a big advantage of ZnO for example; another big advantage is that ZnO is amenable to wet chemical etching. This is particularly important in the device design and fabrication [1-4].

In fabrication and design of device this is very important; ZnO band-gap can be changed by doping with MgO or CdO, where doping with Mg increases the band gap, whereas Cd decreases it, because the changing in ZnO conductivity stills a major case [2,3].

Even relatively small concentrations of native point defects and impurities (down to 10^{-14} cm^{-3} or 0.01 ppm) can significantly affect the electrical and optical properties of semiconductors. Therefore, understanding the role of native point defects (i.e. vacancies, interstitials, and antisites) and the incorporation of impurities is the key toward controlling the conductivity in ZnO. For a long time it has been postulated that the unintentional n-type conductivity in ZnO is caused by the presence of oxygen vacancies or zinc

interstitials. It has been shown that oxygen vacancies are actually deep donors and cannot contribute to n-type conductivity. In addition, it was found that the other point defects (e.g. Zn interstitials and Zn antisites) are also unlikely causes of the observed n-type conductivity in as-grown ZnO crystals [2].

Most of the group-II-VI binary compound semiconductors crystallize in either cubic zinc-blende or hexagonal wurtzite structure where each anion is surrounded by four cations at the corners of a tetrahedron, and vice versa. This tetrahedral coordination is typical of ***sp*3** covalent bonding, but these materials also have a substantial ionic character [5,6].

As mentioned above ZnO is an II-VI compound semiconductor whose ionicity resides at the borderline between covalent and ionic semiconductor. The crystal structures shared by ZnO are wurtzite (*B*4), zinc blende (*B*3), and rocksalt (*B*1), as schematically shown in figure (1.1), at ambient conditions, the thermodynamically stable phase is wurtzite. The zinc-blende ZnO structure can be stabilized only by growth on cubic substrates [3,5].

As demonstrated in figure (1.1), the structure is composed of two interpenetrating hexagonal closepacked (hcp) sublattices, each of which consists of one type of atom displaced with respect to each other along the threefold ***c***-axis by the amount of u = 3/8 = 0.375 (in an ideal wurtzite structure).The internal parameter u is defined as the length of the bond parallel to the c-axis (anion–cation bond length or the nearest-neighbor distance) divided by the c lattice parameter [3,5].

Each sublattice includes four atoms per unit cell and every atom of one kind (group-II atom) is surrounded by four atoms of the other kind (group VI), or vice versa, which are coordinated at the edges of a tetrahedron. In a real ZnO crystal, the wurtzite structure deviates from the ideal arrangement, by changing the *c*/*a* ratio or the *u* value. It should be pointed out that a strong correlation exists between the *c*/*a* ratio and the *u* parameter in that when the *c*/*a* ratio decreases, the *u* parameter increases in such a way that those four tetrahedral distances remain nearly constant through a distortion of tetrahedral angles due to long-range polar interactions [3,5].

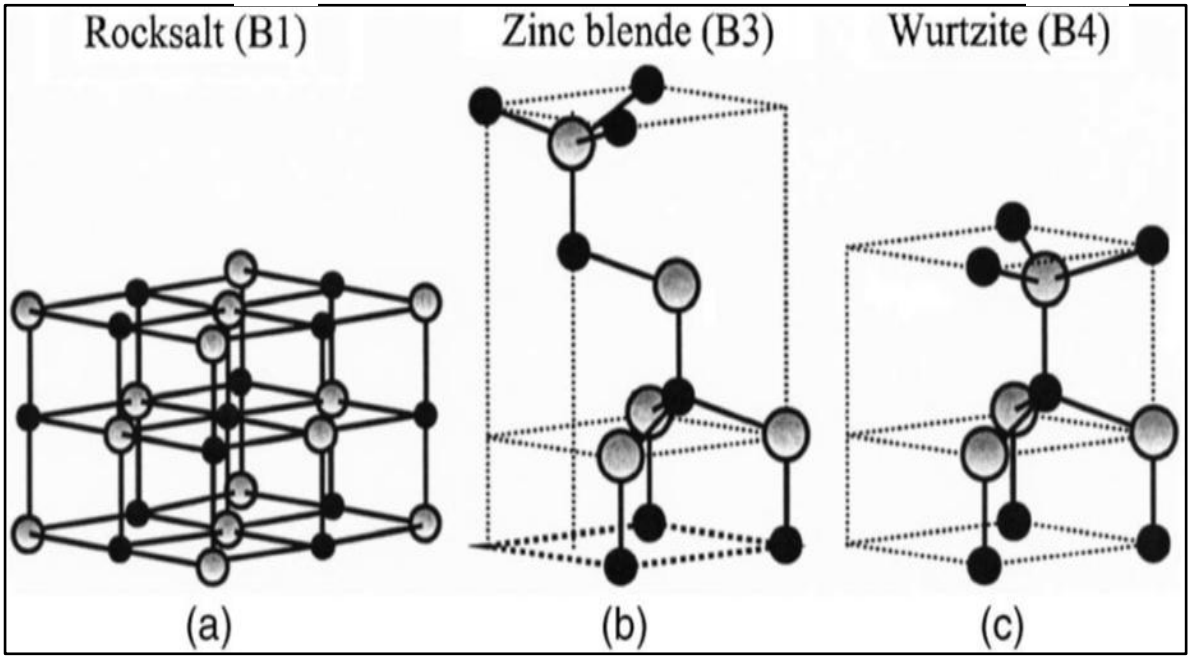

Fig (1.1). ZnO crystal structures: (a) cubic rocksalt (*B*1), (b) cubic zinc blende (*B*3), and (c) hexagonal wurtzite (*B*4) [3,7].

1.4. Electrical Properties Of Pure ZnO

ZnO tends to intrinsically form as an n-type semiconductor material, in which the electrical conductivity is due to excess zinc, presumably interstitially within the lattice and in oxygen vacancies [2,6].

ZnO electrical properties can be modified by appropriate doping either by cationic or anionic substitutional elements. Hence, by doping ZnO with Al, In, B, Ga, or F results in the production of transparent conductors, which is more important in photovoltaic applications. In addition, doping with some rare earth ions, such as erbium, europium, and terbium, ZnO is suitable for applications in high optical gain amplifiers. Furthermore, doping with Al impurity, which is combined in ZnO, can affects the ZnO optical as well as electrical properties. As their potential applications, Al doped ZnO (AZO) thin films can be used as transparent electrodes in flat-panel displays and solar cells [3,7].

1.5. Varistor

Surge protection devices are often used to protect power and electronic equipment from the destructive transient high voltage from lightning or other large-magnitude surge. These devices are used to limit the high voltage to a level which is sufficiently safe for the equipment being protected by diverting the large current to ground. The nonlinearity properties of these devices depend on composition. One type of nonlinear devices is known as Metal Oxide Varistor (MOV). MOV is a ceramic device with highly non-linear electrical properties; similar to those of a back-to-back diode, and has been used for low voltage application (below 1 kV). For higher voltage application that is above 1 kV the protection device is usually known as Metal Oxide Surge Arrester (MOSA) which may consists of several MOV blocks. Due to its high nonlinear properties, these devices have high energy absorption capability which is a good property for high voltage suppressers [8,9].

However, nonlinear properties can be degraded by the effects of electrical and thermal stresses as well as chemical reactions with the surrounding material. Usually, the thermal stress is considered as an effect due to the temperature rise of the metal oxide materials subsequent to the discharge of high energy surges. While, the electrical stress may be the effects of voltage stress by its own operating voltage at ambient temperature or by high current stress due to high voltage occurrence [10,11].

In the past, many investigations of several non-destructive diagnostic techniques have been conducted for reliable condition assessment of the ageing of MOSA. These diagnostic techniques include the standard 1mA reference voltage, lightning impulse discharge residual voltage, voltage decay (VD), polarization or depolarization current (PDC) and Return Voltage (RV) measurements. The modern diagnostic techniques based on dielectric response such as VD, PDC and RV measurements, have also been used to evaluate insulating materials such as cables and transformers [10].

The varistor is an example of a smart material. Smart materials are defined as materials that have the intrinsic ability to respond to their environment in a useful manner. In the case of the varistor (whose name comes from variable resistor) the response to environmental conditions lies in the highly nonlinear current-voltage (I-V) relationship. When exposed to a voltage higher than a certain breakdown value, the varistor loses most of its

electrical resistance and the current is conducted readily. This attribute is very helpful for surge protection so that varistors are widely utilized in protecting electric power lines and electronic components against dangerous voltage surges [12].

Varistors are of particular interest to modern surge protection, which made from zinc oxide. The particular (essential) importance of ZnO varistors is due to the fact that their nonlinear properties and the range of voltage and current over which the device can be used is far superior to those of other materials devices, the most popular surge protectors prior to the advent of the ZnO varistor. The ZnO varistors were first developed in Japan by Matsuoka and his research group in 1968 and commercialized in the following years [12].

In the first decade after their invention various additives improving the electrical specialties were discovered and the processing conditions were optimized. In the next decade, the microstructures and the physical properties of the grain boundaries were gradually identified. At that time applications grew in protection of electrical equipment and electronic components such as transistors and ICs against voltage surges [12,13].

The important effect producing the nonlinear voltage-current properties takes place at the grain boundaries. This is a very small structure and thus difficult to observe directly. Most of the models of varistors action were originally based on macroscopic observations of a bulk sample behavior. To clarify fundamental issues that remain the subject of discussion, techniques are required that allow a direct observation of the local electric field at the grain boundaries [14,15].

ZnO varistors are solid state electronic ceramic components whose key function is to sense and restrict transient voltage surges (short duration spikes in voltage). Most of the rapid variations in the electrical conditions of circuits originate from lightning strikes, electro static discharge, etc. would cause a transient voltage to be generated from the energy stored due to the circuit capacitance and conductance, so that the key of varistor attribute of transient high voltage protection requires the impulse energy to be dissipated at a voltage low enough to ensure the work continuation of the electrical components [13-15].

Varistors are voltage dependent, non-Ohmic devices whose electrical properties are almost similar to ‘back-to-back Zener diodes. When exposed to

a high voltage the varistor impedance varies from a near open circuit to a highly conductive state, thus clamping the transient voltage to a harmless level and protecting electronic components in precious electronic devices [16,17].

As mentioned above ZnO varistors exhibit non Ohmic behavior with resistivity values dependent on the applied voltage, where the main properties of ZnO varistors are described as follows [16].

(a) ZnO varistors have a very fast response to high voltage transients whereby they can sense and restrict transients in nano seconds speed.

(b) ZnO varistors can sense and clamp transients repeatedly, in thousands of times, without being destroyed.

(c) The current voltage characteristic is nonlinear similar to the current voltage properties of a Zener diode.

(d) They can implement Surge suppressing employments on the same level in both polarities, which means that they can work in both reverse and forward biases; like two diodes organized back-to-back.

(e) They can be used in circuits which operate with both alternating current (ac) and direct current (dc), over wide ranges of voltage (one volt to megavolts) and current (1 microampere to kiloamperes).

(f) They have very large energy handling abilities extend from a few joules for smaller models up to thousands of kilojoules for larger models [16].

Lastly, varistors are voltage dependent, nonlinear devices which have an electrical behavior similar to back-to-back Zener diodes. The symmetrical sharp breakdown characteristic enables the varistor to provide excellent transients suppression performance. When exposed to high voltage transients the varistor impedance changes many orders of magnitude from a near open circuit to a highly conductive level, and then restricts the transient voltage to a safe level. The potentially destructive energy of the incoming transient pulse is absorbed by the varistor, then protecting sensitive circuit components [13,16].

1.6. Literature Review

Though the work has been in progress since the early 1970‟s to further improvement the non-Ohmicity of the ZnO varistors, some very promising work has been carried out since the late 1990‟s. This section provides a brief description of the investigations that has been done by researchers all over the world from 2000 till 2014.

In (2000), Almadari. prepared ZnO varistor using high energy milling to enhance its physical and electrical properties, where Bi_2O_3, Sb_2O_3. MnO_3, and SiO_3 Al_2O_3, and Nb_2O_5, pressures value >100MPa, sintering temperature around 1300 ℃ for 2-5 hours, corresponding breakdown voltage is between 1-2 kV/cm, the nonlinearity of 30-35 [18].

In (2003), Kelleher. Prepared ZnO varistor and studied its microstructure and electrical properties, calciner with a peak temperature of 920°C, pressing at 74 MPa produces green compacts of 38 mm in diameter, sintering profile with a peak temperature of 1120°C of total time of 70h [19].

In (2005), Furtado, et al. Studied the execution of ZnO varistor microstructure doped with rare earth, the samples composition is ZnO, Co_3O_4, Pr_6O_{11}, Nd_2O_3, Cr_2O_3 powders. calcined in air at 750 °C for 2 hours. The calcined mixture into discs of 12.4 mm in diameter and 2.1 mm in thickness at a pressure of 80 MPa. The discs were sintered at 1300-1350 °C in air atmosphere for 1 hour, the heating and cooling rates were 6 °C/min, the nonlinear coefficient of 18.7-62, current density 17-49 mA/cm^2, the average grain size increases with increasing of sintering temperature [20].

In (2006), Hove. Studied the improvement of the voltage-current behavior of ZnO varistor doped with Bi_2O_3, CoO, MnO, NiO, LaB_6, $SiTe_2$, sintering temperatures were 800°C for 1h, the nonlinear coefficient of 30.02, the breakdown voltage of 0.80 kV [21].

In (2006), Gunturkun, and Toplan. Studied the variation in grain size and density of ZnO varistor doped with SrO, ZnO (99.7% and $SrCO_3$ powders were used of four basic compositions; ZnO containing 1, 2, 3 and 4 wt.% SrO, pressed at 100 MPa to prepared specimens at 10 mm diameter and 8 mm

thick. The specimens were sintered at 1000, 1100, 1200 and 1300°C for 1, 3, 5 and 10 h using a heating rate of 5 °C /min, The result is that the effect of SrO additions of 1-4 wt.% on sintering behavior and grain growth mechanism. The highest densifications were obtained at high sintering temperatures and high sintering times [22].

In (2007), Lin et.al. Studied the effect of additive ratio on the electrical properties of ZnO varistors, Bi, Sb, and Co were chosen as the additives while cobalt and manganese were selected as the dopants in this study, sintering temperatures were 950 and 1100°C for 1, 3 and 5 h, respectively, breakdown field is 895 V/mm, the nonlinear coefficient reaches up to 48, The grain size is increased with the increase in sintering temperature [17].

In (2008), Kuo and Tuan. Studied the grain growth behavior of ZnO varistor, ZnO and 5 wt% Bi_2O_3 was prepared with laminated together with platinum inner electrodes to inhibit the grain growth, all specimens were firstly fired from room temperature to 400℃ in air for 1h at a heating rate of 1℃ /min to remove the organics, sintering was performed in air at 900–1200℃ for various durations of time, with heating and cooling rates of 5℃ /min, they found that the growth of ZnO grains within the platinum inner electrodes is prohibited due to the decrease of the transportation paths [23]**.**

In (2008), Liang, et al. Studied the effect of rare earth doping on the potential gradient and leakage current of ZnO varistors, the samples of ZnO, 0.5 mol% Bi_2O_3, 1.0 mol% Sb_2O_3, 0.5 mol%MnO, 0.5 mol%Cr_2O_3, 0.5 mol%Co_2O_3, 1.0 mol% SiO_2, and *x* mol% R_2O_3, the powder was pressed into discs of 42 mm in diameter and 16 mm in thickness at a pressure of 80 MPa, the discs were sintered in air for 2 h, at 1130℃, 1170℃, 1190℃ and 1250℃ at heating and cooling rates were 1℃/min and 2℃/min, the sintered samples were lapped and polished to about 10 mm in thickness, covered with aluminum electrodes on the upper and lower surface. The density of 5.08-5.47 gm/cm^3, nonlinear coefficient of 14-53, leakage current 2-45 μA, potential gradient of 263-584V/mm, V_{gb} of 2.64-3.28V [24].

In (2009), Yoon, et al. Studied **e**nhancement of ZnO varistor voltage doping with Y_2O_3 . samples composition of (95.8-X) mol% ZnO, 0.7 mol% Bi_2O_3, 1.25 mol% Sb_2O_3, 0.75 mol% CoO, 0.15

mol% Cr_2O_3, 0.4 mol% NiO, 0.75 mol% MnO_2, 0.2 mol% Nd_2O_3 and X mol% Y_2O_3 (X= 0, 0.3, 0.5, 1.0), calcined at 800^oC for 2 hr , a 3 wt% polyvinyl alcohol (PVA) binder was added the powder was pressed into discs and sintered for 2 hr at heating and cooling rates or 5^oC/min, nonlinearity coefficient of 72-65, potential gradient of 275 - 400 V/mm, and the leakage current of 0.2 - 0.9 μA [25].

In (2009), M.G.M , et al. Studied the effect of temperature stresses and DC bias on nonlinear behavior of ZnO varistor, The composition 99.0 mol % ZnO + 0.5 mol % Bi_2O_3 + 0.5 mol %TiO_2, the and presintered at 800°C for 2 h. The pre-sintered mixture was pulverized using an agate mortar and after 1.75 wt.% (PVA) binder addition, the granulated powder was sieved by using a 75 μm, the discs of 10mm in diameter and 1mm in thickness at a pressure 2 tons were pressed and sintered at various sintering temperatures (1140- 1260°C) and sintering time of 45 and 90 min with heating and cooling rate 2.66°C min^{-1}, Silver paste was coated on both faces 5 mm in diameter of the sample and was heating at 550°C for 10 min. The density of 5.24-5.03 g cm^{-3}, the leakage current of 651.51-807.89, the potential gradient of 1.990-15.75V/mm, and nonlinear coefficient of 1.14-2.21[26]**.**

In (2009), Arefin, et al. Studied the Phase formation at the time of liquid phase sintering of ZnO varistor, where the composition ZnO, Bi_2O_3 and Sb_2O_3. The mixture pressed at 100 MPa, cylindrical compacts were produced with an average diameter of 19 mm and a density of 3.4 g/cm^3 corresponding to a fractional density of 60%, these mixtures and heated at 10 K/min to 1000℃ in atmospheres [27]**.**

In (2009), Dong et al. Studied Bi_2O_3 vaporization of ZnO varistor ceramics, 96.5% ZnO, 0.7% Bi_2O_3, 1.0% Sb_2O_3, 0.8% Co_2O_3, 0.5% Cr_2O_3 and 0.5% MnO_2 (molar fraction), the powder was uniaxially pressed into discs of 12 mm in diameter and 2 mm in thickness, the pressed discs were sintered at sintering temperature of 900, 1000, 1100, 1200, and 1300 ℃ in air for 2 h [28]**.**

In (2009), Abdul Malek. Studied the failure of ZnO varistor ceramic, polarization/depolarization current (PDC), voltage decay (VD) and return voltage (RV) measurements metal oxide varistor. Where the diagnostics method based on dielectric time constants analysis using an equivalent circuit of varistor microstructure which called Maxwell-Model [29].

In (2010), Niti et al. Investigated The effect of barium addition on the densification and grain growth of ZnO-based ceramics, the composition: ZnO + $0.0025Bi_2O_3$+ (x) $BaCO_3$ where x = 0 and 0.005, the mechanical mixture was ball-milled with alumina balls in ethanol for 24 hours, the solutions were dried at 120°C, and calcined at 400°C for 6 hours. The powders were pressed and sintered in air for 6 hours at 900, 1000, 1100, 1200, 1300 and 1400°C, with heating and cooling rates of 5°C/min. The relative density and grain size increase with increasing sintering temperature, where maximum relative density at 1300°C, the averaged crystallite sizes calculated by the Scherer's formula are approximately in between (45 and 50 nm)[30].

In (2010), Mahata. Investigated the synthesis of pure ZnO powder by conventional ceramic processing route to develop ZnO varistor electrical parameters,the maximum values are non-linear coefficient (16), breakdown field (18.72V/cm) and leakage current (132μA), and the variation of capacitance, impedance and phase with respect to frequency variations. [17].

In (2010), Sedky and El-Suheel. Investigated the effect of magnetic and nonmagnetic additives on ZnO varistors properties. Zn1- *x*M*x*O samples with various *x* values ($0.00 \leq x \leq 0.20$, M= Mn, Al) are calcined at 900◦C in air for 12 hours, pressed into disks of 1 cm diameter and 0.3 cm thick, sintered at temperatures of 1200℃ for 10 hours in air and then quenched down to room temperature, the density of Al doped of 4.35-6.94, leakage current of $1.5*10^{-4}$-3.01×10^{-4}, and nonlinear coefficients of 1.61-2.09, and for Mn doped 3.77-5.37, 1.51×10^{-4}- 75.6×10^{-4}, and 1.7-2.19 respectively [31].

In (2011), Zhu et al. Investigated the influence of composite doping on ZnO properties, where the composition 85.33ZnO: $2.76Bi_2O_3$: $3.22Sb_2O_3$: $1.28MnCO_3$: 0.84Cr203: $0.92Ni_2O_3$: $1.83Co_2O_3$:$0.88SiO_2$: $2.25Pr_6O_{11}$, The mixture was calcinated at 500 °C for 2 h followed by 30 min of calcination at 700°C, the dried powder was then pressed into discs of 10 mm in diameter and 2 mm in thickness. The green discs sintered at 1075 °C for 2h with a heating rate of 3 °C/min, and then cooled to room temperature in the furnace. The gradient voltage of 363-561 V/mm, the nonlinear coefficient of 67-75, 0.45-1.08 μA, and the density of 5.36-5.72 gm/cm^3 [32].

In (2011), Sedghi and Noori. Investigated ZnO varistors characters prepared from micro and nano powder, the composition of the sample of ZnO as a body and Bi_2O_3, Sb_2O_3, CoO, Cr_2O_3, and MnO powders as additives, the

powder calcinated at 400 ^{o}C, and pressed into 10 mm diameter and 2 mm height discs by 70 MPa pressure, and the samples were sintered at 1100 ^{o}C for 1 h, and at 1200 ^{o}C for 2 h. Sintered density 5.44 g/cm^3, the nonlinear coefficient 34.8, and gradient voltage of 2920V/cm [33].

In (2012), Yaya, and Arhin, Studied the Bi_2O_3 and Sb_2O_3 effect on the electrical properties and microstructure of ZnO varistor, where the samples compositions consists of (99% ZnO + 1% Bi_2O_3), and (98% ZnO+ 1% Bi_2O_3 + 1% Sb_2O_3) were prepared. The powders were mixed and pressed at 150MPa, and sintered at 800 and 1100℃, the percentage densifications before sintering and after sintering were calculated as well as their weight loses. The densification values of (59.5-86.8%) and the maximum value of potential gradient about ($3*10^4$ V/m) and maximum current density value about (250A/m^2) [34]**.**

In (2012), Dong, et al. Studied the ZnO varistor ceramics microstructural and electrical properties effect as a result of doping with Yb2O3 , where samples composition of (96.5−*x*) % ZnO + 0.7% Bi_2O_3 + 1.0% Sb_2O_3 + 0.8%Co_2O_3 + 0.5% MnO_2 + 0.5% Cr_2O_3 + *x*% Yb_2O_3 (*x* = 0, 0.1, 0.2, 0.3 and 0.4, molar fraction. The powder was pressed into discs of 12.0 mm in diameter and 2.0 mm in thickness, the discs were sintered at 900, 950 and 1000 °C for 2 h with a heating rate of 5 °C/min. The result voltage is between 656-1232 V/mm, the nonlinear coefficient is in the range of 14.1−22.3, and the leakage current is between 0.60- and 19.6 μA [35].

In (2012), Al Abdullah and Bakour. Investigated the development of Stability of ZnO varistor doped with rare earth, where the composition consists of [96.755% ZnO (1-x), 0.5% Bi_2O_3, 0.75% CO_2O_3, 0.5% MnO_2, 0.5% Cr_2O_3, 1% Sb_2O_3, doped with rare earth oxides (Er, Ce, Pr, Y, Dy), where the samples subjected to electrical stresses, then the electrical properties and relative density measured before and after these stresses, where the nonlinear coefficient is in the range of 49-75, threshold voltage of 660-1600 V/mm, and the relative density of 95.99-98.8% [36].

In (2013), Desouky, et al. Studied MnO_2 effect on the electrical properties of ZnO varistor, where MnO_2, in the range 0.5-1.5 mol%, was mixed with a mixture of ZnO-mol% V_2O_5 powder by ball milling with alumina balls and deionized water for 2 h. The mixtures were then dried at

110°C for 24h and calcined in muffle kiln at 750°C for 2h, The green samples were sintered in muffle kiln with a rate of heating of 5°C/min in temperature range between (900-1200) °C for 2 h.(he doesn't displays his results about electrical properties) [37].

In (2013), JIANG, et al. They studied, compared and summarized different results of the rare oxides doping effect on the electrical properties, which include improvement and enhancement the (voltage gradient, nonlinear coefficient, leakage current, energy absorption capability) [38].

In (2013), Ke, et al. Studied ZnO based varistors doped with rare earth, of high potential gradient at low sintering temperature, where (96.5−*X*) mol% ZnO+0.7 mol% Bi_2O_3 +1.0 mol% Sb_2O_3+0.5 mol% Cr_2O_3+ 0.8 mol% Co_2O_3 + 0.5 mol% MnO_2 + *X* mol% Y_2O_3, with *X*equal to 0 or 0.08 . The powder samples were mixed with few drops of a binder addition of 2wt% (PVA) and uniaxially pressed into discs of 10mm in diameter and 1mm in thickness under 150Mpa pressure. The green pellets were, respectively, sintered at 800◦C and 1200◦C for 2 h. The densities of the pellets were measured by Archimedes method. Leakage current I_L of (9.1-396μA), potential gradient of (114.7-2247.2 V/mm), and nonlinear coefficient α of (3-23) [39].

In (2013) Kato and Takada. Investigated the relation between the crystalline phases and electrical properties of ZnO varistor, where ZnO containing 0.5 mol% Bi_2O_3, 1.2 mol% Sb_2O_3, and small amounts of Co, Mn, Ni, Cr, Si, Al, and B oxides**,** with 0.5 mol% of Y_2O_3, Eu_2O_3, Ho_2O_3, Er_2O_3, Yb_2O_3, and Lu_2O_3**.** The powder was pressed at 39 MPa into pellets 40 mm in diameter and 10 mm thick. The pressed pellets were sintered at 1150 °C for 5 h in an atmosphere with heating and cooling rates of 75 °C/h [40].

In (2013) Pillai et al. Studied the preparation of ZnO nano varistors devices and the effect of some oxides additives (Bi_2O_3, CoO, MnO, Cr_2O_3 and Sb_2O_3) on the performance, electrical properties, and microstructure of ZnO varistors using the chemical processing sol–gel and combustion synthesis plasma pyrolysis methods [14].

In (2014) Hong, et al. Studied the effect of Co_3O_4 Doping on the electrical properties of ZnO varistor at different concentrations, where mixtures of ZnO and Co_3O_4 corresponding to 0.1, 0.5, 1.0, 2.0, and 3.0 at. % Co doping, prepared by wet ball-milling, pressed into pellets at 98 MPa, and sintered at 1000°C for 1 h in air at heating and cooling rates of 5°C/min.

Sintered pellets were trimmed into disks of 1 mm thick and 6 mm in diameter and silvered on both sides for the electrical measurements. J-E (characteristics varistor behavior): α of (3 – 35); potential gradient of (5715 -9209 V/cm); J_L of (4 - 628 μA/cm^2); ρ_{gb} of (0.1~22.8 × 10^9Ωcm) [41].

In (2014) AL Mohammed, et al. Studied the influence of (La_2O_3, Ce_2O_3, NiO, MnO_2, Cr_2O_3, Co_3O_4, Nb_2O_5, and Bi_2O_3) on ZnO varistors, in order to get the greatest value for non-linear coefficient, by building a database by performing experimental measurements for I-V characteristic, and recording the values of the non-linear coefficient α corresponding to each change in ratios of these, where the minimum and maximum values were MnO_2 (0.1-0.6), NiO(0.2-1.5), Ce_2O_3 (0.2-0.8), and La_2O_3(0.2-0.8), and the maximum value of α =99.22 [42].

In (2014) Akinnifesi, et al. Studied the microstructure effect on the non-linear behavior of ZnO varistor two sample types were constituted as A (95mol % ZnO, 3 mol % PbO, 2 mol % MnO) and (95 mol % ZnO, 2 mol % PbO, 3 mol % MnO), The mixture was calcinated in air at a temperature of 150 C for about 2 hours. The mixture of each sample was compressed at a pressure of 2.5 x 10^2 N/m^2 into a disc form. The discs were sintered between 750℃ and 850℃ for between 12 and 42 hours, the leakage current of (0.54-1.7μA) , the non-linear coefficient of (0.32-7.29), and the grain size of (1.02-2.2μm) [43]**.**

1.7. Aim Of The Work

Manufacturing of ZnO varistor samples by doping ZnO with transition metal oxides as follow (95.5% ZnO, 0.5% Bi_2O_3, 2.5% Sb_2O_3, 0.5% Co_3O_4, 0.5% Cr_2O_3, 0.5% MnO_2), and then doping by rare earth oxides (Dy_2O_3, La_2O_3, Y_2O_3) with different concentrations (10^{-3}, $5*10^{-3}$, and $10*10^{-3}$), using conventional ceramic fabrication procedure to improve and enhances its electrical properties and microstructure.

And then study their electrical properties and microstructures. Improvement, enhancement of the nonlinear properties of ZnO varistor (is the essential goal) especially the nonlinear coefficient, breakdown voltage, and energy absorption capability, in order to use it in high voltages or high powers applications.

(THEORY)

2.1. Introduction

Transient voltage surges in electrical circuits are the most serious danger for the electrical equipment and power utility. Two forms of transient can be developed in electrical circuits; extraneous transient such as lightning and internal transient such as switching and ground faults. Both of this transient is dangerous and cause heavy damages on the voltage-sensitive equipment and micro-circuits. Lightning, with a voltage peak value extends up to 5000 kV, comes from out of circuit, so it should be suppressed on the incoming power lines. On the other hand, switching or ground fault transients, generally with a very small magnitude, can be generated within the equipment itself. Progression of electronics and solid state physics results in the usage of electronic circuits and systems containing low cost, high reliability solid state components powered by regular 120V AC power line sources. In general, the solid state components are very vulnerable against the small high voltages and cannot withstand the amount of high voltage imposed by typical power system transient. Considering different forms of transient surges, the protection systems should cover a wide range of voltages and energy handling capacities to be able to neutralize all forms of transients [44,45].

There are several methods to suppress the over voltages developed in an electrical circuit; using a safety fuse, a voltage reputational isolation transformer, etc. However, the usage of these methods is generally limited and with some problems. For example; a safety fuse should be replaced after each transient or, the voltage regulation/isolation transformers are effective only in the slow surge areas (typically $25ms$) while the majority of transients in the electrical circuits are very fast (less than $8ms$). A typical rise time for lightning is 600 to 1000 volts per μs and electromagnetic pulses are typically in nanoseconds areas that exceed largely the application area of these methods [44,45].

As mentioned in chapter one ZnO varistors with nonlinear current voltage behavior and high energy handling ability which have been widely used for protecting electronic devices against voltage surges. With the development of microelectronics and large scale integrated circuits, low

voltage ZnO varistors are now being used for surge protection in integrated circuits and in automobiles, etc. These varistors have thus become an important topic in academic and industrial research [16,45].

Most of the transient voltage surge suppressers (TVSS) manufactured today are Metal Oxide Varistors (MOV) especially the ZnO based varistors. TVSS devices are mainly used as a voltage limiting elements which restrict or clamp transient high voltages; which means the transient peak voltage is reduced or limited to a level that is considered safe, as illustrated in Figure (2.1.a) [16].

Normally, a varistor is located at the incoming power line before the power supply reaches the circuitry being protected. If during one fine day, a transient high voltage, or spike, is passed along the power line, the varistor will detect the circuit in time about nanoseconds speed; it will absorb most of the high voltage and reduce it to a small magnitude and safe level above the normal operating voltage of the circuit, this operation is shown in Figure (2.1.b). The "safe level" refers to the voltage magnitude in which the electrical circuit be treated without being destruction [16].

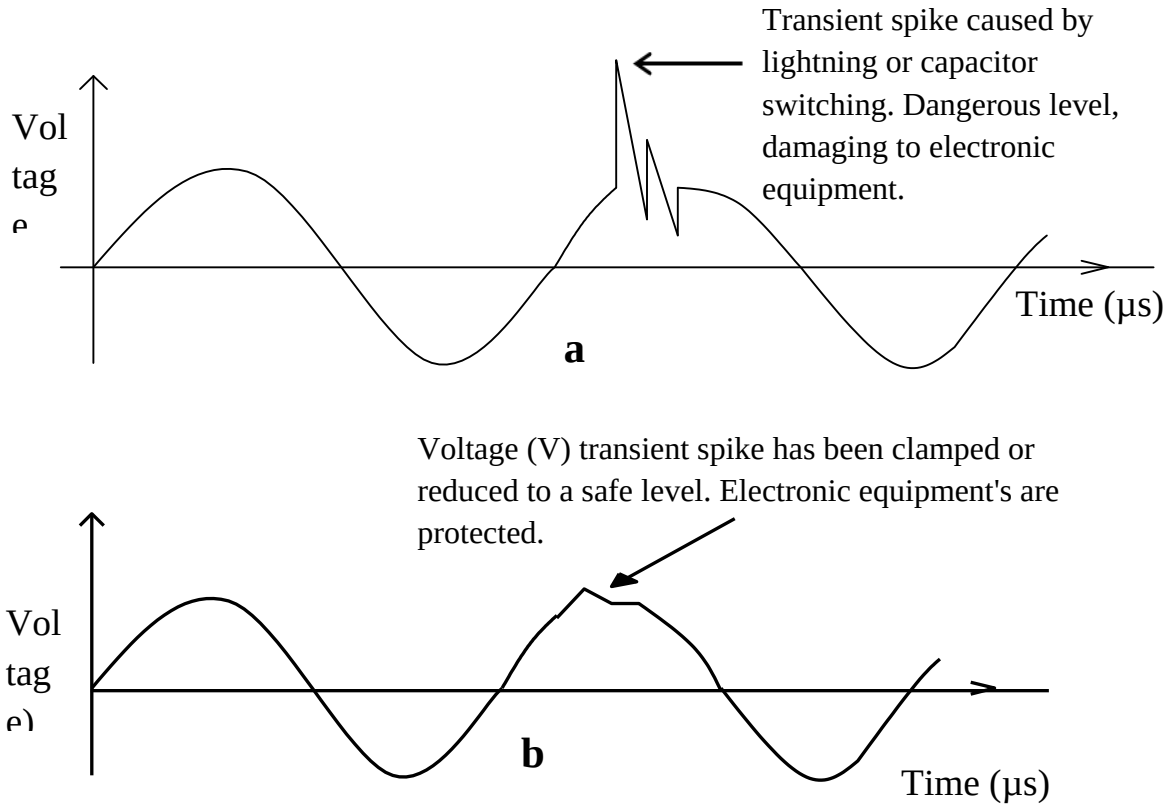

Fig (2.1): (a) Over voltages transient. (b): safe level voltages [16].

2.2. Transient Voltage Surge Suppressers

Electronic and electric circuits possibly subjected to critical high voltage transient generated from electrostatic discharges, lightning, and switching. To solve this problem the designer can over-specify the circuit or incorporate protection. The economic balance generally leans towards protection which authorizes the reduction of component costs by specifying moderate ratings. Those devices which connected in parallel with the equipment, and protects it from getting damaged due to transient high voltages by effectively acting as a short circuit when a transient surge occurs, therefore the current through the equipment (load) is limited, these protectors are called transient voltage surge suppressers, as shown in figure (2.2) [16,45].

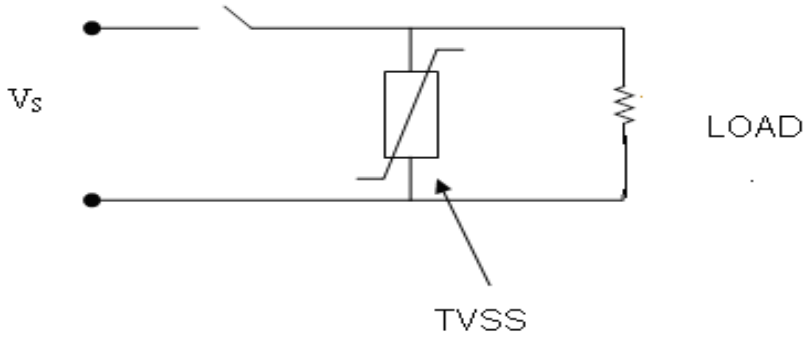

Fig (2.2): Transient Voltage Surge Suppresser (TVSS) [16].

2.3. Types of Transient Voltage Surge Suppressers

The ideal surge suppresser does not exist; it is possible to select the suitable suppresser for a certain purpose. It is difficult to compare efficiency or performance of these transient voltage surge suppressers because of the dissimilarity of models and technology [17]. The following sections explain surge voltage suppressors which are widely used in electric and electronic circuits.

2.3.1. Spark Plug

Spark plug or gas filled protectors are among the oldest voltage surge protection devices. They are suitable for usage as voltage surge suppresser devices because of their large surge current handling capability. The main deficiency of these types is the high response time, which cannot escort with the rapid change in the voltage leaving the equipment unprotected during the voltage changing [17].

2.3.2. Zener Diode

Zener diodes are two terminal semiconductor devices which can act as transient voltage surge suppresser when operated in the reverse bias mode. They exhibit very low response time when a voltage surge occurs. The major advantage of Zener diodes is their very effective clamping. Moreover they can be used at very low voltage. The main disadvantage of these devices is their low transient energy handling capability owing to heat generated in a small volume [17,46].

2.3.3. Varistor Device

ZnO varistor is a semiconducting device, which has greater energy absorption and high transient energy handling capability, a nonlinear current voltage properties with a methodical sharp breakdown identical to that of a Zener diode [20,47].

2.4. Varistor

Varistors (variable resistors) are nonlinear, two-terminal, semiconductor voltage-dependent resistors. Varistors are electronic ceramic materials whose electrical properties are greatly dominated by grain-boundary interface states. Varistors applications are technologically important because of their electrical properties that enable them to be used as solid state switches with large-energy handling capabilities [35,48].

The varistors are also known as Voltage Dependent Resistors (VDR) because they exhibit a highly nonlinear current voltage properties with a highly resistive state in the pre-breakdown region (also known as Ohmic region) and large nonlinearity coefficient (φ) in the breakdown region, as shown in figure (2.14). Several materials with charged grain boundaries show to some extent such non-linearity phenomena. Some examples are ZnO, TiO_2, WO_3, and SnO_2 [47,49].

The nonlinear current voltage relationship is expressed by the empirical equations:

$$J = KE^{\varphi} \quad \ldots\ldots\ldots\ldots\ldots\ldots\ldots\ldots \textit{(2-1)}$$

$$\varphi = \frac{\log(J_2/J_1)}{\log(E_2/E_1)} \ldots\ldots\ldots\ldots\ldots\ldots\ldots \text{(2-2)}$$

or

$$I = KV^{\varphi} \quad \ldots\ldots\ldots\ldots\ldots\ldots\ldots\ldots \textit{(2-3)}$$

$$\varphi = \frac{log(I_2/I_1)}{log(V_2/V_1)} \quad \ldots\ldots\ldots\ldots\ldots\ldots \textit{(2-4)}$$

$$\varphi = \frac{log I_2 - log I_1}{log\ V_2 - log V_1} \quad \ldots\ldots\ldots\ldots\ldots\ldots \textit{(2-5)}$$

Where J represents the current density, E the potential gradient; K constant, and φ represents the nonlinearity exponent (coefficient), and its maximum value of the order of *50*, $J_2 = 1\ mA/cm^2$, $J_1 = 1\ mA/cm^2$, E_2 and E_1 represent the potential gradient at $1\ mA/cm^2$ and $0.1\ mA/cm^2$, $I_2 = 1\ mA$, $I_1 = 0.1\ mA$, V_2 and V_1 represent the voltages at 1 and $0.1mA$ respectively [47,50,51].

From a physical point of view, the nonlinearity in the current voltage characteristics originates from the bias dependence of the interface charge, which controls the barrier height and then the current flow across the junction. When the applied voltage passes the nominal voltage (or breakdown voltage)

the material's resistance strongly decreases, enabling the current to flow throughout the polycrystalline material [10,17].

The VDR's current voltage characteristics are similar to those of Zener diodes in reverse bias region but with much greater current and energy handling capabilities. Functionally, VDR‟s are connected in parallel with circuits to protect them from voltage surges. When they are subject to a voltage below their breakdown voltage, they pass only a leakage current. When the voltage of the circuit exceeds the switch voltage, for instance, during a voltage transient or surge, the VDR becomes highly conducting and draws the current through it. When the voltage returns to normal, the VDR returns to its original high resistance state, usage of such polycrystalline semiconductors to protect resistant equipment from transient high voltage is that the VDR component is chosen to have a switch voltage or breakdown voltage slightly greater than the maximum design voltage applied to the system to be protected [17,49].

2.5. Physics of ZnO Varistors

The nonlinearity behavior in the ZnO varistor due to the grain boundaries process where the barriers of majority charge carriers exist in the depletion layers of the adjacent grains. Schottky barrier has been considered to be the most likely barrier at the grain boundaries of ZnO microstructure. There is no need for physically separate, intergranular, insulating layer between two grains. The negative surface charge at the grain boundaries interface (electron traps) equivalent to the positive charge in the depletion layer at the grains on both sides of the interface. Thermo-ionic emission and tunneling are accepted to be the major transport mechanisms [9,52,53].

2.6. Microstructure Of ZnO Varistors

The microstructure of ZnO varistors can be defined as complex, polycrystalline, multiphase, doped semiconducting ceramics. It is formed by conventional sintering of a mixture of oxides such as Zn, Bi, Co, Mn, Sb, Ni Cr and Al, the major component being ZnO, typically 85 - 95%. Although the microstructures of varistors exhibit considerable variation from one

manufacture to another, they all exhibit the properties of a typical ceramic prepared by liquid phase sintering [19,18,52].

These devices (varistors) consist of conducting ZnO grains, surrounded by a thin insulating oxide layer. The resulting microstructure consists of ZnO grains, spinel ($Zn_7Sb_2O_{12}$) and a number of bismuth rich intergranular phases. The varistor work associated with processes at a ZnO - ZnO grain boundaries. ZnO grains are the predominant phase and consist of relatively small conducting ZnO crystals [19,54].

When designing a varistor for a given nominal varistor, the voltage is basically a matter of selecting devices thickness such that the appropriate number of grains in series between the electrodes. It is possible to control the grain size by altering the composition of oxide dopants in the varistor powder formulation and the sintering temperature, the fundamental merit of the ZnO varistor is the potential gradient across the single interface junction between grains, estimated at (2.3) volts per grain boundary [55,34].

Upon sintering several amorphous and crystalline phases are formed. The main microscopic constituents found in ZnO varistor materials are:

1- ZnO grains.
2- Spinel ($Zn_7Sb_2O_{11}$) grains.
3- Several bismuth-rich intergranular phases including pyrochlore phase ($Bi_3Zn_2Sb_3O_{14}$). Other minor phases are also present which are not detectable by conventional techniques [14,34,35].

Both Bi_2O_3-rich and ($Zn_7Sb_2O_{12}$) spinel phases are also usually existed at the grain boundaries of the ZnO, but the existence of a ($Bi_3Zn_2Sb_3O_{14}$) phase is possible too. ZnO – ZnO grain boundaries, Bi_2O_3-rich phase, which is a highly resistance phase, represent the main reason (principle) of the varistors work, while spinel-ZnO junctions do not contribute to the nonlinear effect [52].

These phases could be identified from the XRD pattern, spinel and pyrochlore are mainly crystallized in intergranular phases, while Bi_2O_3 rich phases are found at the triple points, as shown in figure (2.3) [14,21].

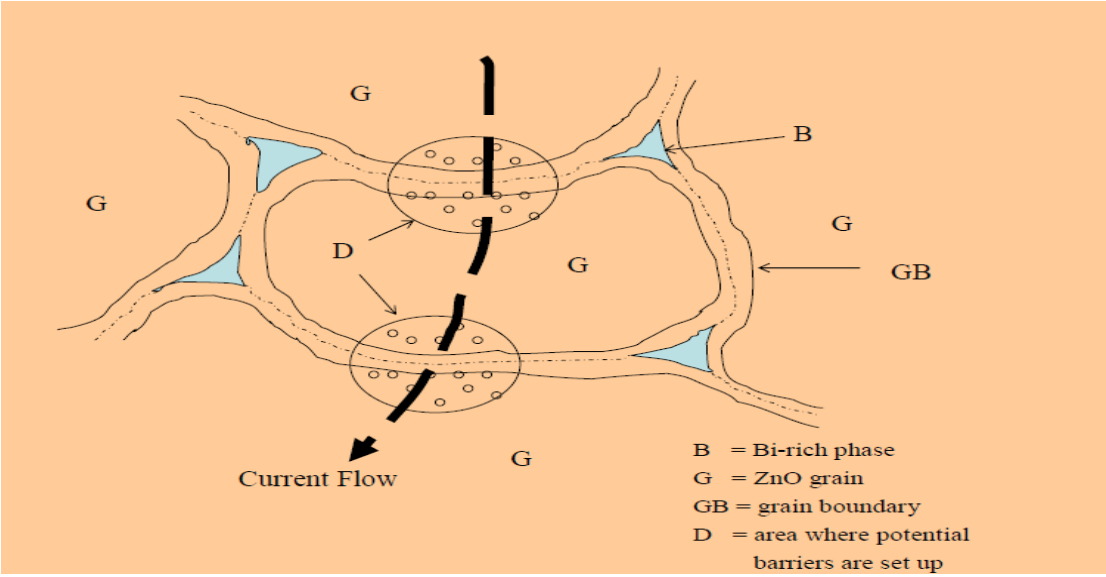

Fig (2.3): The microstructure of ZnO varistor phases [21].

After varistors fabricated (forming), then two electrodes manufactured on two-sided. The bulk of the varistor between contacts is comprised of ZnO grains with average size *d*, as shown in figure (2.4) [21,31].

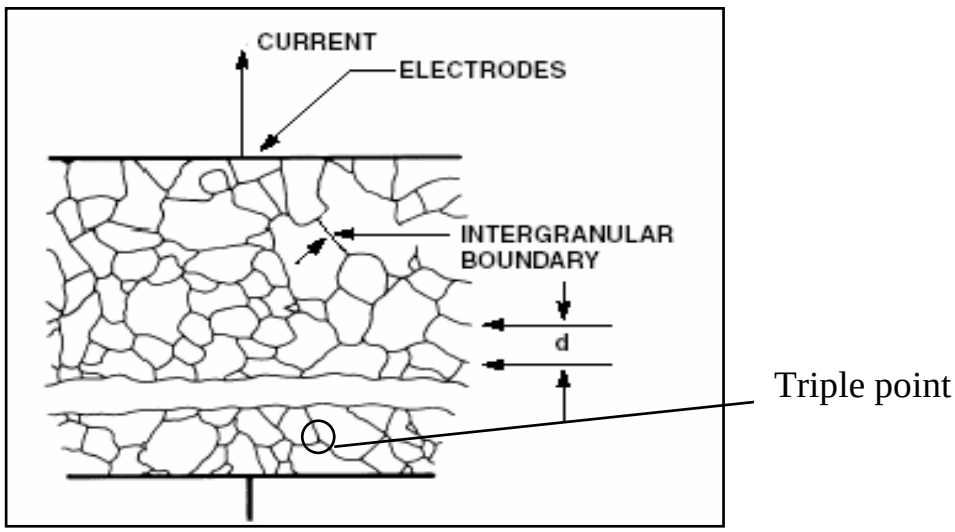

Fig (2.4): ZnO varistor microstructure description [31].

ZnO varistor have highly nonlinear resistance which is primarily zinc oxide added to other materials. Conductive zinc oxide grains separated by boundaries that form semiconductor junctions, similar to a semiconducting diode, a metal oxide varistor microstructure is equivalent to combinations of millions series and parallel semiconducting diodes [21,52].

The simple equivalent model to describe the ZnO material in terms of electrical components is an R_{IG}-C_{IG} where (R_{IG} is the resistance of intergranular layers, and C_{IG} the capacitance of intergranular layers) parallel circuit in series with another resistor, R_{GRAIN} (the resistance of grains). R_{IG} is defined as a highly non-linear resistor with increasing voltage, similar to nonlinear behavior of intergranular layers of ZnO material, the capacitance of ZnO grains is very small and can be neglected, the equivalent circuit of ZnO varistor is as shown in figure (2.5) [**9**,21].

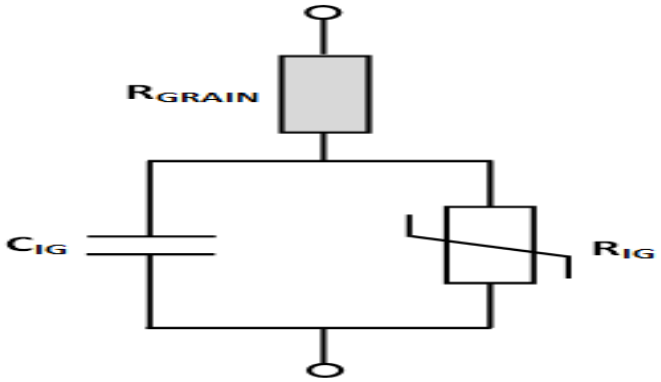

Fig(2.5): Equivalent circuit of ZnO varistor [9].

2.6.1. ZnO Grains

The bulk of the varistor micro structure between the electrodes contacts is comprised of ZnO grains. They are the basic building block of ZnO varistors formed as a result of sintering of ZnO particles together with other metal oxide dopant particles [**19**].

During the sintering process the ZnO particles grow to form grains and become doped by cationic elements. These doped ZnO grains are responsible for the conductivity of the ZnO varistors in the up-turn region of the current voltage properties, and, have a role as heat sink for surge energy absorption, as explained in the electrical properties sections [54,14].

ZnO grains form the main constituent in the present ZnO varistor materials. The grains differ in geometry but they are very similar with respect to chemical composition [8,19].

The grain size may be controlled by sintering temperature and time, whereas the higher sintering temperature and longer sintering times increase the grain size [8,28].

The grain size is also influenced by the presence of metal oxide additives [19].

2.6.2. Spinel Phase

The second phase of ZnO varistors; this phase has a spinel type structure, where its formula is $Zn_7Sb_2O_{12}$ which contains various amounts of chromium, manganese, cobalt, and nickel in solid solution. The spinel phase appears as faceted octahedral crystals predominately situated at the ZnO grain boundaries [19,56].

The Pyrochlore decomposition at a temperature about 1000 ℃ is forming spinel ($Zn_7Sb_2O_{12}$) (as will be explained in section 2.7.2) [35].

$Zn_7Sb_2O_{12}$, residing between the ZnO grains or as thin layers which promote the formation of twin boundaries in ZnO and the presence of the spinel phase inhibit the growth of the ZnO grains during the sintering process [35,52].

The presence of spinel particles is a result of the particular composition and processing of the varistor, two different chemical reaction routes have been identified for their formation, the reaction between ZnO and Sb_2O_3 during heating to higher temperatures and the decomposition of pyrochlore during heating by the sintering process [19,56].

2.6.3. Bi_2O_3 Rich Phases

Bi_2O_3 rich phases are also usually present at the grain boundaries of ZnO. Rich of Bi_2O_3, which is a highly resistive phase, represents the main cause of the varistor effect [52].

Bi_2O_3-rich phases in ZnO varistors can be divided into three major parts

1- Crystalline Bi_2O_3 phase.
2- Amorphous phase.
3- Pyrochlore ($Zn_2Bi_3Sb_3O_{14}$) phase.

The above phases form three-dimensional networks throughout the varistor bulk [19].

2.6.3.1. Crystalline Bi_2O_3 Phase

Pure Bi_2O_3 has four known phases denoted the $\alpha-, \beta-, \gamma-, and\ \delta-$ phases. The $\alpha-$ phase is the stable phase at low temperatures and it undergoes a phase transition at T=730 ℃ into the $\delta-$phase. The $\delta-$phase is stable up to the melting point at 825℃. Bi_2O_3 has a phase hysteresis since cooling the $\delta-$phase can cause the formation of a tetragonal $\beta-$phase or a bcc $\gamma-$phase at temperatures below 730 ℃ before the material finally transforms into α-phase [21,54],.

The grain boundary is also Bi-rich, with an α-Bi_2O_3 phase as the predominant phase present. This material is an insulator, and the insulators by their nature have traps. The overall effect of these materials is the creation of the double Schottky potential barriers, in other words there are interface states formed in the grain boundaries whereas these states originate double Schottky barriers, which controls the electron transport between grains [54,56].

2.6.3.2. Amorphous Bi_2O_3 Phase

The amorphous bismuth-rich phase is found primarily in the grain junctions, especially at the ZnO-ZnO interfaces, and it causes (produces) the Schottky barriers. The intergranular bismuth-rich films are continuous and it is (1-2) nm thick, as shown in Figure (2.6) [19,57].

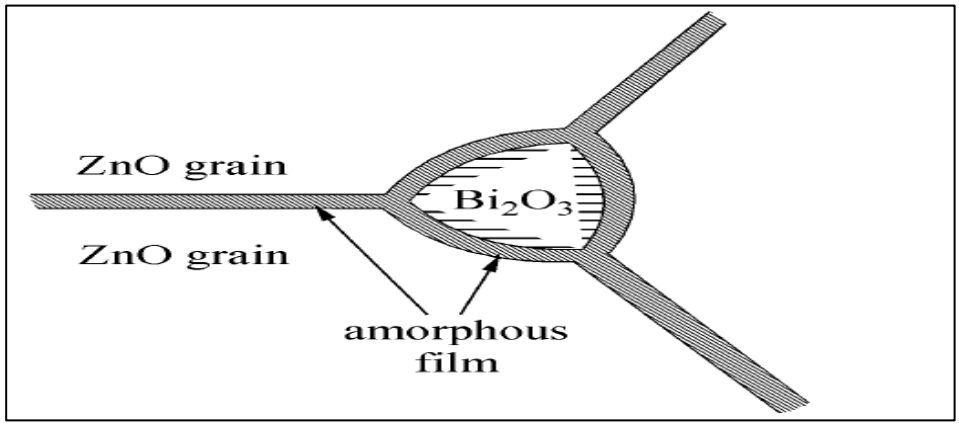

Fig (2.6).Triple grain junction, crystalline Bi_2O_3, amorphous bismuth rich film, and ZnO grains [8].

2.6.3.3. Pyrochlore Phase

Pyrochlore $Zn_2Bi_3Sb_3O_{14}$ phase is formed initially during heating to the sintering temperature between 700- 900℃, the amount of pyrochlore phase formed is inversely dependent with the heating rate [19,14].

Pyrochlore phase formed in the systems always contains Bi_2O_3 and Sb_2O_3.A small amount of Co^{2+}, Mn^{2+} may be dissolved in this phase, which appears to fill the space at some of the multiple grain junctions and sometimes partially surround the ZnO grains [19].

Pyrochlore phase is responsible for the nonlinearity, however, the exact role of pyrochlore phases on the electrical properties of ZnO varistors is unknown [18].

2.6.4. Grain Boundary

Grain boundaries are breaking the three dimensional periodicity of the bulk crystal due to the misorientation of the two lattices [54].

Breaking up the crystal lattice and rotating one part with respect to the rest of it, forms a so called grain boundary where the two crystals orientations meet, this breaking of the crystal symmetry creates a potential barrier for the electrons on both sides of the grain boundary [54].

It is possible for the electron to passes the grain boundary. The barrier at the grain boundary limits the number of electrons which are able to pass. As shown in Figure (2.7) [54].

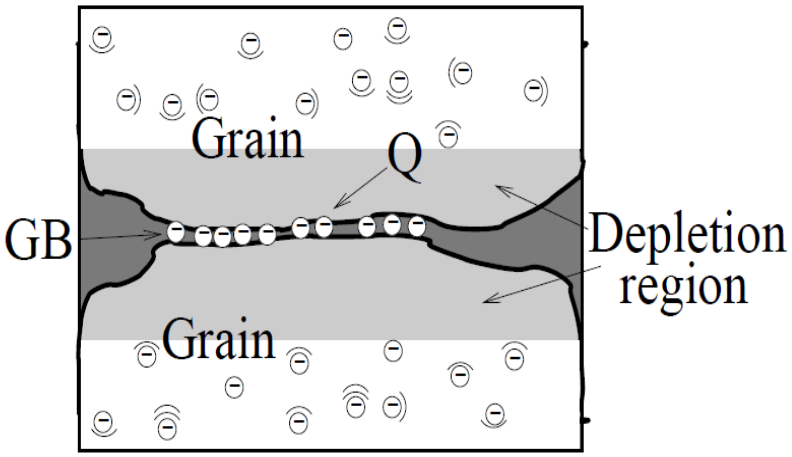

Fig (2.7): The distribution of charges at the neighborhood of the grain boundaries (the shaded region) represents the depletion region [54].

Pyrochlore phase $Bi_3Zn_2Sb_3O_{14}$, spinel $Zn_7Sb_2O_{12}$ and Bi_2O_3 rich with α-Bi_2O_3 based are the predominant phase located at the grain boundaries and triple point regions separating ZnO-ZnO grains, these phases are insulators, and insulators by their nature have traps. The general effect of these phases is the origination of the double Schottky barriers [21,56].

The three dimensional bismuth rich grain boundaries that surround the ZnO grains can be categorized microstructurally into two parts ; the ZnO-ZnO single grain boundary, and the grain boundary at multiple and triple grain junctions [19].

2.6.4.1. ZnO-ZnO Single Grain Boundaries

With respect to the existence of Bi_2O_3 at the boundaries between two ZnO grains, two types of results have been reported; continuous bismuth rich film a few nanometers thick, and 1/2 atomic to atomic layer of bismuth intergranular layer [19].

Until now, there doesn't appear to be an agreement regarding the width of grain boundaries found by microstructural analysis of ZnO varistors [19].

2.6.4.2. Triple And Multiple Grain Junctions

The amorphous bismuth rich film is distributed continuously between the ZnO grains of the material, while the crystalline Bi_2O_3 rich phases are predominantly located in the triple and multiple grain junctions and they are surrounded by an amorphous Bi_2O_3 rich phase [35,19].

2.6.5. Porosity

If the device after fabricated contains high porosity, then the non-regularity arising in density may causes the leakage current which distributes non uniformly over the area of the sample, resulting in a temperature distribution, which varies from site to site [18,19].

2.7. Sintering

Sintering is a high temperature technological process that transforms individual ceramic particles into a compact polycrystalline body, and this process is widely used to fabricate bulk ceramic components [12].

Sintering occurs over a range of temperatures, but is accelerated as the particles approach their melting range. It takes place faster as the particle size decreases, and diffusion distances are shorter . For solid state sintering, it is appropriate to think of sintering with respect to the melting temperature [12].

During sintering the particles of the powder are merged with their neighbors, junctions between them are increased step-by-step with time. The worth mentioning that the sintering process convoyed with the dispersion of the porosity [58].

The sintering process converts the green microstructure to the microstructure of a dense component. In electronic ceramics microstructural properties include density, grain size and pore size, as well as crystalline and amorphous phases [59].

The sintering process consists of solid particle bonding or neck formation, followed by continuous closing of pores from a large open porosity to essentially pore free bodies [57].

The sintering processes can be divided into two types:

1- Solid phase sintering.
2- Liquid phase sintering [60].

2.7.1. Solid phase Sintering

In this type of sintering the shaped green bodies are heated to a temperature that is typically 0.5-0.9 of the melting point. In this process liquid does not exist and atomic diffusion in the solid state produces connecting of the particles and reduction of the porosity [56,61]. Figure (2.8) illustrates the solid phase sintering.

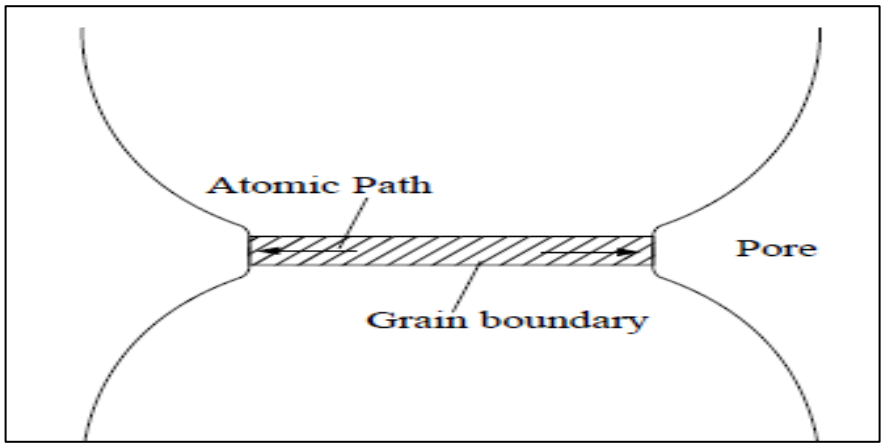

Fig (2.8). Solid phase sintering [56].

2.7.2. Liquid phase sintering

In this type a small amount of liquid, typically less than a few volume percent of the original solid mixture, is present at the sintering temperature. The liquid volume is insufficient to fill the pore space so that additional processes are required to achieve full densification [56]. Liquid phase sintering is an important method for the industrial production of many ceramics products. worth mentioning that the liquid phase enhances and improves the densification process at lower temperatures [61]. The liquid phase performs as a connector during the cooling process, which connects the ZnO and spinel grains together [56], as illustrated in Figure (2.9).

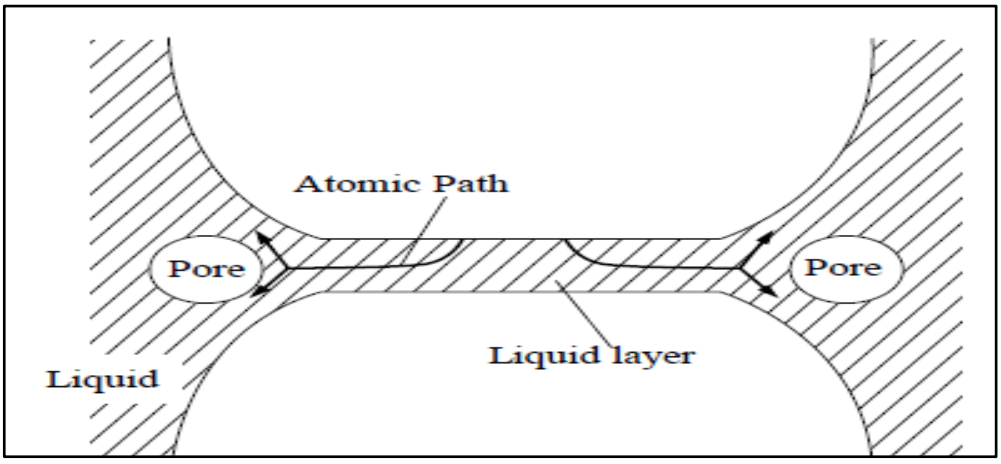

Fig (2.9). Liquid phase sintering [56].

Densification during sintering is a complex phenomenon, where the densification of zinc oxide varistors is predominantly by liquid phase sintering. The predominant liquid phase is bismuth oxide, its viscosity of which is influenced by metal oxide additive dopants. In addition to temperature, its concentration is determined by the amount of bismuth oxide added to the initial formulation, and the level of pyrochlore and spinel formation[56].

Varistors are manufactured by mixing a number of different metal oxides in powder form and the mixture is treated by liquid phase sintering to form the final varistor, this process is called liquid phase sintering because the metal oxides mixture is heated at temperatures in the range of 1000℃ - 1300℃ for a specific time in a furnace. The additives (metal oxides) or most of them

melt at or under these temperatures, while the ZnO grains stay crystalline which means that the ZnO grains are floating in a melt of metal oxides during the sintering process [54,56,62].

Typically, liquid phase sintering begins by mixing two or more small powders of differing compositions. During heating, one powder melts or reacts to form a liquid between the particles that overflows the more refractory phase. The process consists of several overlapping steps involving solid state diffusion, particle rearrangement, solution-reprecipitation, and solid skeleton densification. After sintering the product is a composite of grains that were solid during sintering connected with a solidified liquid [21].

During the initial stage of liquid phase sintering (LPS) rearrangement of the solid phase, in which surface tension forces act to bring about physical movement of the constituents of sintering body, takes place causing rapid densification. This process assumes that if there is good wetting between liquid and solid phases, solid grains can rearrange themselves under the action of surface tension forces, producing more stable packing. Therefore it is interesting to investigate how the solid grains rearrange [63].

The exceptional current-voltage behavior of ZnO varistors was attributed mainly to the presence of the numerous oxides which segregate at the ZnO-grain boundaries. These additive-oxides are categorized in three main groups:

a- The varistor-action oxides.

b- Specific current voltage regulator.

c- Spinel forming grain growth inhibitors [45,56].

Bi_2O_3, being the varistor-action oxide, forms the liquid through a eutectic melting with ZnO at 740°C which promotes densification and enables liquid phase sintering. During cooling Bi_2O_3 forms tunnel barriers at the ZnO grain boundaries and this leads to the non-Ohmic behavior , Sb_2O_3, on the other hand, is the spinel forming grain-growth inhibitor which produces the spinel phase ($Zn_7Sb_2O_{12}$) [14,28] .

Microstructure development of $ZnO{-}Bi_2O_3$-based varistor ceramics during reactive liquid phase sintering in the temperature range of 500−1050 °C is as following:

$Sb_2O_3(s) + O_2 \rightarrow Sb_2O_5$ (l) At 527℃.

Sb_2O_5 (l) + ZnO (s) $\rightarrow ZnSb_2O_6$ (s) At 700-800℃.

$3ZnSb_2O_6$ (s) + $3Bi_2O_3$ (s) + ZnO(s) → $2Zn_2Bi_3Sb_3O_{14}$ (Pyrochlore) between 700- and 900℃.

$2Zn_2Bi_3Sb_3O_{14}$ (s) (Pyrochlore) +17ZnO (s) →$3Zn_7Sb_2O_{12}$ (s) (Spinel) +$3Bi_2O_3$ between (950−1050 ℃). [14,34,35].

Sintering arises during three stages: initial, intermediate, and final stages. The first stage consists of the growth of weld necks between individual particles, the second stage involves the isolation of the pores, and finally disappearance of pores occurs at the third stage. A schematic Figure of three stages of sintering is shown in figure (2.10) [18].

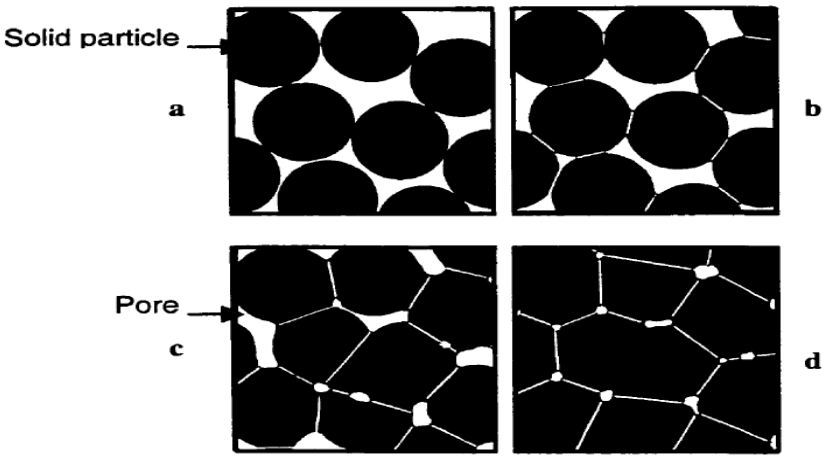

Fig (2.10) .The three stages of sintering process.(a) bound growth starting (initial stage), (b) shrinkage of pores volume (intermediate stage), (c) formation of grains boundaries (final stage) [18].

2.8. Development Of Microstructure

The binary system Bi_2O_3–ZnO is characterized by an asymmetric location of the eutectic at (740℃). The initial melt only dissolved a small quantity of zinc oxide and therefore the extent of the liquid phase in the system is basically controlled by the Bi_2O_3 fraction in the sample. However, Sb_2O_3 incorporation leads to a depression of the solidus from (740℃) to (590℃), because of the comparatively lower melting point of Sb_2O_3 (melting point equals to (656℃), for Sb_2O_3 and (825℃) for Bi_2O_3), the low temperature melt is dominated by Bi_2O_3/Sb_2O_3 [28,64].

Figure (2.11), explains the formation of the liquid phase in the Bi_2O_3–Sb_2O_3–ZnO ternary system with increasing of the temperature.

It may be noted that the eutectic melting is not depressed below a temperature of 740℃. Under these conditions, four major phases can be identified: $(Bi,Sb)_2O_3$ liquid and Sb_2O_4, Sb_2O_5 and ZnO solid phases. At (790°C), Sb_2O_5 disappears and the liquid is saturated with ZnO and Sb_2O_4, as shown in Figure (2.11.c), [46,56].

Grain growth in varistor ceramics occurs by the creation of ZnO–Bi_2O_3 binary structures during the liquid phase sintering process. Therefore, a substantial enhancement of grain growth is expected above the eutectic liquid temperature, compared with the grain growth of pure undoped ZnO, this is due to the creation of liquid bismuth along the ZnO grain boundaries, which enhances the grain boundary movement and thus facilitates the grain growth [14,65].

During sintering various phases in the microstructure are distributed in such a way that the grain boundary region converts to a highly resistive phase (ρ_{gb}~$10^{12}\,\Omega cm$) and then the grain interior (ZnO grains) becomes highly conductive (ρ_{gb} 1-10 Ωcm) [14,19].

A sharp drop in resistivity from grain boundary region to the ZnO grain usually occurs within a very small space. This is normally considered as a depletion layer. Thus at each grain boundary area there exists a depletion layer extending into the nearby ZnO grains, and then the varistor action produced as a result of the presence of these depletion layers between the ZnO grains [14,19].

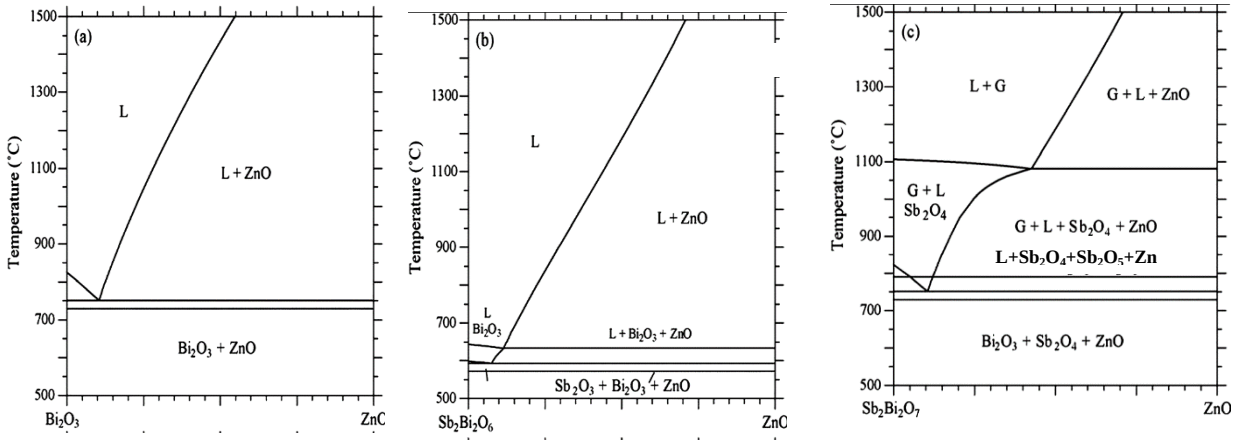

a b c

Fig (2.11). temperature composition sections(a) ZnO–Bi_2O_3, (b) ZnO–Bi_2O_3–Sb_2O_3 and (c) ZnO–Bi_2O_3–Sb_2O_4 (L =liquid, G = gas) [27,56].

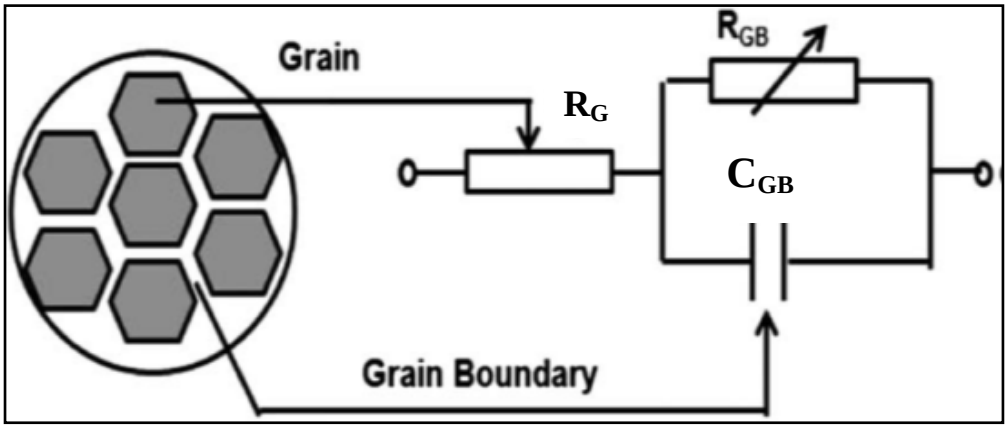

Fig (2.12). Electrical circuit proportional to varistor component [14].

The nonlinearity of the voltage current properties results from phenomena occurring mainly on the boundary of the grains. Potential barriers appear between grains, and they regulate the intensity of currents depending on voltage [53].

The simple equivalent model to describe the ZnO varistor material in terms of electrical components is an R_{IG}-C_{IG} parallel circuit in series with another resistor (R_{Grain}) the resistance of conducting ZnO grains. R_{IG} is defined as a highly nonlinear resistor with increasing voltage. Similar to nonlinear behavior of intergranular layers of ZnO material, we have the grain boundary capacitance C_{IG}. ZnO grains capacitance of is very small and can be neglected. The equivalent circuit modeled is as shown in Figure (2.12). [21,56].

Metal oxide varistors (MOV) protect any equipment revealable to permanent damage from rapid, long term lightning strikes. Figure (2.13) shows the MOV act as the protection component of the equipment. Under normal operation, MOV has very high impedance up to several mega ohms and it can be considered as open circuit [54,**56**], therefore, all of the current in circuit will flow through the equipment and bypassing the MOV, but when subjected to high voltage, instantly, the impedance of the ZnO varistor declines to a few ohms or less for severe surges to avoid large current flows through equipment. After the surge absorption is completely done, immediately the varistor returns to its normal high impedance and restores its original properties. Nonlinear properties would eliminate the power follow current flowing through it after the surge was done, this is the main advantage

of the varistor where its residual voltages at high currents can be reduced [29,54].

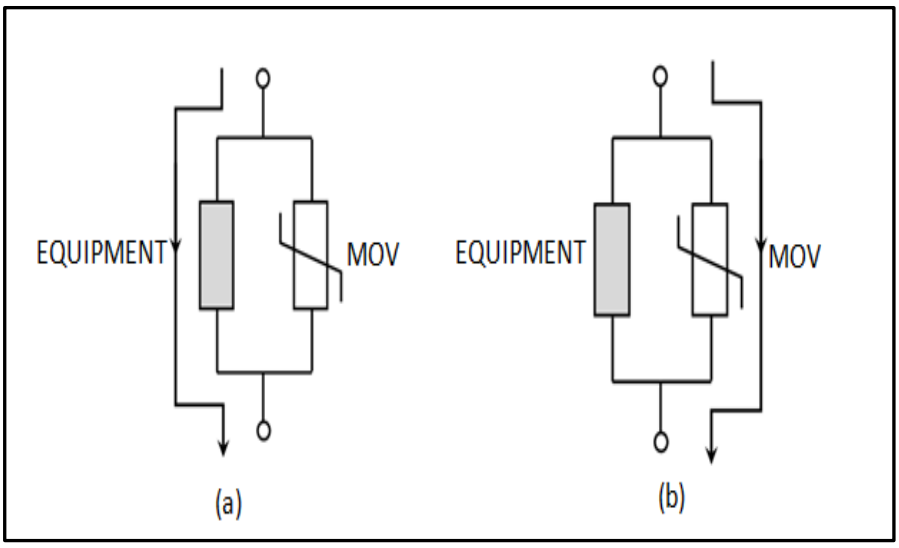

Fig (2.13). Influence of varistor (a) at conventional working, (b) at high voltage working [29].

2.9. Varistor Electrical Regions

ZnO varistors are complex, multiphase, polycrystalline, doped, metal oxide, solid state, and semiconducting ceramics. They are made of ZnO plus other metal oxide additives such as antimony, bismuth, cobalt, manganese, and nickel etc. and their electrical resistance is a nonlinear (non Ohmic) function of applied voltage. Their unique nonlinear electrical properties arise from internal interfaces between the ZnO grains and grain boundaries in the ceramic. The ZnO varistor has a very steep nonlinear current-voltage curve and therefore can support widely varying currents over a narrow voltage range [48,66,67].

The most important property of varistor is the nonlinear current voltage properties of this device. The current voltage properties of a typical varistor is shown in Figure (2.14), where three regions can be distinguished [19]:

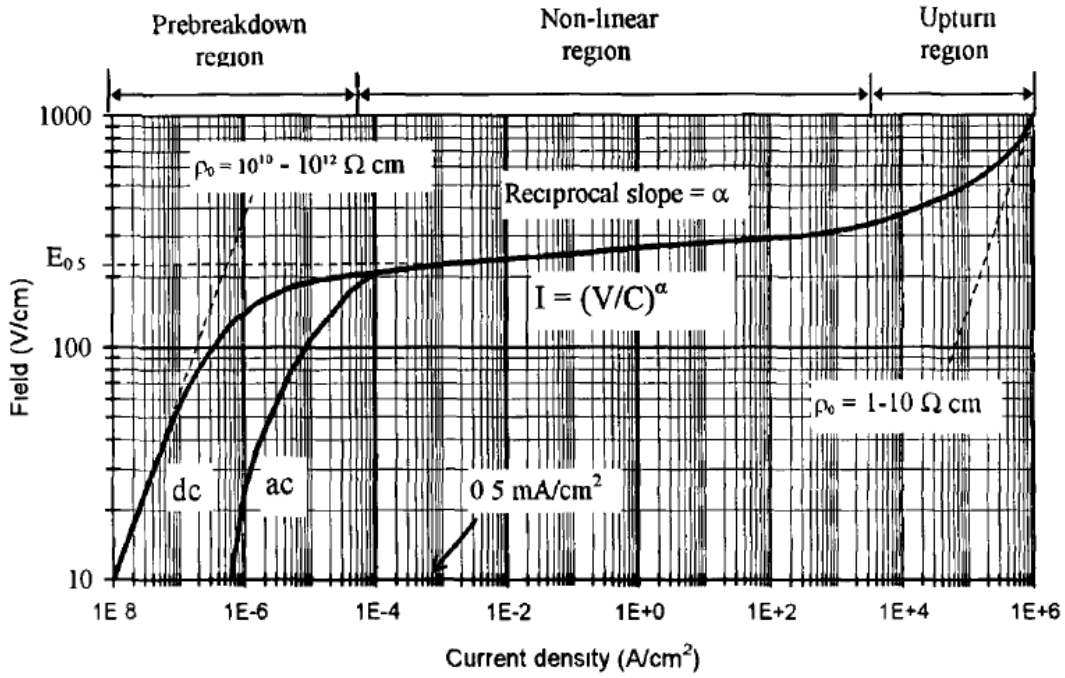

Fig (2.14). Current voltage graph of typical metal oxide varistors [13].

Zone 1: Leakage region (pre-breakdown region): At low voltages, varistor is highly resistive of the order of $10^{12}\ \Omega cm$ and it can be regarded as an excellent insulating device [17,18].

In this region, the current voltage behavior of varistor is described by Ohm's law, and is controlled by the resistivity of the grain boundary, this region corresponds to the varistor operation in the absence of all high voltages, (the pre-breakdown region determines the steady state joule heating and the nominal voltage of the varistor), the current is governed by a thermo-ionic emission process which results in a weak nonlinearity. The leakage current is a function of temperature i.e. it increases with increase in temperature [10,21,55].

Zone 2: Breakdown region (action region): When the voltage exceeds a certain value, often called breakdown voltage or breakdown field, the varistor becomes highly conducting and it conducts an increasingly large amount of current for a small increase in voltage. The resistivity of the device in this region drops dramatically down to values of 1-10 Ωcm and the current voltage properties can no longer be described by Ohm's Law. The relationship

between current and voltage in this case is generally expressed by the varistor empiric power equation [14,21]:

$$I = \left(\frac{V}{C}\right)^{\varphi} \ldots\ldots\ldots\ldots\ldots\ldots\ldots\ldots\ldots\ldots\ldots (2-5)$$

$$K = \left(\frac{1}{C}\right)^{\varphi} \ldots\ldots\ldots\ldots\ldots\ldots\ldots\ldots\ldots\ldots\ldots\ldots (2-6)$$

When $\varphi = 1$ the Equation above will be simplified to the Ohm's law and the current would be proportional to the applied voltage. In this case, the device will act as an Ohmic resistor[14].

If $\varphi \to \infty$ the current will varies infinitely for small changes in the applied field in the closeness of the breakdown voltage, and the device will be a perfect one. In practice, the varistors behave between a perfect varistor and an Ohmic resistor. The higher the value of φ, the better the device and, the higher the protection level [18,19].

And $\varphi = \frac{R}{R_D} \ldots\ldots\ldots\ldots\ldots\ldots\ldots\ldots\ldots\ldots\ldots (2-7)$

Where R represents Ohmic resistance and R_D is differential resistance.

$$\varphi = \frac{R}{R_D} = \frac{V/I}{dV/dI} \ldots\ldots\ldots\ldots\ldots\ldots\ldots\ldots\ldots\ldots (2-8)$$

$$\varphi = \frac{V/I}{dV/dI} = \frac{dI/I}{dV/V} \ldots\ldots\ldots\ldots\ldots\ldots\ldots\ldots\ldots\ldots\ldots\ldots (2-9)$$

$$\varphi = \frac{\int dI/I}{\int dV/V} \ldots\ldots\ldots\ldots\ldots\ldots\ldots\ldots\ldots\ldots\ldots\ldots\ldots (2-10)$$

$$\varphi = \frac{\log I_2 - \log I_1}{\log V_2 - \log V_1} \ldots\ldots\ldots\ldots\ldots\ldots\ldots\ldots\ldots\ldots\ldots\ldots (2-11)$$

Where, φ is known as the degree of nonlinearity or nonlinear coefficient, V is the applied voltage on the device, I is the current passing through the device, C is a constant and, the nonlinear region determines the

clamping voltage upon the application of transient surge and this region represents the heart of the varistor [14,68].

The current voltage properties in this region is almost independent of temperature [12].

Zone 3: (Upturn region): Again current voltage behavior of varistors exhibits another Ohmic region at very high currents. This happens at current densities of about 10^3 A/cm^2. This region is often called upturn region in which the current again increases linearly with the voltage [21,55].

2.10. Varistor Electrical Properties

2.10.1. Non Linear Coefficient

The correlation between the electrical behaviors with the principal microstructural features emerges for the ZnO varistor. The microstructure of zinc oxide varistors has been described as consisting of functional (effective) and non-functional phases [19].

The functional phases are those that are considered to have a direct influence on the electrical properties. These are doped ZnO grains; three-dimensional network of bismuth rich phases lying along the multiple grain junctions and interfaces between ZnO grains. The non-functional phases are considered not to directly contribute to the electrical properties of the varistor; these are the spinel secondary phases. A third "non-constituent" in the microstructure that has received least attention in the literature is porosity, some discussion has been reserved on its influence on energy capability and capacitance [19,69].

Multiple dopants such as a combination of antimony, cobalt, manganese and silicon oxides are added to produce greater nonlinearity than the single dopant. It is well recognized that the basic building block of the ZnO varistor is the ZnO grain formed as a result of sintering process, and that the nonlinear varistor behavior is a grain boundaries effect. During sintering, various chemical elements are distributed in such a way in the microstructure that the near grain boundary region becomes highly resistive phase, and the grain

interior becomes highly conductive. A sharp drop in resistivity from grain boundaries to ZnO grains occurs which known as the depletion layer [14,29].

At each grain boundary, there exists a depletion layer on both sides of the grain boundary extending into the adjacent grains. The varistor action arises as a result of the presence of this depletion layer within the grains [19].

Additionally, the presence of two depletion layers on both sides of the grain boundary makes the ZnO varistor insensitive to polarity changes; therefore, the varistor appears as a back-to-back diode. Furthermore, since the region near the grain boundary is depleted of electrons, a potential gradient appears across the grain boundary upon application of an external voltage. This is known as the barrier voltage, V_{gb} and typically is of the order of 3.2 Volt per grain boundary and is composed of a resistive R and a capacitive C component. The number of grains in series between the electrodes determines the overall voltage of the varistor device [14,19].

The microstructure of ZnO varistors essentially consists of the conductive grains and the insulating grain boundaries giving rise to the double Schottky barrier model. The electrical properties of ZnO varistors are interpreted as due to potential barriers formed at the grain boundaries of the varistors bulk. It is considered that the junction between two semiconducting ZnO grains ($n-type$ semiconductor) behaves as a $p-type$ semiconductor. Therefore the process of charge transfer between the grains and the interface takes place [55,56].

Schottky barrier model was originally derived to explain the rectifying properties of metal-semiconductor contacts; the metal attracted the conduction electrons in the semiconductor close to the contact. This creates a depletion region in the semiconductor and this causes a band bending of the valence and conduction bands [54].

Double Schottky barrier model is based on the assumption that localized interface states of acceptor type are localized in the grain boundary in a similar way as the metal induced gap states are formed in the metal-semiconductor contact. Interface states act as traps for the conduction electrons in the neighborhoods of the grain boundaries; this creates a depletion region on both sides of the grain boundary as explained in figure (2.15). The depletion region leads to a Schottky barrier on each side of the grain boundary [54].

As a consequence of this process, donors in the grains nearby the interface are ionized, giving electrons to the interface states, which also become ionized. The region near the junction is depleted of charges, and therefore, a potential barrier appears. Since two opposite Schottky type barriers are formed, this is also called the double Schottky barrier [48,55].

In other words, the microstructure of ZnO varistors consists of highly conductive $n-type$ ZnO grains and electrically insulating grain boundaries therefore double Schottky barrier will be formed between them [28].

As indicated in Figure (2.15), double Schottky barriers are generated when majority carriers are trapped at interface states formed at grain boundaries. When the concentration of additives in layer A is not equal to that in layer B, the difference in the Fermi levels gives rise to an electrical potential barrier across the ZnO grain boundaries at zero bias [48].

Amorphous Bi-rich phase is found primarily in the grain junctions, especially at the ZnO-ZnO interfaces and it affects Schottky barriers [55].

Last, Schottky barrier at each interface can explains the non-Ohmic properties (nonlinearity properties) of ZnO varistor, the temperature dependence of the current voltage curve, effect of additives, and dielectric properties [19,55].

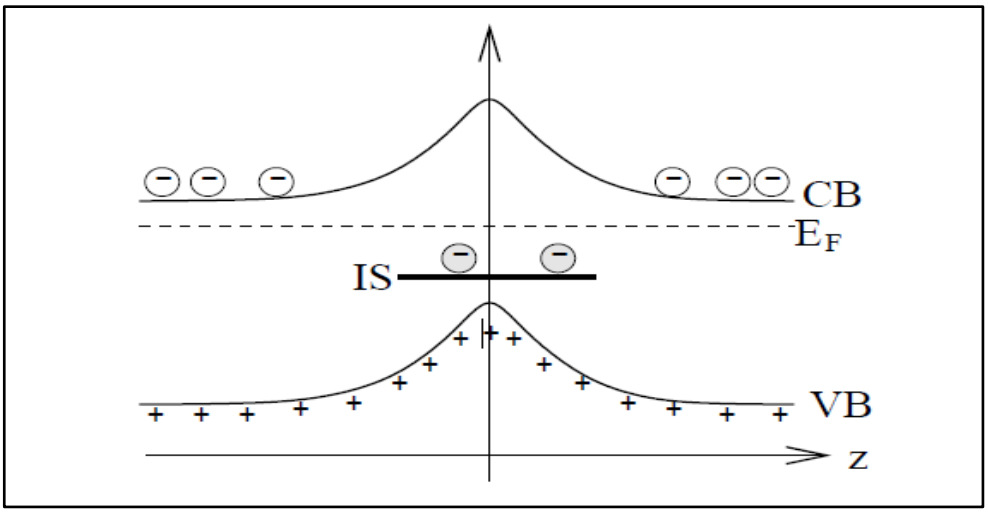

Fig (2.15). Grain boundary, double Schottky barrier in ZnO varistor. The localized Interface state is indicated by IS [54].

2.10.2. Potential Barriers At Grain Boundaries

The high resistivity in the closeness of grain boundaries in ZnO varistors is a consequence of potential barriers in that region. To some degree, such potential barriers of grain boundaries always exist in polycrystalline semiconductors, since the potentials of grain boundary regions are shifted from the bulk value by the deficiency of perfect periodicity. A more pronounced change of the potential can be created by vacancies, impurities, or other phases in the boundaries [12,21].

2.10.3. Breakdown Voltage

The voltage at which the onset of nonlinearity occurs and it means that the device changes from insulating regime to conducting regime. It is conventionally defined as the voltage under which the device passes 0.5 mA of current and is designated as $V_{0.5}$. In practice, the steady-state voltage of circuit is set at a certain percentage of the breakdown voltage; generally in power applications it is set at (70 to 80%) of $V_{0.5\ mA}$, as shown in equation (2.12) [14,21].

$$V_b = 0.8\, V_{05\ mA} \ldots\ldots\ldots\ldots\ldots\ldots\ldots\ldots\ldots\ldots\ldots\ldots (2-12)$$

The breakdown voltage is associated with the number of ZnO insulator boundaries within the device. The higher the value of $E_{0.5}$, is the smaller the device for a given protection level. In this respect, a high $E_{0.5}$ value can leads to fabricate miniaturized varistors for electronic applications or to reduce the size of the power surge varistor. It will be advantageous to increase the breakdown voltage without losing the other electrical properties [18,21].

2.10.4. The Leakage Current

It is the current which passes through the device in the pre-breakdown region. Ideally, a varistor should have no leakage current; it means that the device should be an ideal insulator in the fields below the breakdown field. However, an ideal varistor does not exist and all varistors exhibit a small current in this region which increases with the applied voltage [35,70].

The leakage current is measured as:

$$I_L = 0.75\, V_{0.1mA} \quad \ldots\ldots\ldots\ldots\ldots\ldots\ldots\ldots\ldots\ldots\ldots\ldots (2\text{-}13)$$

Or

$I_L = 0.80\ V_{0.1mA}$ ……... (2-14)

If the leakage current is high, the device will lose electrical energy during steady state operation. Besides, the high leakage current can lead to heat the device and to affect the other electrical properties. If the generated heat due to leakage current is not transferred to the outside environment, it may cause a thermally run away of the device. Therefore, the tendency of the manufacturers is to reduce the leakage current to as small levels as possible [14,70].

The Leakage current after time (t) minutes can be calculated from the following equation:

$I_L = I_{L0} + K_T\ t^{1/2}$ …….. (2-15)

Where I_L the current after time (t), I_{L0} the leakage current at (t=0) , K_T degradation rate coefficient [70].

2.10.5. Energy Absorption Capability

The ability of varistor for absorbing transient energy and handle it, since varistors are supposed to limit the transient voltage surges repeatedly without being destroyed. Therefore one of the cases where the device can be destroyed is when a high current passes through the device within a relatively long time, if the device is not able to handle the applied energy, it wiI1 be destroyed. Therefore, the absorption energy represents one of the critical parameters in the characterization of varistors. The higher the energy absorption, the more performance has the device [38,46].

$E = VIt$ … … …

2.10.6. The Average Grain Size

The average grain size *(d)* can be determined by the lineal (linear) intercept method from the scanning electron microscopy images (SEM), given by the following equation:

$$d = 1.56\ L/MN \ldots\ldots\ldots\ldots\ldots\ldots\ldots\ldots\ldots\ldots\ldots\ldots\ldots\ldots (2-20)$$

Where (*L)* is the random line length on the micrograph, (*M)* is the magnification of the micrograph, and *N* is the number of the grain boundaries intercepted by the lines [70,71].

Or from the X-Ray diffraction data by using Scherer equation as following:

$$d = \frac{K\,\lambda}{\beta(2\theta)cos\theta} \ldots\ldots\ldots\ldots\ldots\ldots\ldots\ldots\ldots\ldots\ldots\ldots\ldots (2-21)$$

Where (d) is the grain size, (K) is a constant, (λ) is the wavelength of the incident X-ray beam, β full width at half maximum FWHM (radians), θ Bragg angle (peak position) [72,73].

The voltage per grain boundary (V_{gb}) can be calculated from the following equation[74]:

$$V_{gb} = V_b \left(\frac{d}{D}\right) \ldots\ldots\ldots\ldots\ldots\ldots\ldots\ldots\ldots\ldots\ldots\ldots\ldots\ldots (2-22)$$

Where (V_b) the breakdown voltage, (d) represents the average grain size, and (*D*) is the thickness of the varistor [74].

2.10.7. Clamping Ratio

Clamping ratio (efficiency) is a very important parameter which defined as the ratio of voltages in the non-linear region. This parameter affirms the ability of a varistor to limit the transient voltage and the level of protection; it can be calculated as follows [19,46,70]:

Clamping ratio (clamping voltage) can be calculated from the following equation:

$$C_r = \frac{V_2}{V_1} \ldots\ldots\ldots\ldots\ldots\ldots\ldots\ldots\ldots\ldots (2\text{-}23)$$

Threshold voltage has often been described in some literature as the voltage observed at (0.1 mA) ($V_{0.1\ mA}$). Other authors have used the voltage at (1 mA) ($V_{1\ mA}$) as the reference voltage. The more (C_r) is near (1), the better the varistor protects [19,70].

2.11. Conductivity Mechanism

Breaking up the crystal lattice and rotating one part with respect to the rest of it, forms a so called grain boundary where the two crystals orientations meet. This breaking of the crystal symmetry creates a potential barrier for the electrons on the both sides of the grain boundary. The potential barrier has the same effects as a mountain to a human being. It is possible for the electrons to pass the grain boundary, but it takes an effort similar to that of scaling a high peak. The barrier at the grain boundary limits the number of electrons which are able to pass [54].

2.12. Roles Of Doping

Pure ZnO has exceptional current-voltage properties but not be able to produce varistor effect without dopants [**56**].

Without dopants it's a non-stoichiometric $n-type$ semiconductor with a linear or Ohmic behavior. To produce a nonlinear material, various metal oxides have to be incorporated into the ZnO. These oxides are added to control one or more of the properties such as the electrical properties (breakdown voltage, nonlinearity and leakage current), grain growth or sintering temperature [14].

The varistor functionality largely depends on the chemical compositions and density of the grain boundaries. With very large grain sizes the effective number of grain boundaries is reduced and with very low impurity content the varistor may show more linear current voltage behavior which is not accepted for a surge-arrestor [56].

As mentioned above Bi_2O_3 is molten above 825℃, assisting in the initial densification of the polycrystalline ceramic. This polycrystallinity is the key to varistor action in ZnO. The addition of Bi_2O_3 has been found to be the most essential component for forming non-Ohmic behavior. However, addition of transition oxides such as Co_3O_4 and MnO_2 also improve and

enhance the nonlinearity characters. Similarly, multiple dopants such as a combination of Bi_2O_3, Sb_2O_3, MnO_2, Co_3O_4, Cr_2O_3 and other oxides can produce greater nonlinearity than a single dopant [14,56].

Foreign atoms in the crystal structure influence the properties of the material because they change the local environment for the electrons. If there is a foreign atom that occupies one of the sites in the lattice, this atom is called an impurity atom but if the impurity atom has been introduced in the material for specific purposes, it is called a dopant [54].

Dopants are divided into three basic groups according to the functional applications, as follows:

1- Those that participate in the formation of the basic microstructure of ZnO varistors in sintering provide for the formation of inter-granular layers; Bi_2O_3 is one such dopant.
2- Those used in ensuring the non-linearity of the varistor ceramic promote the creation of deep charge carrier traps and cause the formation of the surface potential of the grains; Co_3O_4 and MnO_2 are such dopants.
3- Those that stabilize inter-granular layers under electrical loads and external environmental factors (temperature and humidity) and increase the stability of the electrical properties and reliability of the varistors; Sb_2O_3 is one such dopant [52,71].

2.12.1. Effect Of Bi_2O_3

Bismuth oxide (Bi_2O_3) is one of the most important additives in varistors, whereas the interaction between Bi_2O_3 and ZnO in varistors is believed to be important for the I-V properties. The Bi atoms are observed to be highly concentrated to the grain boundary regions in the varistor materials, whereas a large fraction is found in the form of Bi_2O_3 phases located in the triple junctions. The Bi-atoms also appears in the grain boundaries either as more or less amorphous Bi_2O_3-phases which coat the ZnO grains or as individual atoms decorating the grain boundary [54].

Bi_2O_3 concentration inside the ZnO grains is very low and it also seems as Zn concentration in the phase at the triple junctions is fairly low [75].

The Bi_2O_3-phases that cover the ZnO grains could then be the host of the acceptor states which are responsible for the formation of the double Schottky barrier in Bi-doped ZnO varistors[[54].

Bi_2O_3 is an essential additive of ZnO varistors because it has melting point that is far lower than that of ZnO and other additives, and thus exists in liquid phase in a relatively low temperature, which promotes other oxide to be distributed evenly in the ZnO grains and grain boundary [23,9].

When cooled down, Bi_2O_3 can't be found in the ZnO grains but separate in the grain boundary for the Bi^{3+} ion which has a much bigger diameter (1.10×10^{-10} m) than that of the Zn^{2+} ions (0.74×10^{-10} m) [9].

This will cause all additives separating together in the grain boundary to form a very thin interface that has a very high level of grain-boundary potential barrier and thus increase the nonlinear coefficient of ZnO varistors and the capacity of permitted accessing current consequently [23].

The sintering temperature has essential effect on the electrical properties of ZnO varistors. But if the temperature is too high, many of the Bi atoms will volatilize, and thus bring about many air pores in ZnO varistor to deteriorate the structural uniformity so as to affect its electrical properties. On the other hand, since that phase is relevant to the materials leakage current I_L and the nonlinear coefficient (φ), with the increase of the sintering temperature, the electric field strength of the low-voltage ZnO varistor E_{1mA} will decrease, while (I_L)will increase and (φ)will decrease. Generally, the appropriate sintering temperature for low-voltage ZnO varistor ceramics should not be more than (1250℃) [9].

Bi_2O_3-based ZnO varistors show good nonlinear properties, where Bi_2O_3 easily reacts with some metals used in preparing multilayer chip nonlinear varistors and it destroys the multilayer structure [75].

2.12.2. Effect Of Sb_2O_3

Besides Bi_2O_3, Sb_2O_3 also plays important roles in varistor functionality. This dopant creates a pyrochlore phase ($Zn_2Bi_3Sb_3O_{14}$) with the other two constituents at very low temperature (~600℃) which later decomposes into a spinel phase ($Zn_7Sb_2O_{12}$) above (900℃) by reacting with ZnO. The growth of ZnO grains has found to be inhibited by spinel grains which act as anchor (pinning) points and ceases the grain boundary migration of ZnO. The pyrochlore phase also has an inhibiting effect on the ZnO grain growth [27,56].

In other words, the $Zn_7Sb_2O_{12}$ particles at the grain boundaries hinder the ion transfer which results in suppression of grain growth. Small grain sizes

further improve the nonlinear property. Furthermore, the I-V properties become stable against electrical stresses. This is important in the practical applications of these materials [54,56].

Effects of Sb_2O_3 on densification of pure ZnO is that the densification temperature is higher than that of pure ZnO, where when Sb_2O_3 is added, this was explained by the volatile nature of Sb_2O_3 so that Sb_2O_3 evaporates during oxidation at about 500°C and condenses on ZnO particle surfaces as a non-crystalline phase with an unknown composition. This hinders the materials transport across ZnO particles and thereby retards densification [27,56].

2.13. Grain Growth Inhibition

Dopants may have an indirect effect on grain growth by increasing diffusivity, and consequently, reducing the sintering time. When a doped compact is exposed to high temperature for a short time grain growth is inhibited. Dopants may also have a direct effect on grain growth suppression by pinning grain boundaries. This occurs when the dopant concentration is larger than the solubility limit. In this case, the excess of dopant results in the formation of a second phase at grain boundaries [18].

Depending on the nature of this second phase, it may have different effects on grain growth suppression.

1- When a stable phase with high melting point forms, it will preferentially crystalize at grain boundaries rather than in the grain interior because by this way, it reduces total gain boundary area, reducing the total energy of the system. The precipitated phase will pin grain boundaries and prevent gain boundary motion. In this case, the amount, morphology, and dispersion of the second phase at grain boundaries determine its efficiency on grain growth suppression [18,66].

2- An excess of dopant may lead to the formation of an eutectic phase with low melting point. At the sintering temperature, this phase melts and forms a continuous liquid film wetting most gain boundaries. The presence of a liquid phase cm control and homogenize gain boundary diffusion and prevent exaggerated or abnormal grain growth and, on the other hand, it may accelerate diffusion and sintering processes [14,18].

2.14. Effect of MnO_2, Co_3O_4 , and Cr_2O_3

The presence of Bi_2O_3 is essential for the varistor effect, but without the other components only very low α values are obtained. Bi_2O_3 forms a thin layer around the ZnO grains and is also incorporated in the ZnO grain surfaces, causing atomic defects to form at the ZnO–ZnO grain boundaries. Some other additives, such as Cr_2O_3, Co_3O_4 and MnO_2 and combinations of them, enhance the nonlinearity. All these additive oxides also have a more or less strong influence on the sintering behavior and on the final microstructure, the grain sizes in a varistor, mainly controlled by spinel and pyrochlore formation. Those oxides used in ensuring the nonlinearity of the varistor ceramic promote the creation of deep charge carrier traps and cause the formation of the surface potential of the [52,45,71].

The incorporation facilitates the liquid phase of MnO_2 ,and as a result facilitates Bi_2O_3 liquid phase formation to improve the nonlinear properties of the varistor by increasing nonlinear coefficient [55].

2.15. Rare Earth Oxides

The rare earth elements, which include the 15 lanthanide elements (Z = 57 through 71) and yttrium (Z = 39), are so called because most of them were originally isolated in the 18^{th} and 19^{th} centuries as oxides from rare minerals. Because of their reactivity, the rare earth elements were found to be difficult to refine to pure metal [76,77].

The lanthanide elements traditionally have been divided into two groups: the light rare earth elements (LREEs) - lanthanum through europium (Z = 57 through 63); and the heavy rare earth elements (HREEs) - gadolinium through lutetium (Z = 64 through 71). Although yttrium is the lightest REEs, it is usually grouped with the HREEs to which it is chemically and physically similar [76,77].

The electrical properties of ZnO varistors are greatly improved with small amounts of rare earth dopants, but severely deteriorated when excessive amounts of rare-earth dopants are added [39,78].

The rare-earth dopants can also greatly improve I_L and φ. Small grain size and good grain boundary barrier are helpful to increase the single grain/grain boundary voltage and improve the electrical stability of ZnO varistors, improve the homogenization of the size of the grains in material, and grain growth inhibitor [52,68,79].

Doping with rare earth oxides appears to be promising for the preparation of ZnO-based varistors with a high breakdown voltage and also high energy-absorption capacity. This can be a successful step because our objective is to have smaller and lighter surge arresters in power network. This aim involves such varistors, which have high conduction threshold voltage, while their energy absorption capacity remains enough high [52].

The addition of rare-earth oxides in the starting composition decreases the average grain size, and doping with rare earth oxides would affect the formation and decomposition of the $Bi_3Zn_2Sb_3O_{14}$ pyrochlore phase, which promotes the generation of the new phases. In the meantime, doping with rare earth oxides would affect the time that the varistor ceramics spend in the liquid phase, and as this process becomes longer [35].

In other words, rare earth oxides are commonly added to control the grain growth of ZnO through the presence of the spinel phase at the grain boundaries of ZnO [25].

The rare earth dopants have an effect on the low current region of varistors and determine the breakdown voltage. The rare-earth doping could significantly improve the voltage gradient, as well as the leakage current and the nonlinearity exponent [68].

Because the diameter of rare-earth element cation is large than Zn^{2+} cation, the rare-earth additive cannot be melted into ZnO grains during the sintering process, and can only exist at grain boundaries [24].

There are new types of spinel secondary phase formation of Bi-Zn-Sb-R-O existing in ZnO varistor doped with rare-earth oxide, and the rare earth element did not exist in Bi_2O_3-rich phase [24].

2.16. XRD Testing:

XRD testing depending on Bragg's law as explained in the following:
An X-ray which reflects from the surface of a substance has travelled less distance than an X-ray reflects from a plane of atoms inside the crystal. The penetrating X-ray travels down to the internal layer, reflects, and travels back over the same distance before being back at the surface. The distance travelled depends on the separation of the layers and the angle at which the X-ray entered the material. For this wave to be in phase with the wave reflected from the surface it needs to have travelled a whole (integer) number of wavelengths

inside the material. Bragg expressed this in an equation now known as Braggs Law [80]:

$n\lambda = 2dsin\theta$……(2-24)

λ is the wavelength of the incident X-ray beam, d the spacing of the crystal layers (path difference), θ the incident angle (the angle between the incident ray and the scatter plane), n an integer [80].As shown in the following figure:

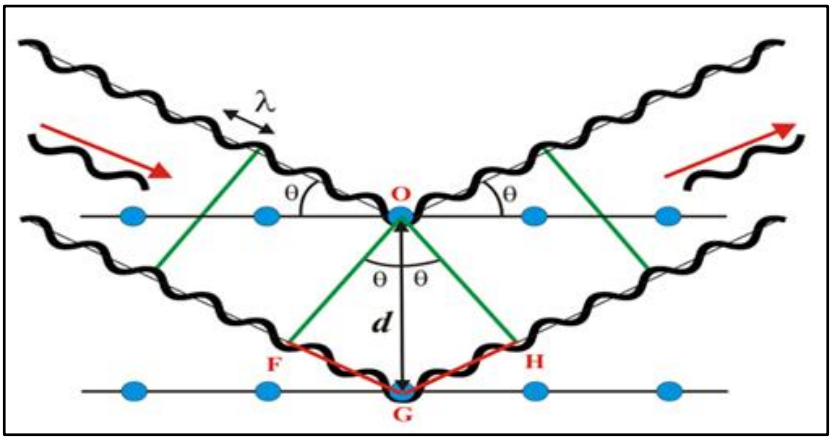

Fig (2.16). Diffraction of X-rays from a set of planes[80].

SAMPLES PREPARATION

Varistors samples were fabricated by the conventional ceramic fabrication procedure as explained in the following sections.

3.1. Weighing:

This process has been accomplished by using four digit balance (Sartorius M-Power Analytical Balance 210g, German). The samples prepared using appropriate oxides which includes ZnO (>99%, Fluka, Switzerland), Bi_2O_3 (99.5%, Himedia, India), Sb_2O_3 (99%, Himedia, India), Co_3O_4 (99%, Fluka, Switzerland), Cr_2O_3 (99%, Himedia, India), MnO_2 (99%, Himedia, India), Dy_2O_3 (99%, Fluka, Switzerland), La_2O_3 (99%, Fluka, Switzerland), and Y_2O_3 (99%, Fluka, Switzerland), the details of samples compositions are explained in Table (3.1).

Table (3.1).The details of samples compositions.

Type	Sample Composition (molar fraction)	REO	ST ℃	
Sample 1	ZnO pure	ZERO	1050	
Sample 2	ZnO pure	ZERO	1100	
Sample 3	ZnO pure	ZERO	1150	
Sample 4	95.5% ZnO, 0.5% Bi_2O_3, 2.5% Sb_2O_3, 0.5% Co_3O_4, 0.5% Cr_2O_3, 0.5% MnO_2	ZERO	1050	
Sample 5	95.5% ZnO, 0.5% Bi_2O_3, 2.5% Sb_2O_3, 0.5% Co_3O_4, 0.5% Cr_2O_3, 0.5% MnO_2	ZERO	1100	
Sample 6	95.5% ZnO, 0.5% Bi_2O_3, 2.5% Sb_2O_3, 0.5% Co_3O_4, 0.5% Cr_2O_3, 0.5% MnO_2	ZERO	1150	
Sample 7	(95.5-R)% ZnO, 0.5% Bi_2O_3, 2.5% Sb_2O_3, 0.5% Co_3O_4, 0.5% Cr_2O_3, 0.5% MnO_2+10^{-3} %R	10^{-3}	1050	R=(Dy_2O_3, La_2O_3, Y_2O_3)
Sample 8	(95.5-R)% ZnO, 0.5% Bi_2O_3, 2.5% Sb_2O_3, 0.5% Co_3O_4, 0.5% Cr_2O_3, 0.5% MnO_2+10^{-3} %R	10^{-3}	1100	R=(Dy_2O_3, La_2O_3, Y_2O_3)

Type	Sample Composition (molar fraction)	REO	ST ℃	
Sample 9	(95.5-R)% ZnO, 0.5% Bi_2O_3, 2.5% Sb_2O_3, 0.5% Co_3O_4, 0.5% Cr_2O_3, 0.5% MnO_2+10^{-3} %R	10^{-3}	1150	R=(Dy_2O_3 , La_2O_3, Y_2O_3)
Sample 10	(95.5-R)% ZnO, 0.5% Bi_2O_3, 2.5% Sb_2O_3, 0.5% Co_3O_4, 0.5% Cr_2O_3, 0.5% MnO_2+$5*10^{-3}$%R	$5*10^{-3}$	1050	R=(Dy_2O_3 , La_2O_3, Y_2O_3)
Sample 11	(95.5-R)% ZnO, 0.5% Bi_2O_3, 2.5% Sb_2O_3, 0.5% Co_3O_4, 0.5% Cr_2O_3, 0.5% MnO_2+$5*10^{-3}$%R	$5*10^{-3}$	1100	R=(Dy_2O_3 , La_2O_3, Y_2O_3)
Sample 12	(95.5-R)% ZnO, 0.5% Bi_2O_3, 2.5% Sb_2O_3, 0.5% Co_3O_4, 0.5% Cr_2O_3, 0.5% MnO_2+$5*10^{-3}$%R	$5*10^{-3}$	1150	R=(Dy_2O_3 , La_2O_3, Y_2O_3)
Sample 13	(95.5-R)% ZnO, 0.5% Bi_2O_3, 2.5% Sb_2O_3, 0.5% Co_3O_4, 0.5% Cr_2O_3, 0.5% MnO_2+$10*10^{-3}$%R	$10*10^{-3}$	1050	R=(Dy_2O_3 , La_2O_3, Y_2O_3)
Sample 14	(95.5-R)% ZnO, 0.5% Bi_2O_3, 2.5% Sb_2O_3, 0.5% Co_3O_4, 0.5% Cr_2O_3, 0.5% MnO_2+$10*10^{-3}$%R	$10*10^{-3}$	1100	R=(Dy_2O_3 , La_2O_3, Y_2O_3)
Sample 15	(95.5-R)% ZnO, 0.5% Bi_2O_3, 2.5% Sb_2O_3, 0.5% Co_3O_4, 0.5% Cr_2O_3, 0.5% MnO_2+$10*10^{-3}$%R	$10*10^{-3}$	1150	R=(Dy_2O_3 , La_2O_3, Y_2O_3)

3.2. Mixing

After weighing the raw powders of constituent oxides of the desired samples were mixed using a magnetic hotplate stirrer (LabTech Hotplate Stirrer LMS-1003 Specification Electronically controlled Stirring from 60 to 1500 rpm. Durable bearing type motor. Temperature range: ambient (+5℃) to (380℃) max. Power consumption max (500 watt), (3.0 amperes). Electric supply : (110 V 60 Hz or 220 V 50/ 60 Hz.) With (500) rounds per minute with magnetic bar in a glass container (dry mixing) for 24 hours to increase the homogeneity among the constituents of the samples.

3.3. Calcination

Calcination process accomplished to remove the gases and the humidity in the powders and this process accomplished In atmosphere at (600℃) for two hours and heating rate equals to (5 ℃/min) using ceramics crucibles in a muffle furnace (Carbolite, England, 1200℃).

After that the temperature of the furnace decreased in cooling rate equals to(5 ℃/min) and in the end the furnace turns off at (300℃).

Illustration (3.1). Powder calcination.

3.4. Remilling and Binder Adding

After calcination process, the powders are remiled using agate mortar and PVA binder added to the powders wt 3%, and the powders mixed again in glass containers using the same magnetic hotplate stirrer for two hours.

3.5. Pressing

The following step is pressing, whereas the powders uniaxially pressed into discs (pellets) of (14.5mm) in diameter and (2mm) in thickness under a pressure equals to (25MP) for (*2 minutes*) using a press made in (Mega company, Spain,15 tons), the green pellets are shown in Illustration (3.2).

Illustration (3.2). The results of the pressing process samples .

3.6. Sintering

After pressing the green pellets sintered under different temperatures to accomplish the final shapes and reach the desired properties of the samples, as explained in the following:

1- **First Sintering Temperature**: Which equals to(1050℃): This process applied on all samples for (2 hours), and the heating rate equals to (5 ℃/min), and finally the furnace turns off at (1050℃).
2- **Second Sintering Temperature**: Which equals to(1100℃): This process applied on all samples for (2 hours), and the heating rate equals to (5 ℃/min), and finally the furnace turns off at (1100℃).
3- **Third Sintering Temperature**: Which equals to(1150℃): This process applied on all samples for (2 hours), and the heating rate equals to (5 ℃/min), and finally the furnace turns off at (1150℃).

The samples produced from sintering process are shown in Illustration (3.3):

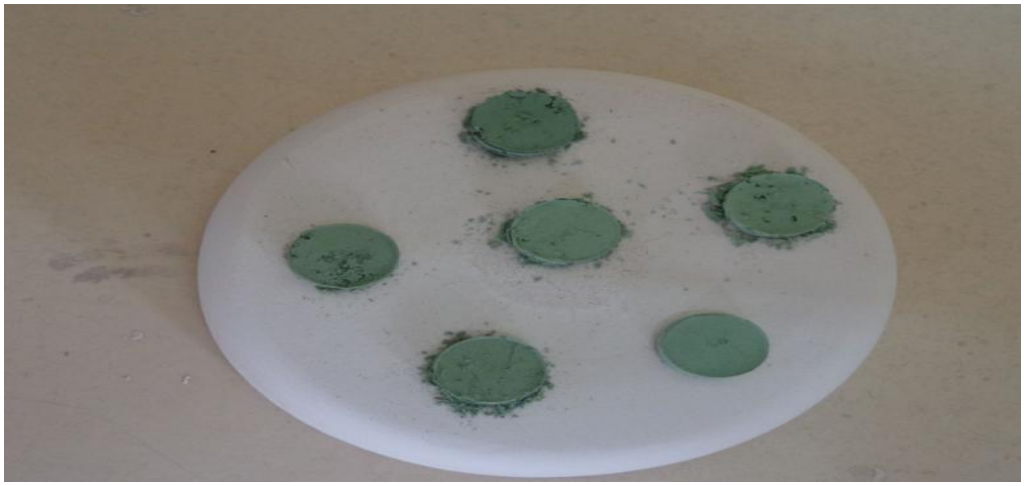

Illustration (3.3). The samples produced after sintering process.

3.7. Presintering:

Because of defects appear in the result of product of the samples after sintering process, these samples presintered under the same conditions of sintering process, to reach superior macro and mechanical properties. As shown in Illustration (3.4).

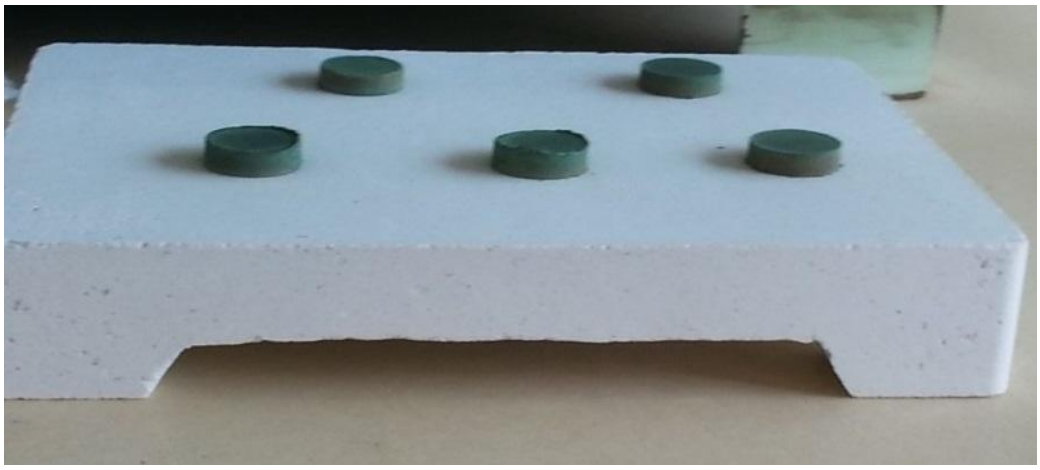

Illustration (3.4). The samples produced after presintering process.

3.8. XRD Testing:

The final samples result from Presintering performed to XRD testing to study, determine, and verification the crystal structure, lattice parameters of the samples and be assured of the phases of bulk varistor resulted from preparation processes.

In addition to measure the grain size from XRD data by using Scherer's equation.

The type of XRD source was Shimadzu XRD-6000 which of the following features ($Cu_{K\alpha}$, Voltage: 40kV, Current: 30mA, Wavelength:1.5406 Å, and the samples were scanned in a Continuous mode from $10^{\circ} - 80^{\circ}$).

We compared the data of XRD of the samples tests with the references and data basses.

3.9. Measurement Of Density:

The densities of sintered samples (pellets) were measured by using Archimedes Principle, mercury liquid used in this test, depending on the following relations[82,83]:

$$\rho = \frac{m}{V} \dots\dots\dots\dots\dots\dots\dots\dots\dots\dots\dots\dots\dots\dots\dots\dots\dots\dots (3-1)$$

Where ρ the density of the material, m the mass of the material and V the volume of the material.

Using the known density of mercury and the mass of the displaced mercury we can calculate the volume of mercury displaced by the sample (pellet)[82,83]:

$$V_{displaced\ \ liquid} = V_{sample} \dots\dots\dots\dots\dots\dots\dots\dots\dots\dots (3-2)$$

Therefore the density of the sample can be measured by applying the upper relations[82,83].

$$\rho = \frac{m}{V} \dots\dots\dots\dots\dots\dots\dots\dots\dots\dots\dots\dots\dots\dots\dots\dots\dots\dots (3-1)$$

Where ρ represents the density of the sample, m the mass of the sample in air and V the volume of the sample.

The relative density of the samples and the percentage value of the porosity measured by the following equations [84,85].

$$P\% = \left(1 - \frac{\rho_s}{\rho_{th}}\right) * 100 \ldots\ldots\ldots\ldots\ldots\ldots\ldots\ldots\ldots\ldots\ldots (3-4)$$

Where $P\%$ represents the percentage of the porosity, ρ_s the practical (measured) value of the samples density, and ρ_{th} the theoretical value of ZnO. Since zinc oxide (ZnO) is more than (90) percent of the constituent materials of the varistor, the theoretical density value of ZnO (which equals to $5.68\, gm/cm^3$) can be conveniently considered to be the theoretical density of varistor material [20,36,68].

3.10. Polishing

The aim of this process is to remove the increment parts or undesirable edges (which result because of the mold) from the coarse pellets (specimens) to achieve a smooth surface, and prepared the specimens to the next process (coating) and then to accomplish the SEM and electrical tests. Polishing process can be divided into three parts:

1- Polishing: this part has been done by using three degrees of emery papers (1000, 2000, and 3000 micron) respectively.
2- Cleaning: after polishing the specimens cleaned by using a solution (Hydrofluoric acid is a solution of hydrogen fluoride (HF) in water) consists of (90%) deionized water and (10%) HF to remove a thin layer from the pellet, and then washing by using deionized water.
3- Drying: it's the last step of polishing process at a temperature equals to (150℃) for (2) hours.

3.11. SEM Testing

The samples of ZnO varistors samples doped with rare earth oxides were examined by scanning electron microscopy (SEM) for three purposes, the first purpose is to correlate the microstructural results with the processing parameters grain size, sintering temperature, concentrations of REOs, with the electrical properties of the samples. The second purpose is to determine the composition of the samples at the grains, grain boundaries and triple points. And the third purpose is to investigate the influence of rare earth oxides concentration changes on the grain size of the samples which affect the electrical properties.

In SEM test the samples of ZnO varistor doped with the three oxides (Dy_2O_3, La_2O_3 and Y_2O_3) at (1150℃) sintering temperature and two

concentrations (10^{-3} and $5*10^{-3}$) were examined at different Magnifications power (16000, 20000, and 24000x).

The type source of SEM was S50 (Magnification: 13-1000000x, Resolution of 3.0 nm at 30 kV, Europe).

3.12. Electroding:

This process accomplished by using a thin film instrument to cover the two faces of the samples using aluminum element (under vacuum as a preparation step to the electrical tests), the electrode diameter equals to ($10mm$) on both faces leaving a small edge at the border.

3.13. Electrical Testing

This test includes the following measurements:

1- Non-linear coefficient.
2- Breakdown voltage.
3- The leakage current.
4- Energy absorption capability.
5- Voltage per grain boundary.
6- Clamping ratio.

These properties measured and accomplished by using An instrument Homemade, DC Power supplies are used for this purpose, the first (HIRANUMA EP-1500, Japan, $0-1500V, 50$ mA) and the other (PHYWE, 0-10 kV, 2mA), where the voltage changed manually during the tests, and two multimeters of type (Victor 88E digital multimeter, Taiwan), one used as a DC voltmeter (0.1mV-1000V) while the other used as DC micrometer (0.1 $\mu A - 20A$), as shown in illustration (3.5).

After connecting the samples to the circuit the test accomplished as following:

1- Non-linear coefficient:

a- Raising the current from the power supply step by step (manually), beginning of (zero mA- 0.1 mA) each step equals to 0.02mA until the current reach (0.1mA), and from (0.1mA to 1mA) each step

equals to (0.1mA), and at each step registration the values of the voltages opposite to the current values.

b- Calculate the non-linear coefficient value by using equation (2-11):

$$\varphi = \frac{\log I_2 - \log I_1}{\log V_2 - \log V_1} \dots\dots\dots\dots\dots\dots\dots\dots\dots\dots (2-11)$$

Where V_2,V_1 represent the voltage values at I_2=1mA, and I_1=0.1mA respectively, at the breakdown region.

2- Breakdown voltage:

a- As mentioned in the steps of number (1.a) above.

b- Registration the voltage value ($V_{0.5mA}$) which opposites to the current value equals to (0.5mA).

c- Finally calculate the break voltage value by using equation (2-12):

$$V_b = 0.8\, V_{0.5\,mA} \dots\dots\dots\dots\dots\dots\dots\dots\dots\dots\dots (2-12).$$

Where V_b represents the break down voltage, and $V_{0.5mA}$ the voltage opposite to the current pass through the sample equals to (0.5mA).

3- **The leakage current:**

a- As mentioned in the steps of number (1.a) above.

a- Measure the current value opposites to the voltage value of ($V_{0.1V}$).

b- Measure the leakage current of each samples by using equation (2-13):

$$I_L = 0.75\, I_{V_{0.1mA}} \dots\dots\dots\dots\dots\dots\dots\dots\dots\dots\dots\dots (2\text{-}13)$$

Where I_L represents leakage current value, $I_{V_{0.1mA}}$ the current value of ($V_{0.1V}$), and $V_{0.5mA}$ the voltage opposite to the current pass through the sample equals to (0.5mA).

4- Energy absorption capability:

a- As mentioned in the steps of number (1.a) above.

b- Calculate the constant (C) by using equation (2-5), the constant (β):

$$I = \left(\frac{V}{C}\right)^{\varphi} \dots\dots\dots\dots\dots\dots\dots\dots\dots\dots\dots (2-5)$$

Where (I,V) represent the current pass through the sample which equals to (1mA), and the opposite voltage value (V_{1mA}), (C) is a constant, and (φ) the non-linear coefficient, ($\beta = 1 / \varphi$).

c- Calculate the energy absorption capability by applying equation (2-19).

$$E = CI^{\beta+1}\, t \ldots\ldots\ldots\ldots\ldots\ldots\ldots\ldots\ldots\ldots\ldots\ldots\ldots\ldots\ldots\ldots (2-19)$$

Where E the energy absorption capability, and (t) the time.

5- Voltage per grain boundary.

a- As mentioned in the steps of number (1.a) above.

b- Using the data of the break down voltage to calculate the voltage per grain boundary by applying equation (2-22)

$$V_{gb} = V_b \left(\frac{d}{D}\right) \ldots\ldots\ldots\ldots\ldots\ldots\ldots\ldots\ldots\ldots\ldots\ldots\ldots\ldots\ldots\ldots (2-22)$$

Where (V_{gb}) represents the Voltage per grain boundary, (V_b) the breakdown voltage, (*d)* the average grain size, and (*D*) the thickness of the sample.

6- Clamping ratio:

a- As mentioned in the steps of number (1.a) above.

b- Calculate the Voltage per grain boundary by applying equation (2-23):

$$C_r = \frac{V_2}{V_1} \ldots\ldots\ldots\ldots\ldots\ldots\ldots\ldots\ldots\ldots\ldots\ldots\ldots\ldots\ldots\ldots (2\text{-}23)$$

Where (C_r) represents the Clamping ratio, (V_1) voltage observed at (0.1 mA) or ($V_{0.1\ mA}$), and (V2) the voltage at observed (1 mA) or($V_{1\ mA}$).

Illustration (3.5). Homemade instrument with PHYWE High voltage power supply.

RESULTS AND DISCUTION

4.1. XRD Results

The following figure explains the XRD results which shows the different phases of five samples, (a) pure ZnO, (b) ZnO + other oxides without rare earth oxides, (c) and ZnO + other oxides + rare earth oxides at concentration equals to (0.001) (Dy_2O_3, La_2O_3, and Y_2O_3) respectively, as shown in the following figure.

The samples was examined with XRD , where the XRD diffraction patterns demonstrate more accurate than others in determining the nature of phases formed as a result in the search, to be ensured of the phases of pure ZnO sample and other samples under test, this process accomplished after calcination at (600℃) and sintering at (1100℃), where figure(4.1.a) explains the compatibility of the data with ASTM cards for ZnO which has hexagonal phase, while figure (4.1.b) shows the effect of adding Bi_2O_3 and Sb_2O_3 on ZnO primary phase pattern, which shows appearance (rising) of Bi_2O_3 and Sb_2O_3 and spinal ($Zn_7Sb_2O_{12}$) phases, where these oxides affect (decrease) the intensities of the peaks of ZnO phase in addition to translate its crystal structure from hexagonal to orthorhombic.

While figure (4.1.c) illustrates the effect of ZnO doping with rare earth oxide, where the doping changed (decreased) the intensity of ZnO, Bi_2O_3 and Sb_2O_3 and spinal ($Zn_7Sb_2O_{12}$) phases, in addition to increasing sintering temperature may have reduced the intensity of these phases, as a result of evaporation (volatilization) in these temperatures. While the crystal structure had kept orthorhombic system with change of the grain size (increase and decrease) depending on the type of the rare earth oxide as described in section (4.2). The XRD data were used too to calculate the grain size using Shearer method.

The matching X-ray evidence to ASTM cards and also with some references to ensure data validity (36-1451), (27-0050), (43-0661), [14,34,35].

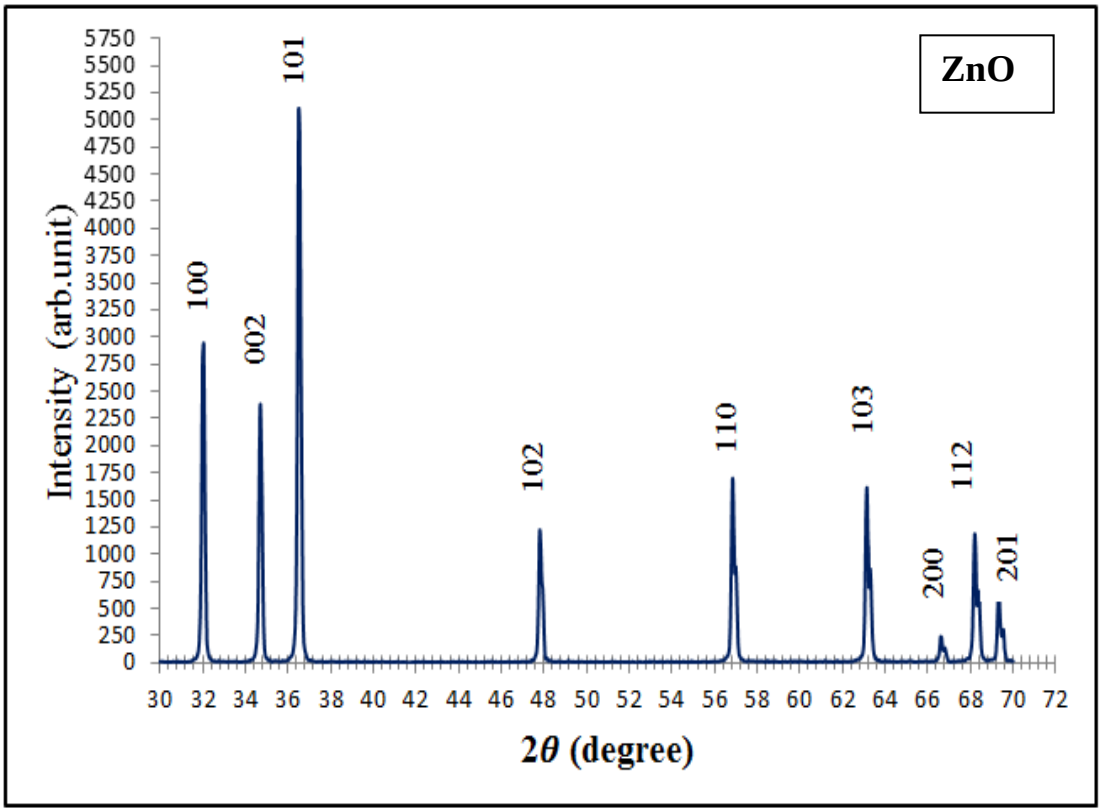
ZnO
Intensity (arb.unit)
2θ (degree)
100
002
101
102
110
103
200
112
201

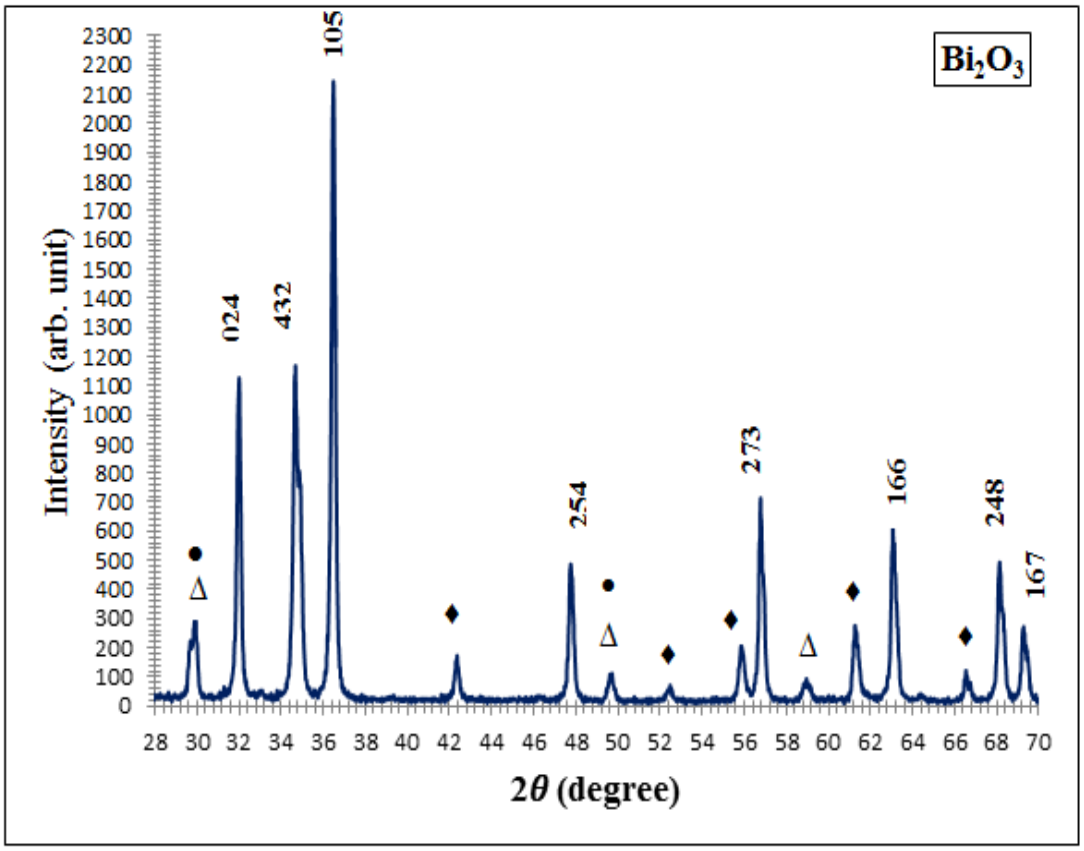
Bi2O3
Intensity (arb. unit)
2θ (degree)
024
432
105
254
273
166
248
167

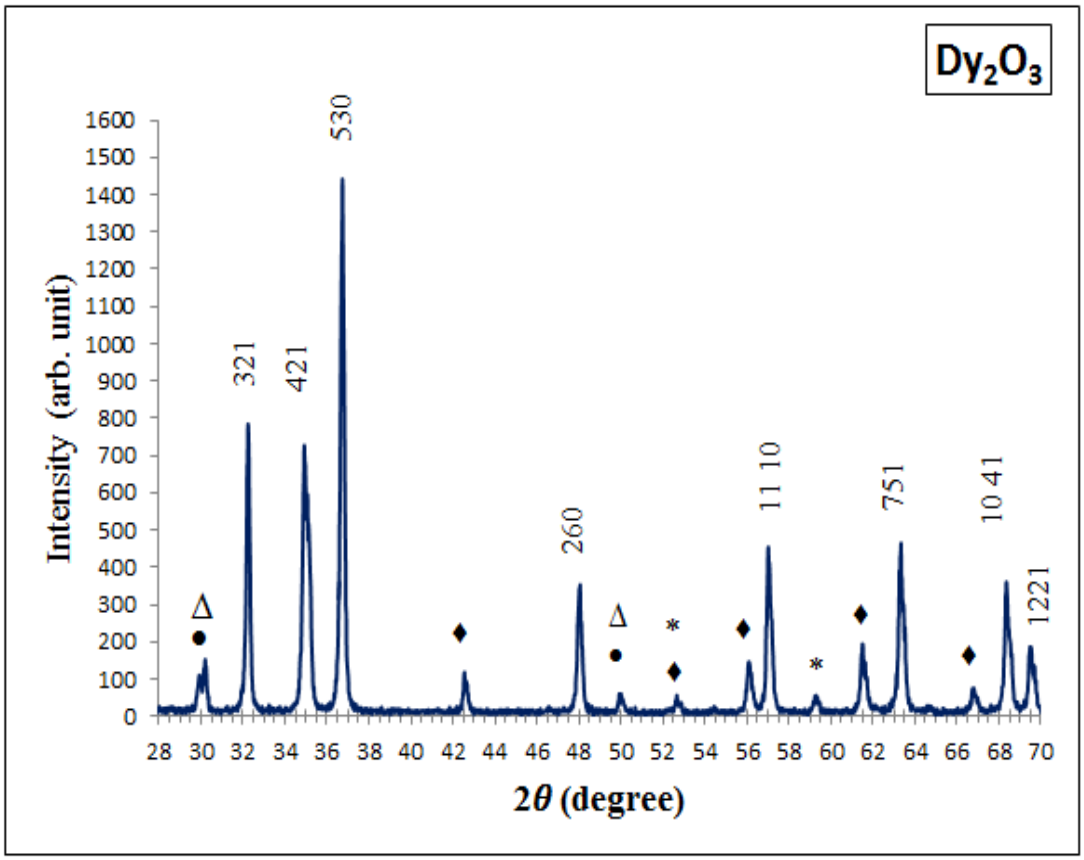
Dy2O3
Intensity (arb. unit)
2θ (degree)
321
421
530
260
11 10
751
10 41
1221

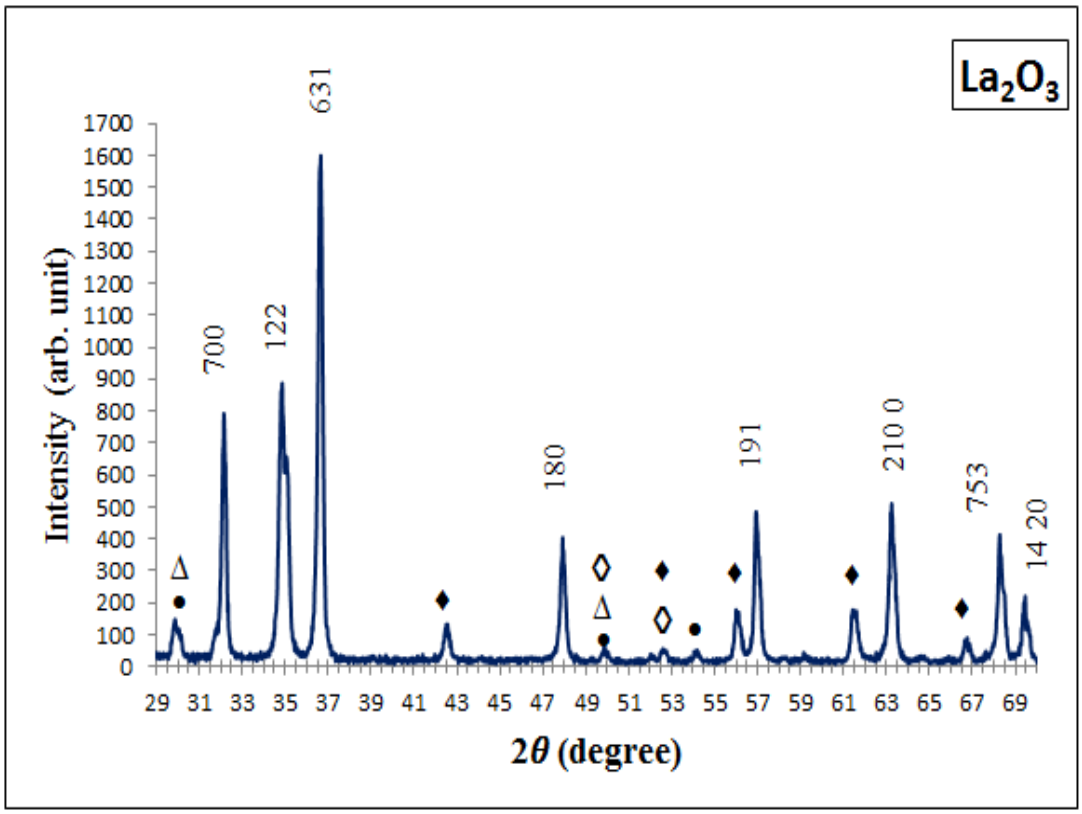
La2O3
Intensity (arb. unit)
2θ (degree)
700
122
631
180
191
210 0
753
14 20

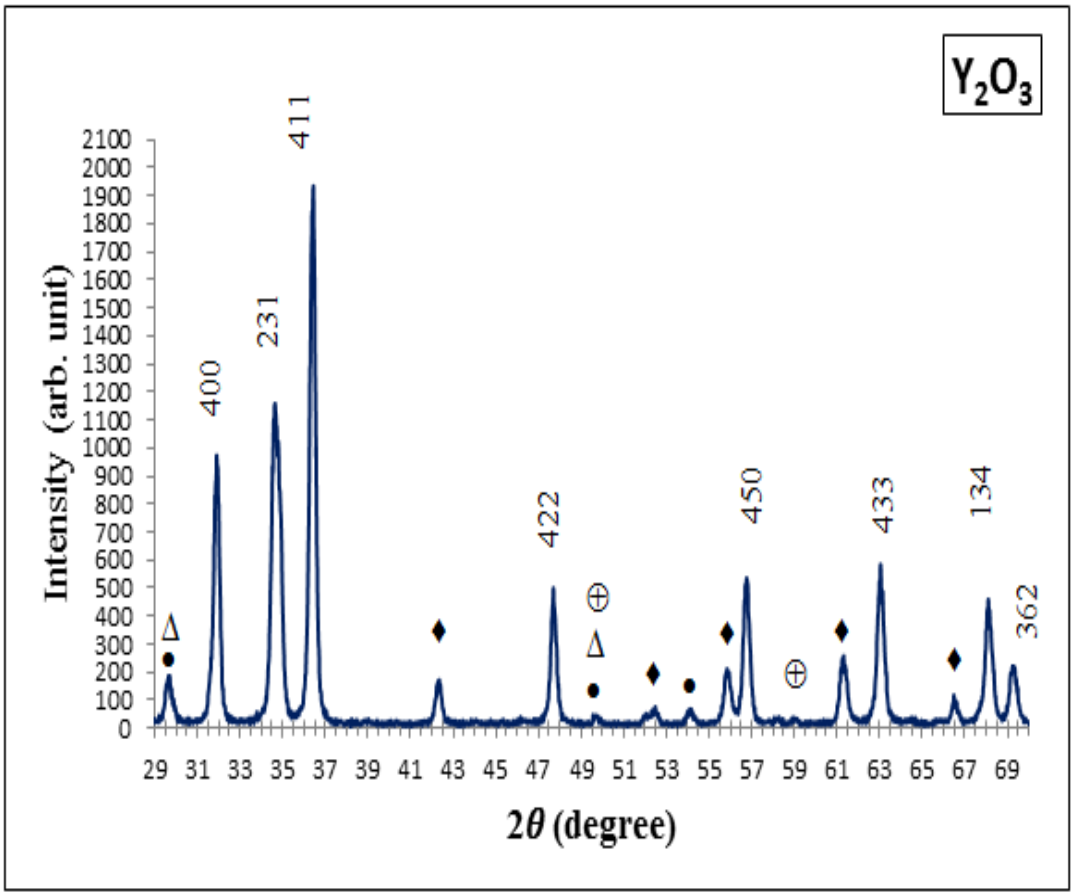

Fig (4.1). XRD of five samples of varistor, (a) ZnO pure, (b) ZnO with other oxides (without REO) where and (c) the samples doped with REO, where, • Bi_2O_3, Δ Sb_2O_3, ♦ $Zn_7Sb_2O_{12}$, * Dy_2O_3, ◊La_2O_3, and ⊕Y_2O_3 phases (from up to down respectively).

It must be observed that the X-ray diffraction peaks of the rare earth oxides are very weak, because of the small concentration of these oxides in the samples. But the effect of them on the electrical properties is obvious as explained in section (4.5).

4.2. Grain Size

The results of grain size measured are explained in table (4.1) and figures (4.2), which obtained using Scherer method from X-ray data, and linear intercept method from scanning electron microscopy images, at concentration equals to (10^{-3}) for all rare earth oxides.

The presented data in table (4.1) confirm the grain growth (increasing the grain size), which affected with three parameters:

1- Increasing of sintering temperature only (because we have the same sintering time for all samples therefor it doesn't affect the results), and this interpretation is compatible with the sintering process theory [57,58].
2- Doping by Bi_2O_3 because the radius of (Bi^{3+} 1.1nm) is larger the radius of Zn^{2+} (0.74nm) [9].
3- Doping by Dy_2O_3 and Y_2O_3 because the radius of (Dy^{3+} 0.89), and (Y^{3+} 0.91 nm) are larger the radius of Zn^{2+} (0.74nm) [68].

While the doping with La_2O_3 decreases the grain size of the sample [86].
In addition to the rapid evaporation (volatilization) of spinel phase ($Zn_7Sb_2O_{12}$) causes rapid increment in grain size [27,56].

Table (4.1).The values of grain size measured by using Scherer's method and SEM images.

No	Sample	Sintering Temperature (℃)	Grain Size (nm)	Method
1.	$Bi_2O_3$1	1050	41.5613	Scherer
2.	$Dy_2O_3$1	1050	44.1574	Scherer
3.	$La_2O_3$1	1050	29.9715	Scherer
4.	$Y_2O_3$1	1050	47.5688	Scherer
5.	ZnO	1100	45.8050	Scherer
6.	$Bi_2O_3$2	1100	50.4091	Scherer
7.	$Dy_2O_3$2	1100	51.5167	Scherer
8.	$La_2O_3$2	1100	47.1375	Scherer
9.	$Y_2O_3$2	1100	55.8724	Scherer
10.	$Dy_2O_3$3	1150	1305	SEM
11.	$La_2O_3$3	1150	1256	SEM
12.	$Y_2O_3$3	1150	1390	SEM

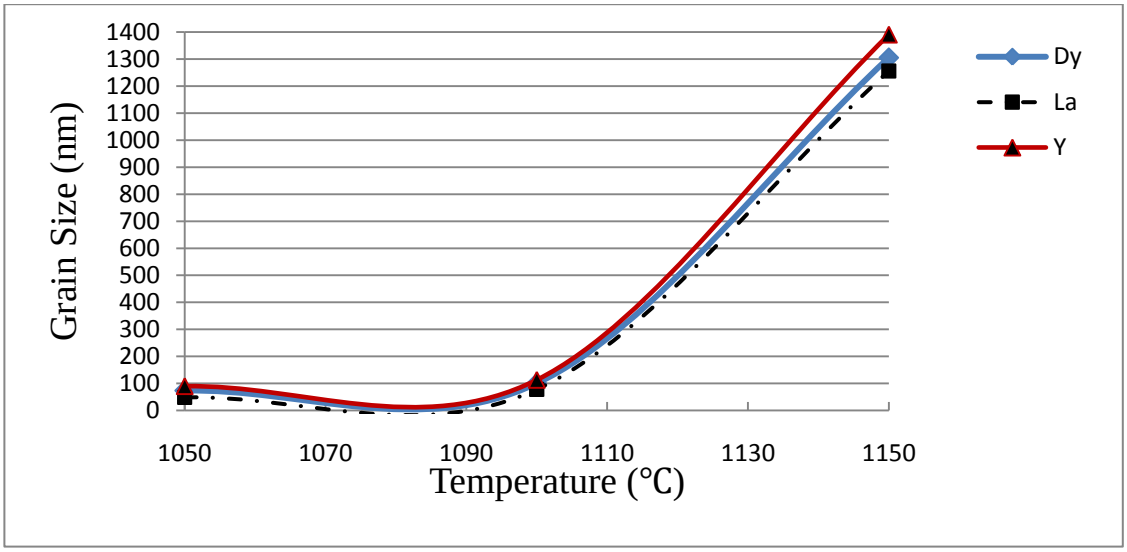

Fig (4.2). The grain size against sintering temperature, of samples doped with REO, where Dy, La, Y represents the samples doped with Dy_2O_3, La_2O_3, and Y_2O_3 respectively.

4.3. Microstructure

As mentioned in section (4.1) the existence of the additives translate the crystal structure of ZnO from hexagonal close packed to orthorhombic crystal system. The lattice parameters were measured from XRD test which confirm the grain growth (as explained in table (4.2)), therefor we can conclude and observe sintering temperature increase the lattice parameters, for example the lattice volume increases from (76.61 $Å^3$) at sintering temperature of (1050℃) to be (99.97 $Å^3$) at (1100℃). Furthermore the doping with rare earth oxides change lattice parameters too, where Dy_2O_3,and Y_2O_3 increases the lattice volume from (76.61 $Å^3$) to be (116 $Å^3$) and (95.59 $Å^3$) respectively, and that because the (Dy^{3+} 0.89), and (Y^{3+} 0.91 nm) are larger than the radius of Zn^{2+} (0.74nm) [68]. While the doping with La_2O_3 decreases the lattice volume from (76.61 $Å^3$) to be (75.81$Å^3$) [86].

From SEM images, we can observe the existence of ZnO grains, the grain boundaries, the triple points, and the porosities. In addition to the grain size measured from SEM confirms that the grain size at rare earth oxides concentration of ($5*10^{-3}$) is larger than the grain size of (10^{-3}).

Table (4.2). The crystal system parameters of samples doped with oxides . (where S.T and R.C mean sintering temperature and rare earth oxides concentration respectively).

Sample	a (Å)	b (Å)	c (Å)	System	Volume ($Å^3$)	S.T (℃)	R.C
$Bi_2O_3$1	10.42	2.82	2.60	Orthorhombic	76.61	1050	ZERO
$Bi_2O_3$2	6.83	5.20	2.80	Orthorhombic	99.97	1100	ZERO
$Dy_2O_3$1	10.28	4.04	2.77	Orthorhombic	116	1050	10^{-3}
$La_2O_3$1	10.4	2.80	2.59	Orthorhombic	75.81	1050	10^{-3}
$Y_2O_3$1	5.64	5.21	3.25	Orthorhombic	95.59	1050	10^{-3}
$Dy_2O_3$2	8.86	5.05	2.75	Orthorhombic	123.57	1100	$5*10^{-3}$
$La_2O_3$2	5.96	5.19	2.79	Orthorhombic	86.61	1100	$5*10^{-3}$
$Y_2O_3$2	7.6	6.33	3.36	Orthorhombic	163.98	1100	$5*10^{-3}$

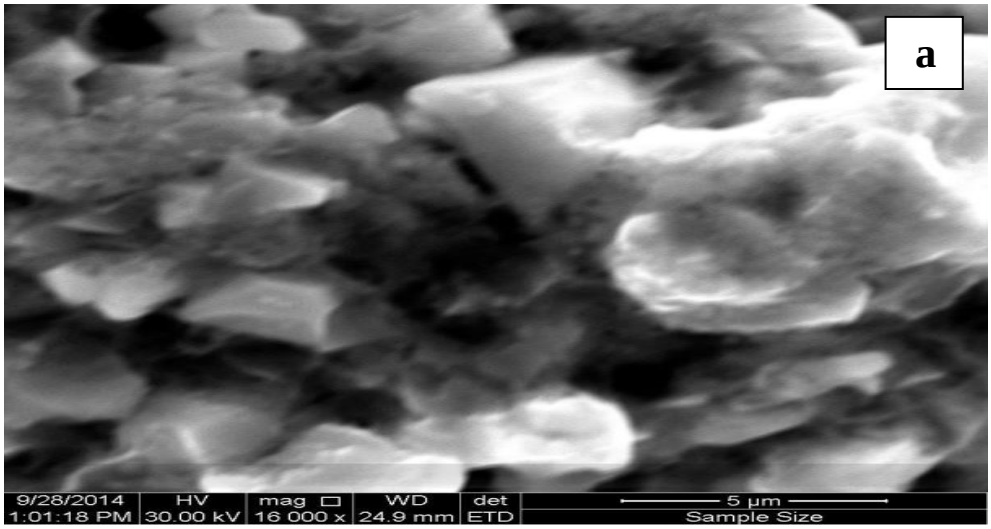

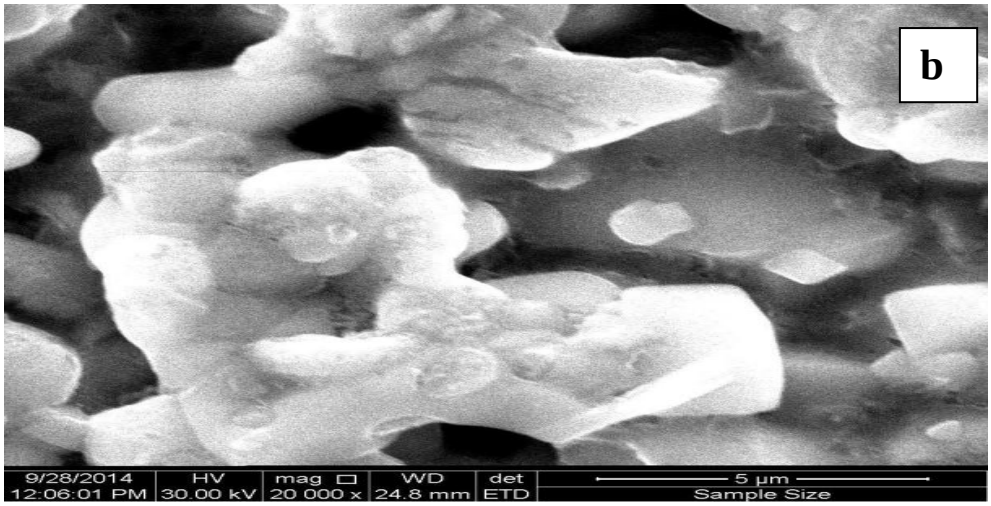

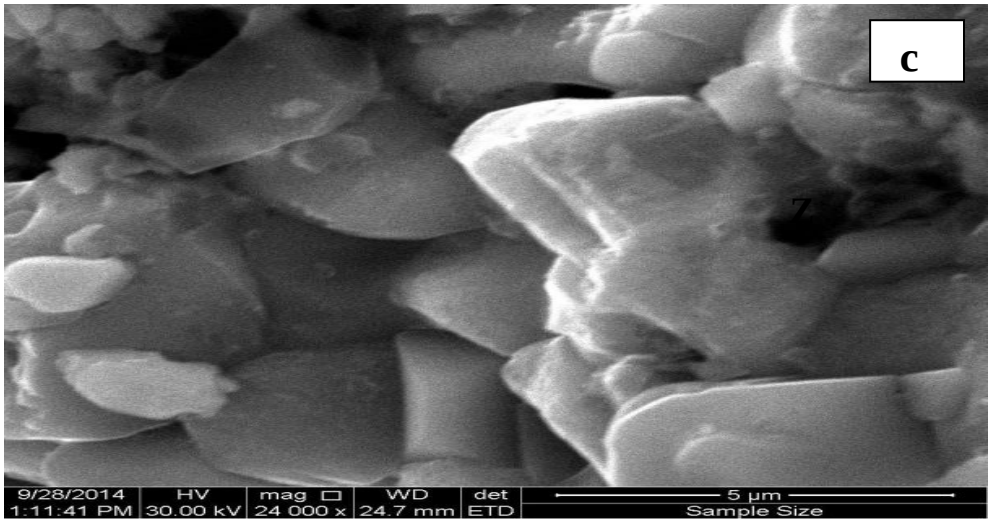
c
9/28/2014
1:11:41 PM
HV
30.00 kV
mag
24 000 x
WD
24.7 mm
det
ETD
5 µm
Sample Size

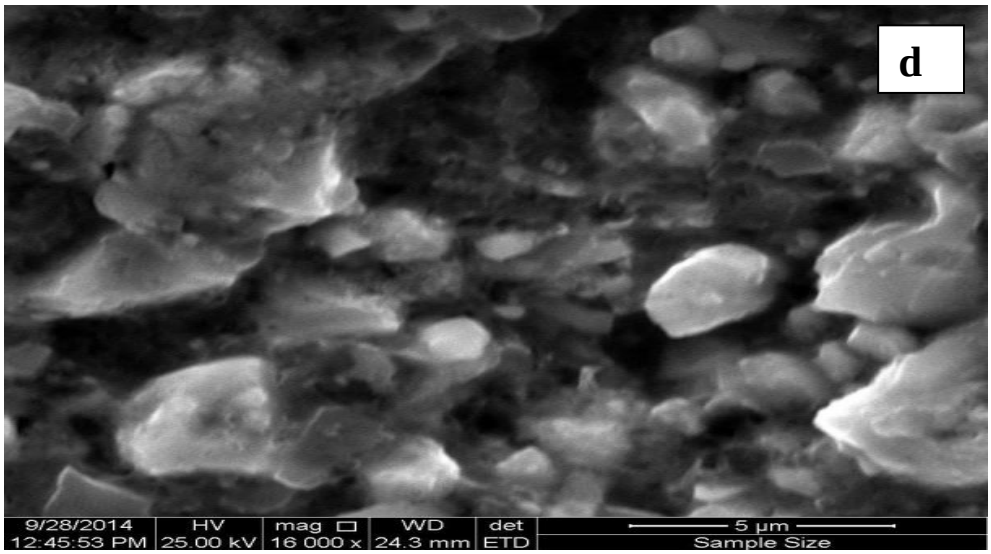
d
9/28/2014
12:45:53 PM
HV
25.00 kV
mag
16 000 x
WD
24.3 mm
det
ETD
5 µm
Sample Size

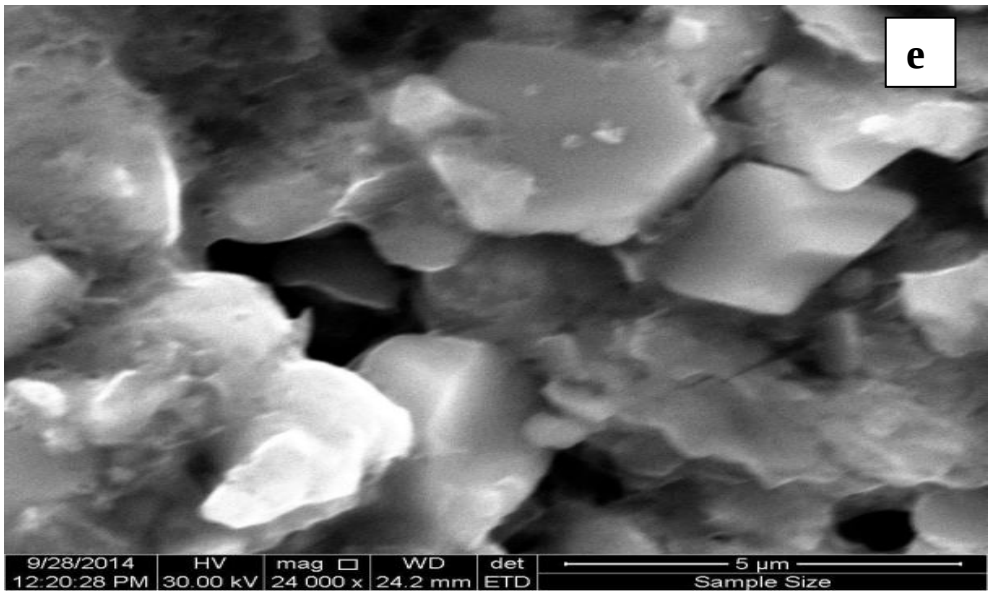
e
9/28/2014
12:20:28 PM
HV
30.00 kV
mag
24 000 x
WD
24.2 mm
det
ETD
5 µm
Sample Size

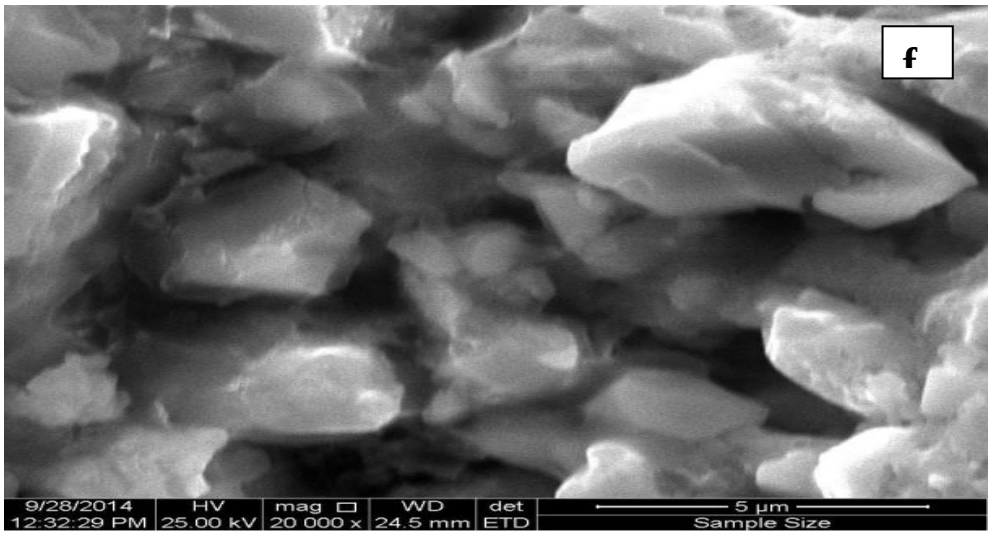

Fig (4.3). SEM images of sizes ($5\mu m * 5\mu m$), of the samples doped with Dy_2O_3, La_2O_3, and Y_2O_3, at sintering temperature (1150℃), where (a, b, c) at concentration (10^{-3}), while (d,e,f) at concentration ($5 * 10^{-3}$) .

4.4. Density

The rising (increasing) of sintering temperature of the samples leads to grain growth (grain size increasing) and gases volatilization which leads to increase the density of the samples (more densification) convoying with decreasing the porosity of the samples by different amounts.

Since the forming pressure of the press which has been used to prepare the samples was constant i.e. all samples compressed under the same pressure, the sintering times, heating rate, cooling rate was the same for all samples, and the concentrations of Bi_2O_3, MnO_2, Co_3O_4, Cr_2O_3, and Sb_2O_3 Remained unchanged for all samples. From the density curves we can observe that there are two parameters affect (changes) the density, and they are:

1- Sintering temperature, where the density increases with increasing sintering temperatures reaching to the saturation state as a result of grain growth in solid and liquid phase sintering, where this processes is convoying with decreasing the porosity [20,24,35].
2- Rare earth oxides concentration as a results of the grain growth effect of rare earth oxides doping convoying with decreasing the porosity, (as mentioned in previous sections) [24,34].

Density, relative porosity with respect to sintering temperature and rare earth oxides concentration, are illustrated in table (4.3), figure (4.4), figure (4.5), figure (4.6), and figure (4.7).

Table (4.3).The values of the density (gm/cm$^{3)}$ and Porosity.

Sintering temperature (℃)	Concentration=10^{-3}					
	Density (gm/cm^3)			Porosity %		
	Dy_2O_3	La_2O_3	Y_2O_3	Dy_2O_3	La_2O_3	Y_2O_3
1050	4.1043	4.0998	3.763	27.73	27.82	33.75
1100	4.3219	4.6570	3.9027	23.91	18	31.28
1150	4.5894	4.8955	4.8035	19.19	13.8	15.42

Sintering temperature (℃)	Concentration=$5 * 10^{-3}$					
	Density (gm/cm^3)			Porosity %		
	Dy_2O_3	La_2O_3	Y_2O_3	Dy_2O_3	La_2O_3	Y_2O_3
1050	4.3457	4.1776	4.3173	23.48	26.44	23.98
1100	4.9717	4.9717	4.5604	12.47	12.47	19.7
1150	5.0341	5.3971	5.1483	11.36	4.972	9.352

Sintering temperature (℃)	Concentration=$10 * 10^{-3}$					
	Density (gm/cm^3)			Porosity %		
	Dy_2O_3	La_2O_3	Y_2O_3	Dy_2O_3	La_2O_3	Y_2O_3
1050	4.8626	4.2895	4.7013	14.39	24.48	17.22
1100	5.5141	5.1949	5.1495	2.919	8.535	9.335
1150	5.5164	5.5181	5.3534	2.878	2.845	5.741

ZnO+ Other Oxides (Without Rare Earth Oxides)		
Sintering temperature (℃)	Density (gm/cm^3)	Porosity %
1050	72.64	27.36
1100	82.97	17.02
1150	83.86	16.14

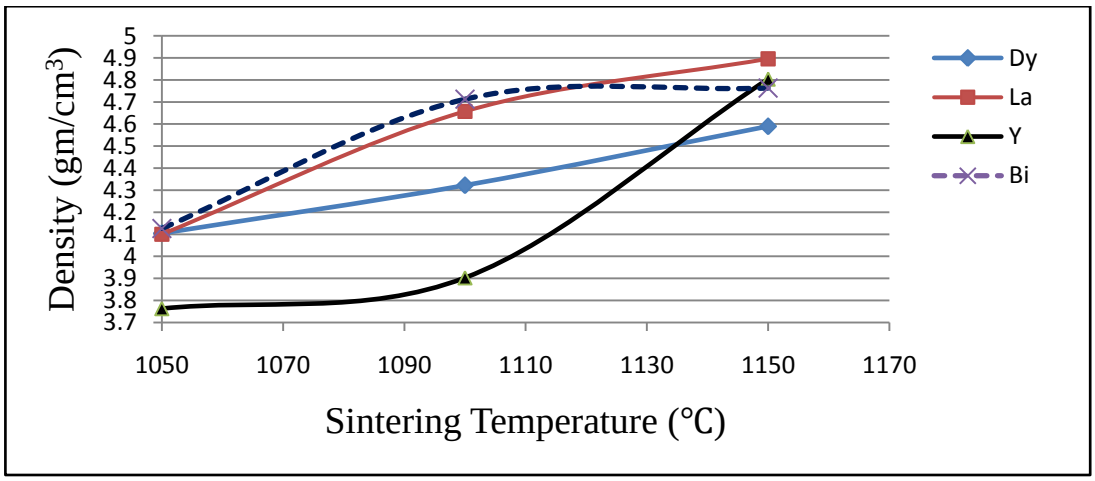

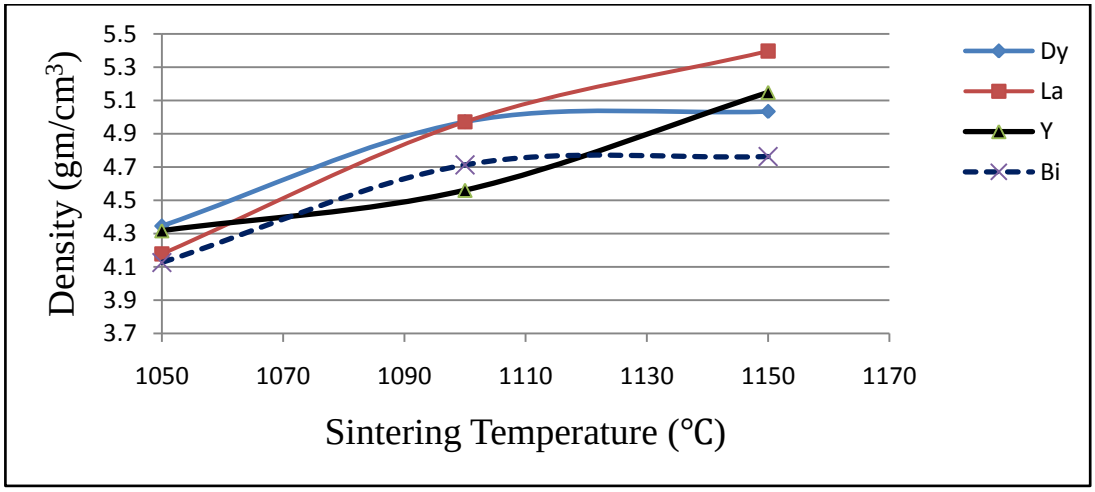

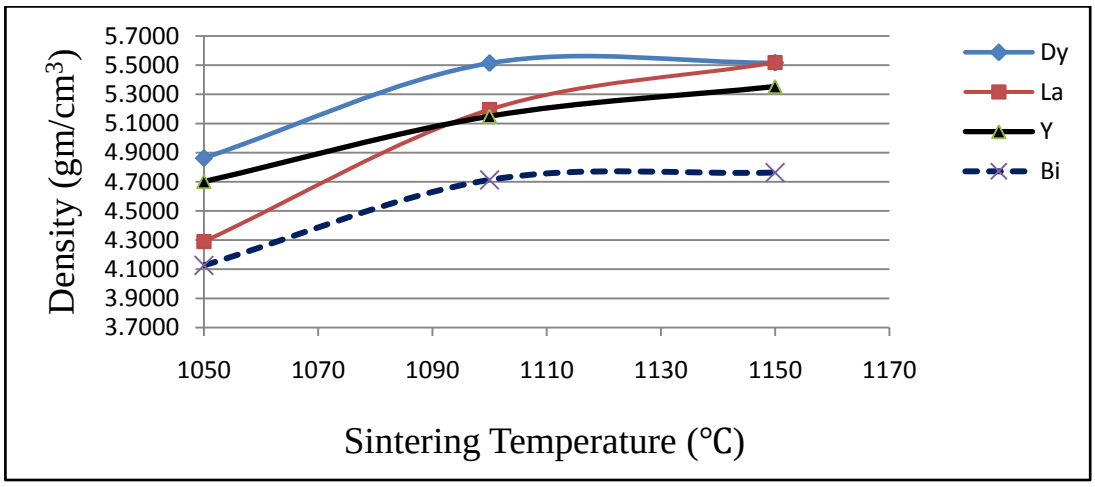

Fig (4.4). Density against temperature, at rare earth oxides concentrations (10^{-3}, $5 * 10^{-3}$ and $10 * 10^{-3}$ mole %), respectively.

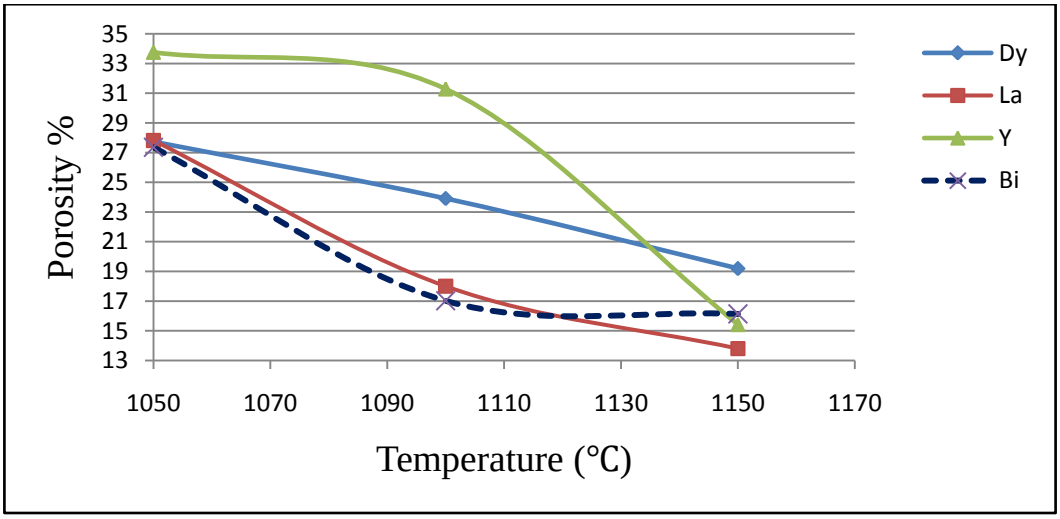

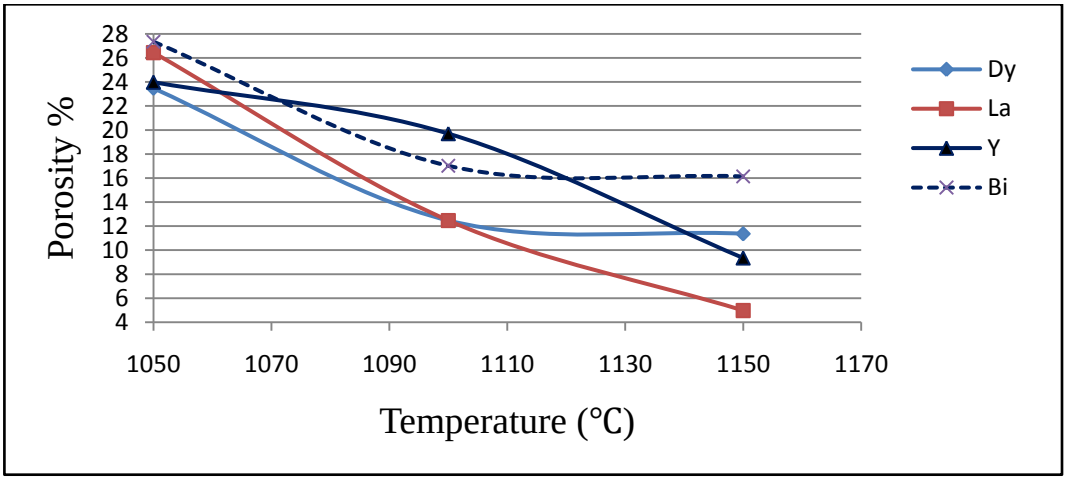

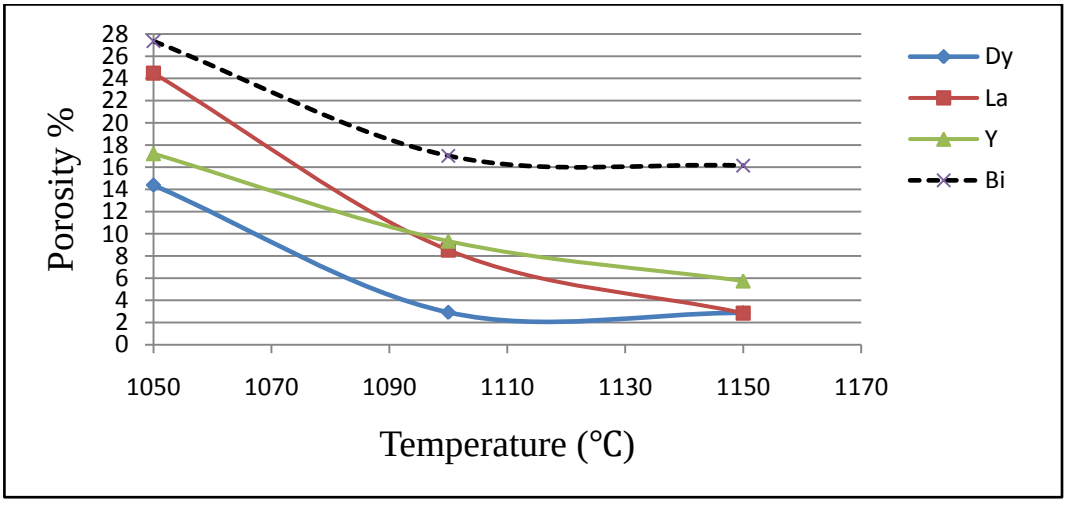

Fig (4.5). Relative porosity against temperature, at rare earth oxides concentrations (10^{-3}, $5 * 10^{-3}$ and $10 * 10^{-3}$ mole %), respectively.

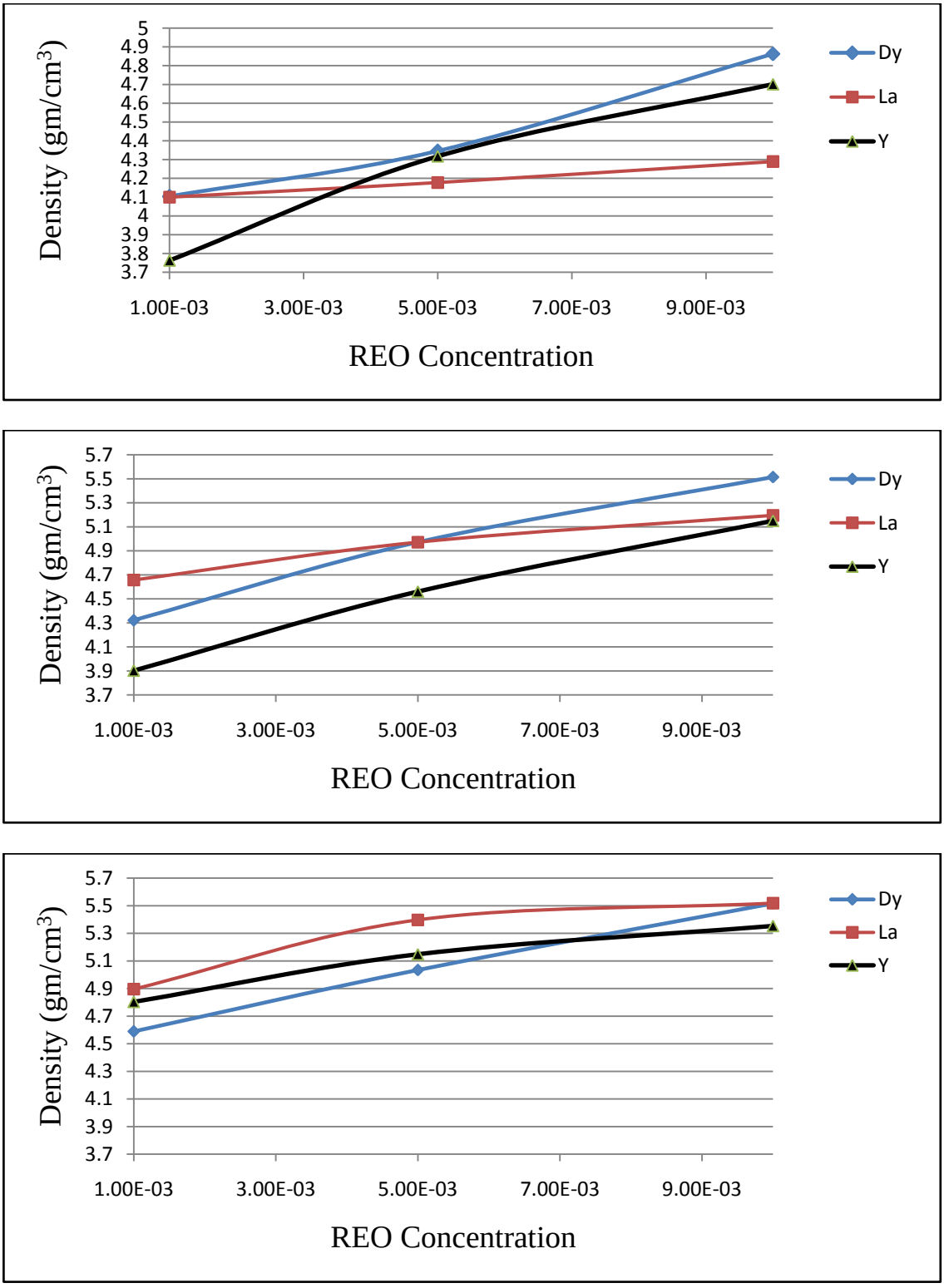

Fig (4.6). Density against rare earth oxides concentrations, at sintering temperature (1050, 1100, and 1150℃), respectively.

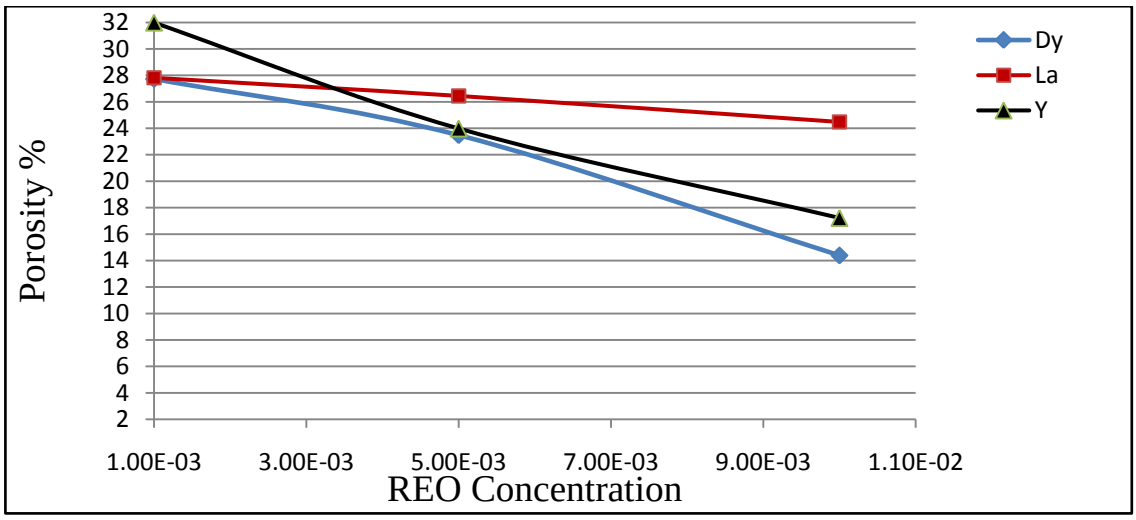

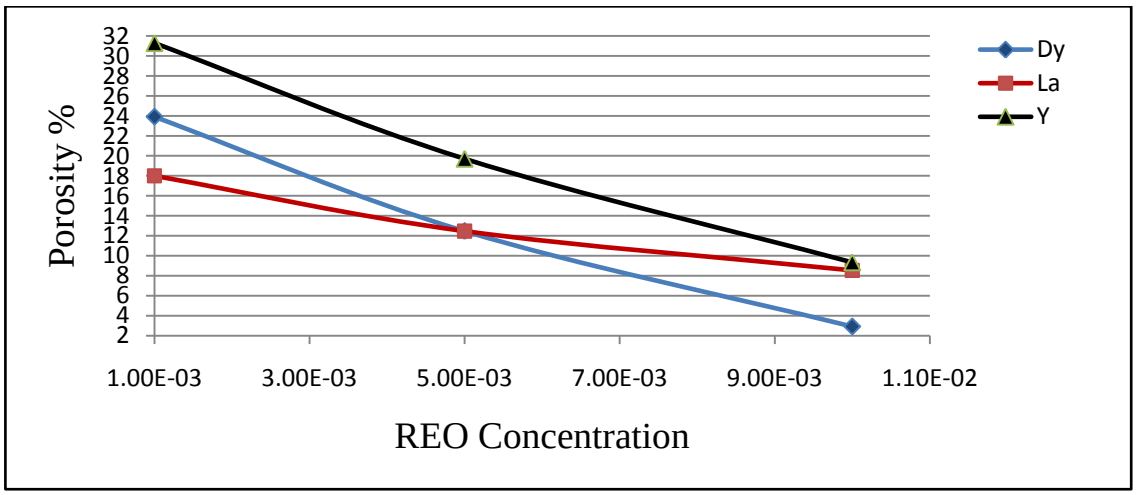

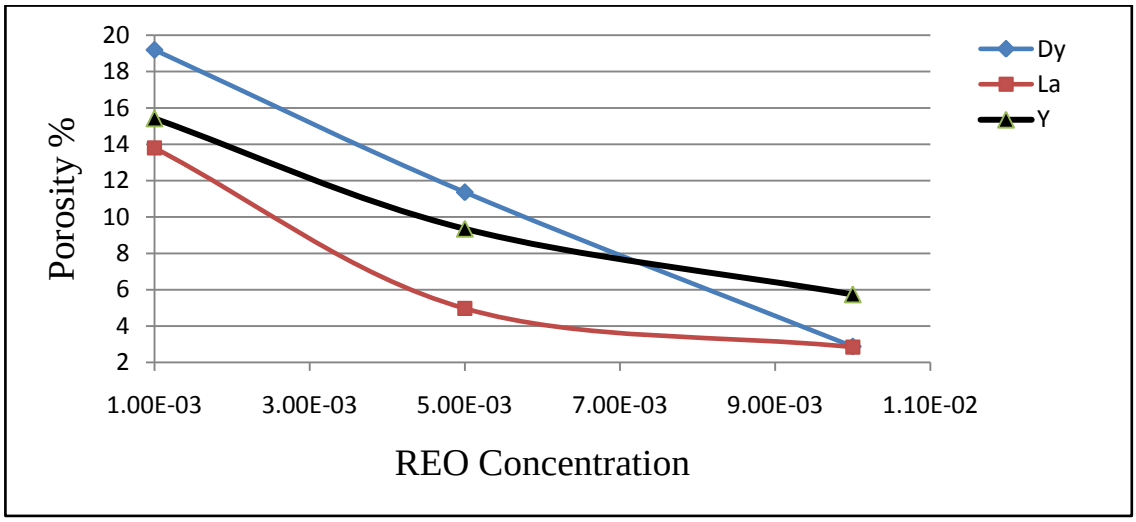

Fig (4.7). Relative porosity against rare earth oxides concentrations, at sintering temperature (1050, 1100, and 1150℃), respectively.

4.5. Electrical Properties

4.5.1. I–V Properties Curve

Because of the limitation of available testing instruments, therefore we constrained to reduce and decrease the thickness of the samples to be compatible or suitable with the capability or ability of the available testing instruments, but this procedure decreased the obtained results.

Figure (4.9). Demonstrates the behavior of ZnO varistors samples starting from ZnO pure samples which illustrates the ohmic (linear) behavior of ZnO pure (where the sample has been damaged when the potential gradient reach about (45V/cm)).

From figure (4.9) we can observe that the doping of ZnO change the behavior from linear to non-linear as a result of Schottky barrier generation between ZnO grains and the grain boundary, while the doping with rare earth oxides improves and enhances the non-linearity of the varistor [38,53,67].

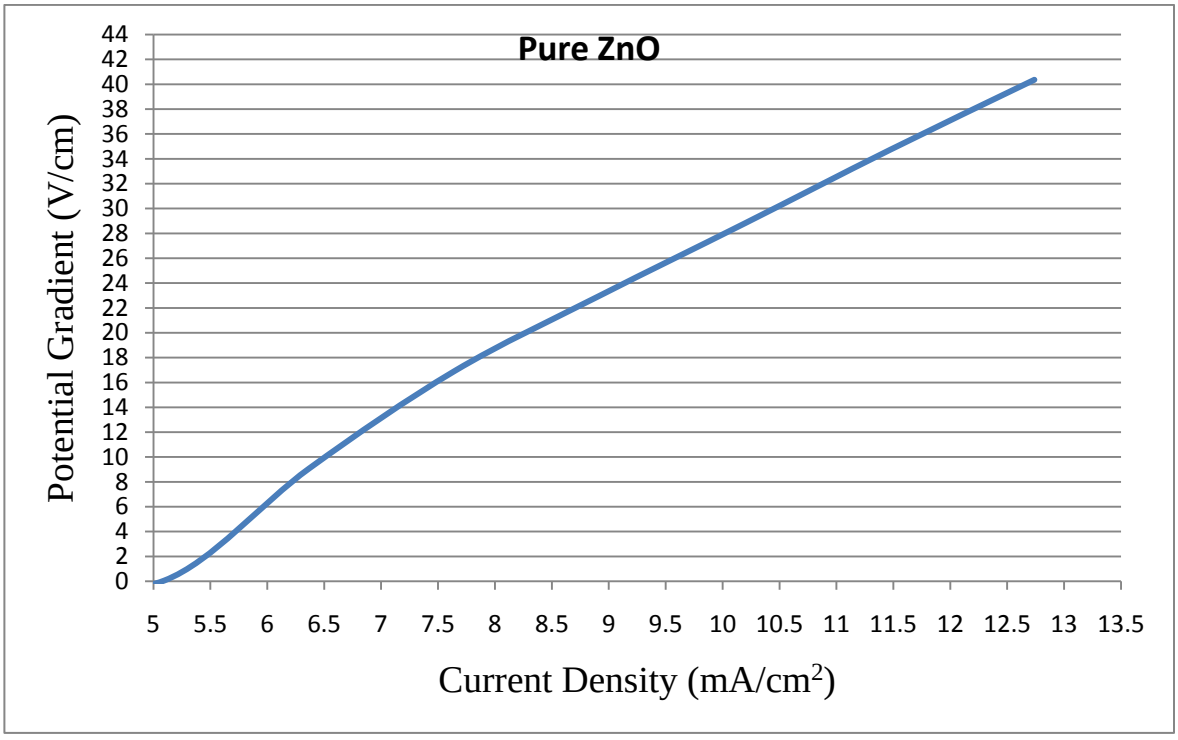

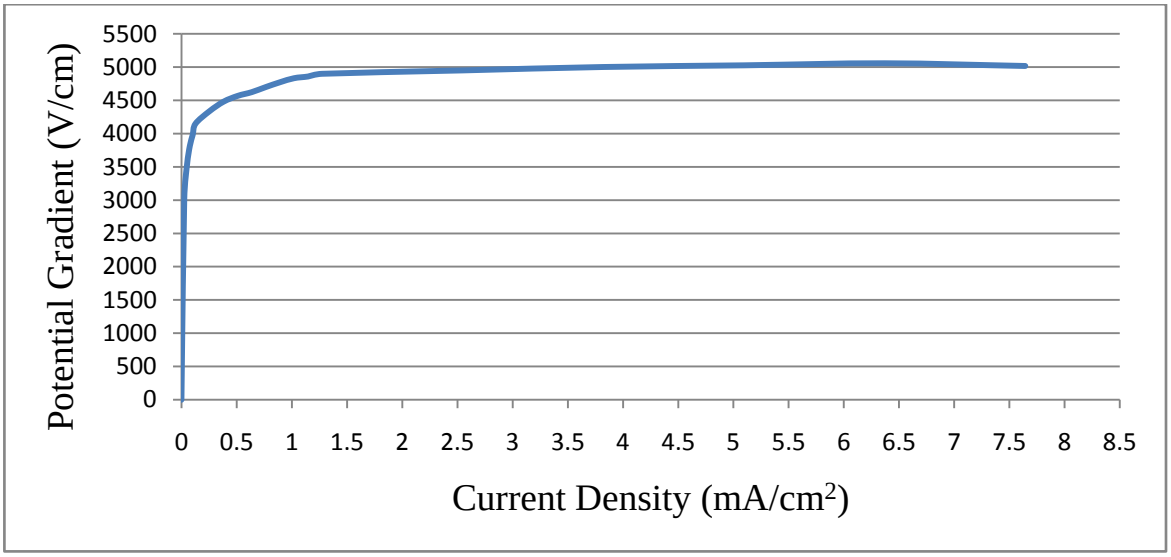
Potential Gradient (V/cm)
5500
5000
4500
4000
3500
3000
2500
2000
1500
1000
500
0
0 0.5 1 1.5 2 2.5 3 3.5 4 4.5 5 5.5 6 6.5 7 7.5 8 8.5
Current Density (mA/cm2)

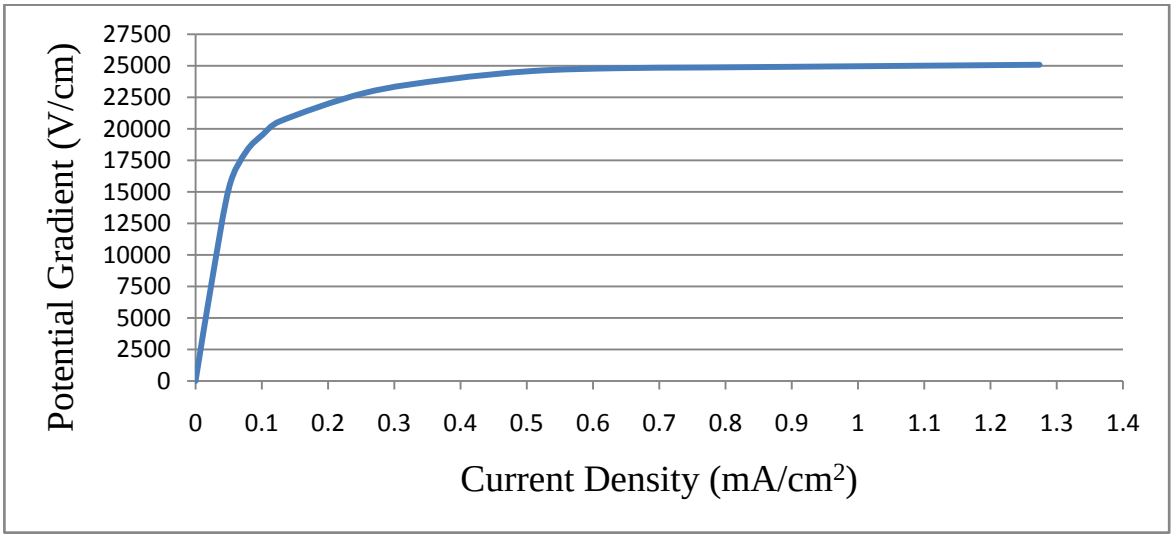
Potential Gradient (V/cm)
27500
25000
22500
20000
17500
15000
12500
10000
7500
5000
2500
0
0 0.1 0.2 0.3 0.4 0.5 0.6 0.7 0.8 0.9 1 1.1 1.2 1.3 1.4
Current Density (mA/cm2)

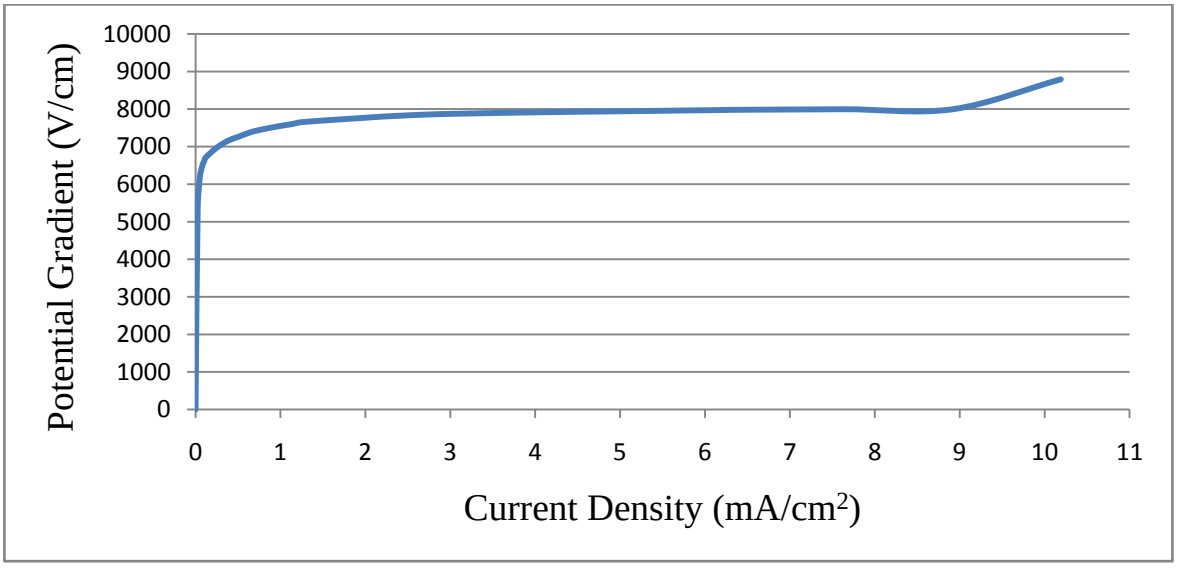
Potential Gradient (V/cm)
10000
9000
8000
7000
6000
5000
4000
3000
2000
1000
0
0 1 2 3 4 5 6 7 8 9 10 11
Current Density (mA/cm2)

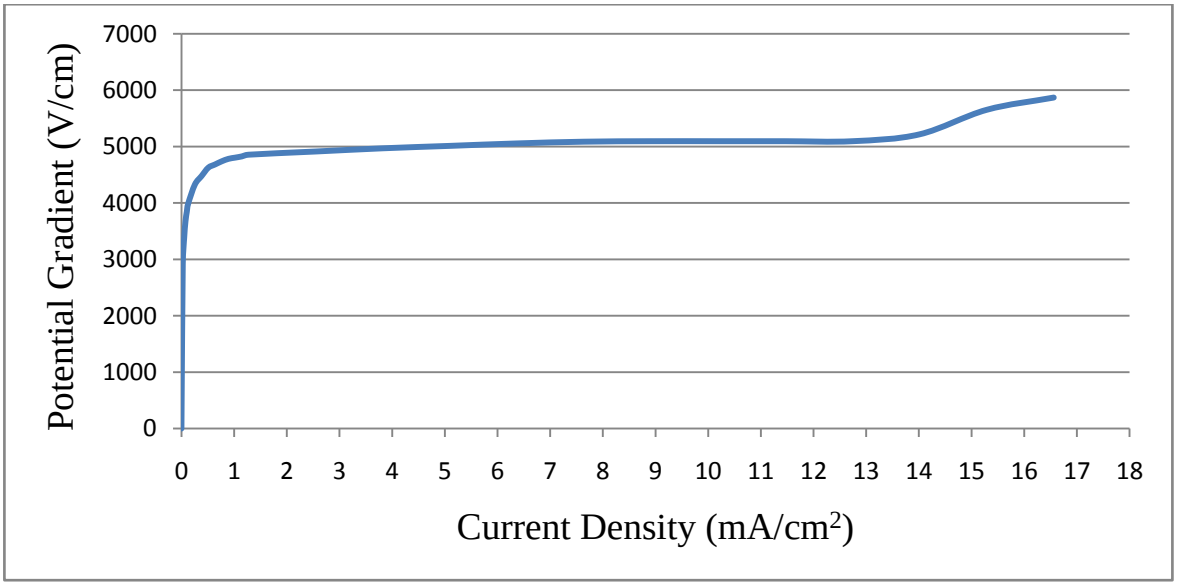

Fig (4.8). I–V characteristic curve of samples (from up to down), pure ZnO , ZnO with other oxides (without rare earth oxides), and finally doped with rare earth oxides, Dy_2O_3, La_2O_3, and Y_2O_3 respectively .

4.5.2. Non-Linear Coefficient (φ)

The non-linear coefficient **(φ)** is the most important parameter in varistor work or it represents the superior criterion parameter among the other parameters or properties of varistor, and its value whenever to be larger that means higher superiority (efficiency) of varistor, and vice versa when (φ) value is small that means low superiority or (efficiency).

Table (4.4) and figure (4.10) explain the variety of non-linear coefficient versus the sintering temperature at a fix concentration of rare earth oxides, while figure (4.11) explain the variety of non-linear coefficient versus rare earth oxides concentration at a fix the sintering temperature.

The doping with Bi_2O_3 and Sb_2O_3 generates Schottky barrier at the grain boundary which represents the reason of the non-linearity of ZnO varistor, from figure (4.10) we can observe that the non-linear coefficient of pure ZnO is very small, while the doping with other oxides enlarge (increases) it, but the rapid volatilization (vaporization) of Bi_2O_3 and spinel phase ($Zn_7Sb_2O_{12}$) after sintering temperature (1100℃) decreases the insolation layer between the ZnO grains therefore the height of Schottky barrier will decreased and the non-linear coefficient will decreased too [46,56].

from figure (4.10) and figure (4.11) we can observe that the non-linear coefficient increased by doping with rare earth oxides and with rare earth oxides concentration because rare earth oxides radius are larger than the radius of Zn^{2+} which enlarged the depletion layer width and the Schottky barrier height, but the volatilization (vaporization) of Bi_2O_3 and spinel phase ($Zn_7Sb_2O_{12}$) after sintering temperature (1100℃) still has an essential role in decreasing the non-linear coefficient [36,56,68].

Table (4.4). Non-linear coefficient values with respect to sintering temperature at fixed rare earth oxide concentration.

Sintering Temperature (℃)	$Concentration = 10^{-3}$			ZnO	ZnO+ Bi_2O_3
	Dy_2O_3	La_2O_3	Y_2O_3		
1050	9.737	7.594	13.63	1.255	4.46
1100	16.74	14.11	17.83	1.331	6.46
1150	12.068	11.67	14.953	1.54	5.5

Sintering Temperature (℃)	$Concentration = 5 * 10^{-3}$		
	Dy_2O_3	La_2O_3	Y_2O_3
1050	13.013	11.6847	16.536
1100	30.082	24.388	46.566
1150	18.641	17.16	23.408

Sintering Temperature (℃)	$Concentration = 10 * 10^{-3}$		
	Dy_2O_3	La_2O_3	Y_2O_3
1050	15.69	12.59	12.99
1100	27.13	19.21	27.47
1150	24.15	16.79	19.67

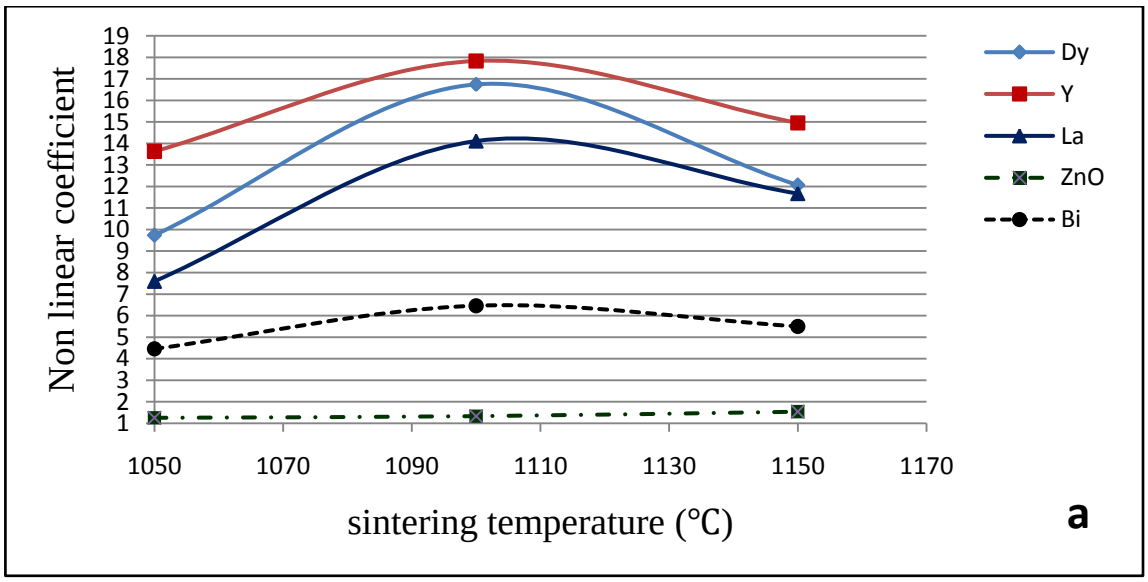

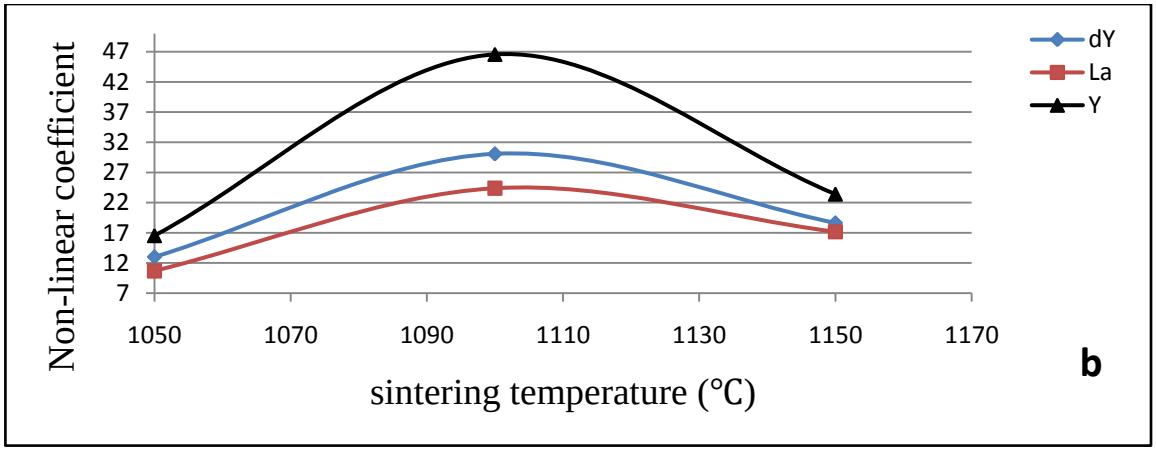

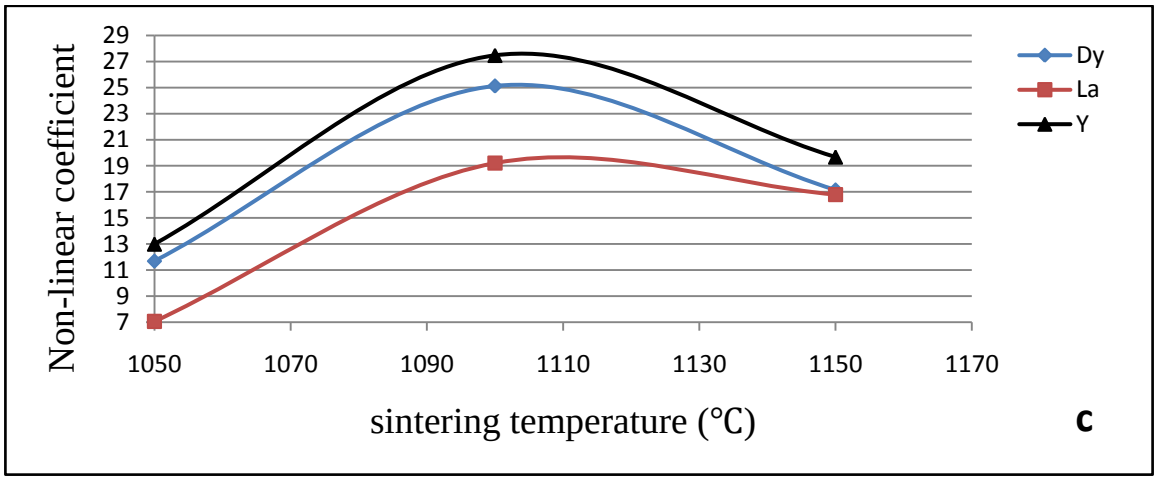

Fig (4.9). Non-linear coefficient with respect to sintering temperature, (a) pure ZnO, ZnO + other oxides (without REO), and doped with REO at 10^{-3}, (b) $5*10^{-3}$, and (c) $10*10^{-3}$.

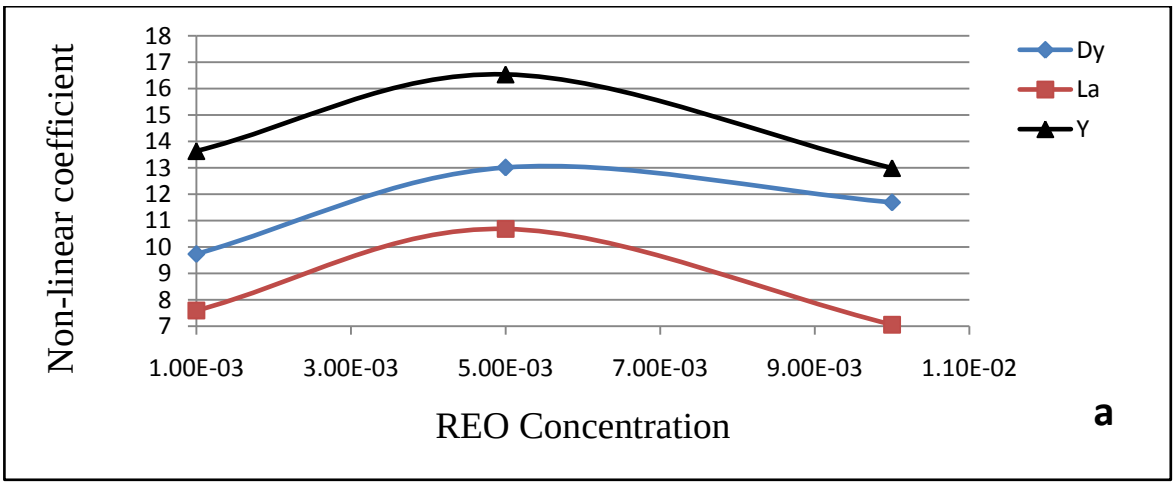

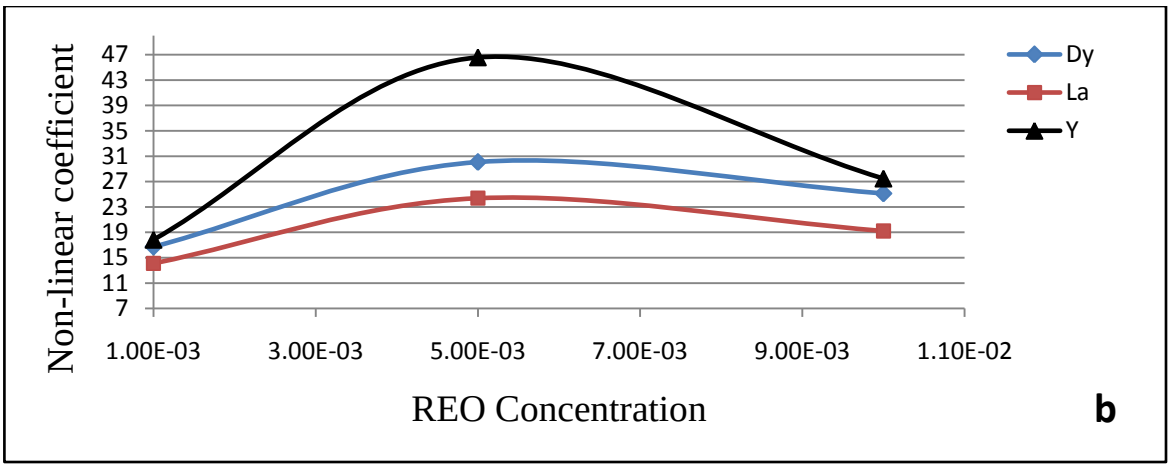

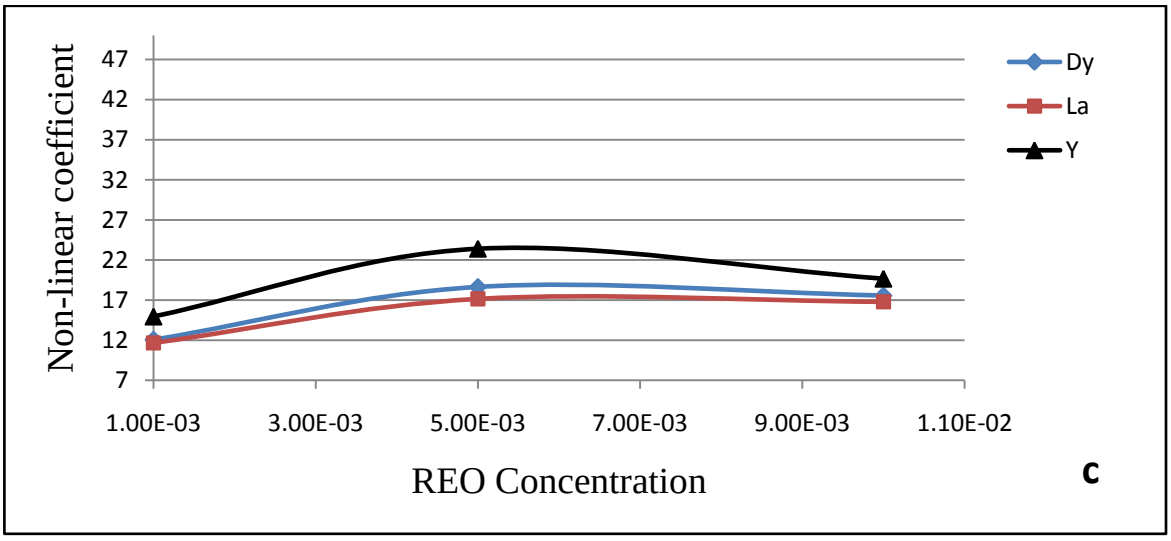

Fig (4.10). Non-linear coefficient with respect to REO concentration at fixed sintering temperature, where (a) at 1050℃, (b) 1100℃, and (c) 1150℃, respectively.

4.5.3. Breakdown Voltage

Table (4.5), figure (4.12), and figure (4.13). Demonstrate the results of breakdown voltage with respect to sintering temperature at fixed rare earth oxides concentrations, and with respect rare earth oxides concentrations at fixed sintering temperature, we can observe obviously that the breakdown voltage decreases with increasing of sintering temperature, and this because of the increasing of grain size (with increasing sintering temperature as mentioned in previous sections) where the breakdown voltage represents the resultant of the number of Schottky barriers in the samples (as shown in equation (2-22)) and these numbers decreased with increasing temperature, on the other hand the volatilization (vaporization) of Bi_2O_3 and spinel phase ($Zn_7Sb_2O_{12}$) with increasing of sintering temperature which leads to decreasing of the layer between ZnO grains [46,74].

$$V_{gb} = V_b \left(\frac{d}{D}\right) \dots\dots\dots\dots\dots\dots\dots\dots\dots\dots\dots\dots\dots\dots\dots\dots (2-22)$$

In addition to the above the rare earth oxides increase the breakdown voltage because of the large melting points of them which inhibit the grain growth at (fixed sintering temperature), increasing the height of Schottky barrier [38,87].

Table (4.5). Breakdown voltage (Volt) with respect to sintering temperature at fixed rare earth oxide concentration.

V_B (Volt)					
Sintering Temperature (℃)	$Concentration = 10^{-3}$			ZnO	ZnO+Bi_2O_3
	Dy_2O_3	La_2O_3	Y_2O_3		
1050	3340	2064	2880	56.8	2320
1100	1180	1132.8	1136	4.8	950.4
1150	818.4	858.4	861.6	6.2E-04	724.8

V_B (Volt)			
Sintering Temperature (℃)	$Concentration = 5 * 10^{-3}$		
	Dy_2O_3	La_2O_3	Y_2O_3
1050	3632	2208	3376
1100	1322	1992	1556
1150	867.6	888.8	988

V_B (Volt)			
Sintering Temperature (℃)	$Concentration = 10 * 10^{-3}$		
	Dy_2O_3	La_2O_3	Y_2O_3
1050	3920	2720	4040
1100	1908	2042.4	2712
1150	1008	1208.8	1132

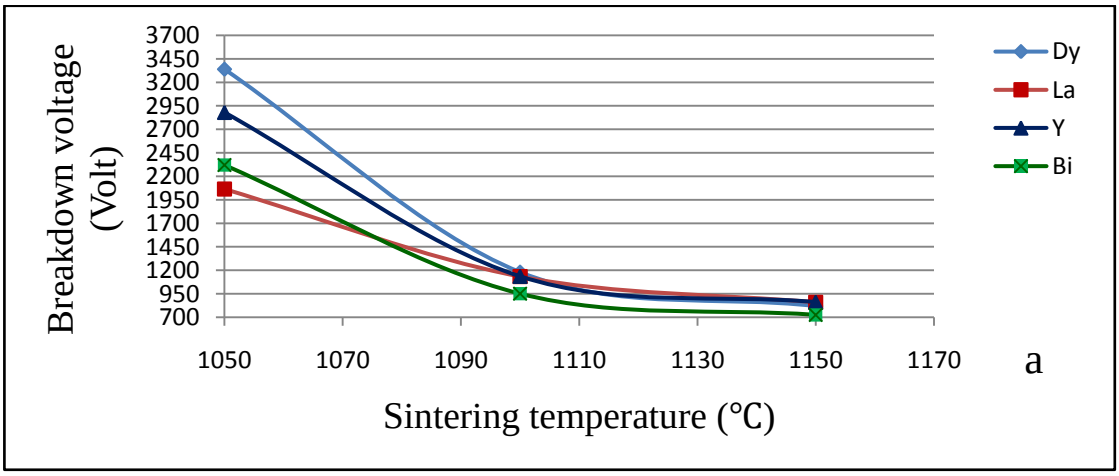

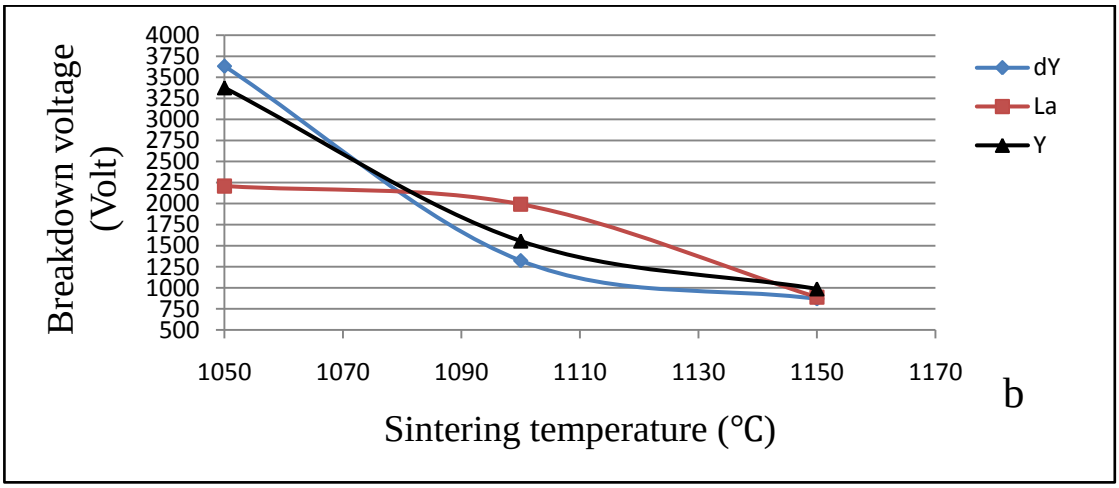

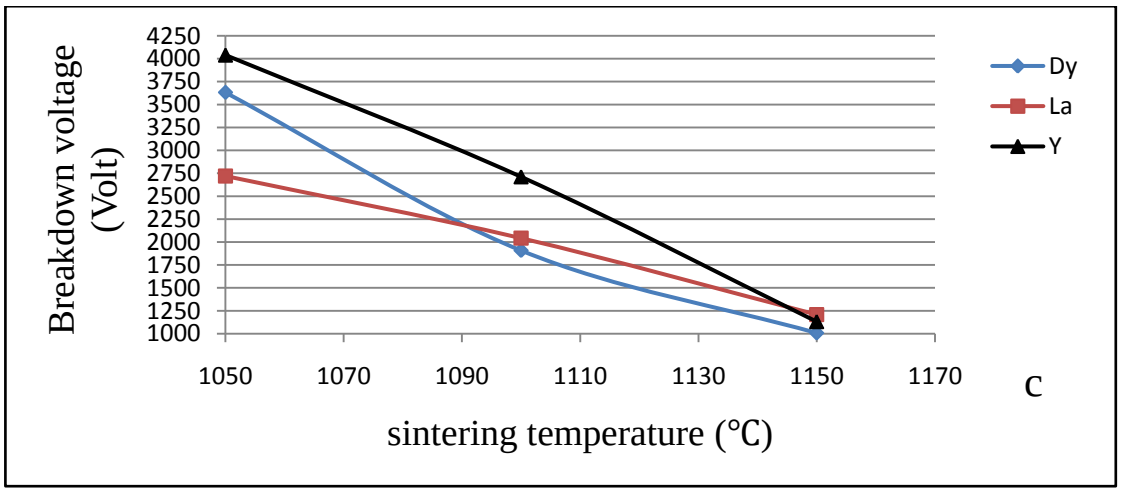

Fig (4.11). Breakdown voltage with respect to sintering temperature, (a) ZnO + other oxides (without REO), ZnO + other oxides+ REO at 10^{-3}, (b) $5*10^{-3}$, and (c) $10*10^{-3}$.

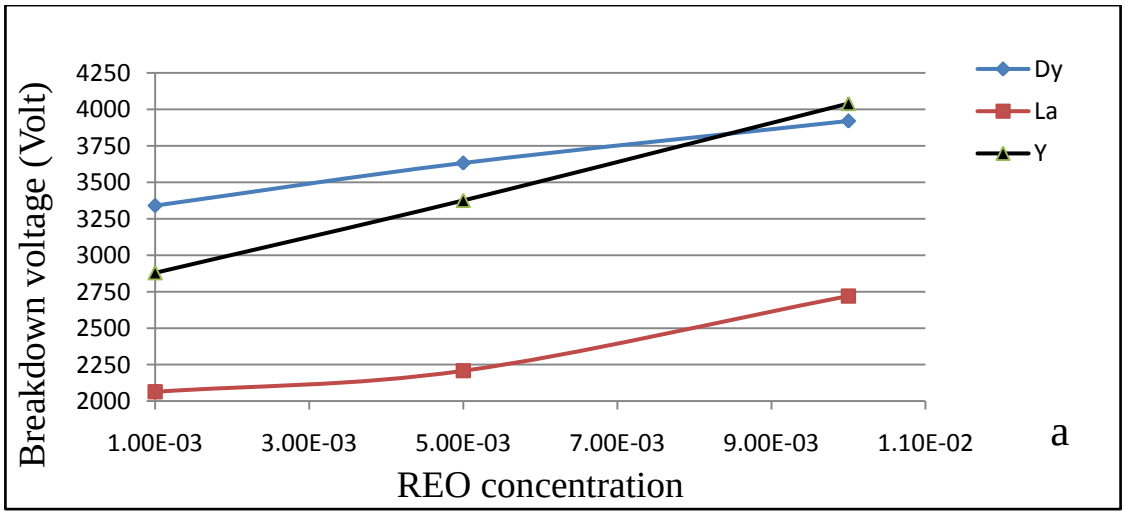

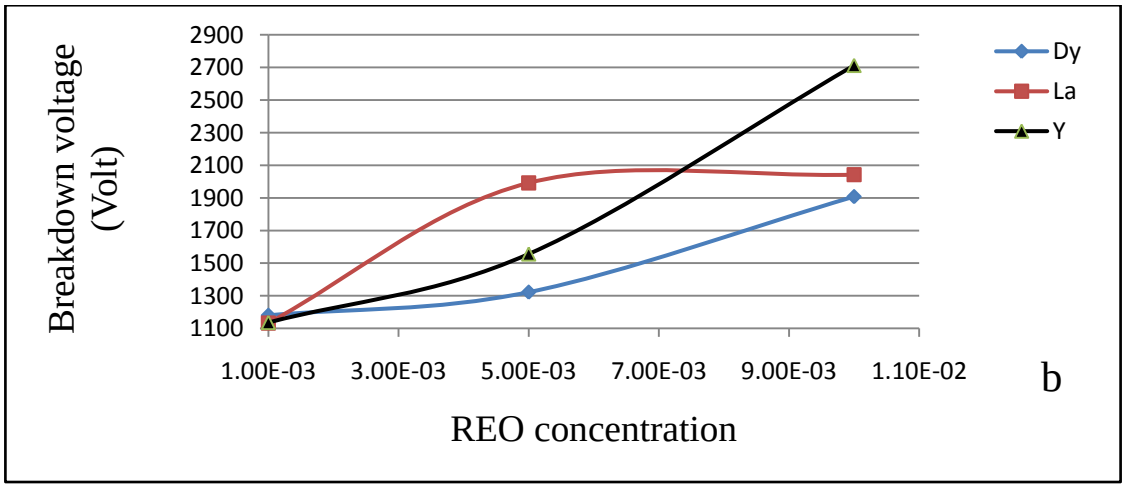

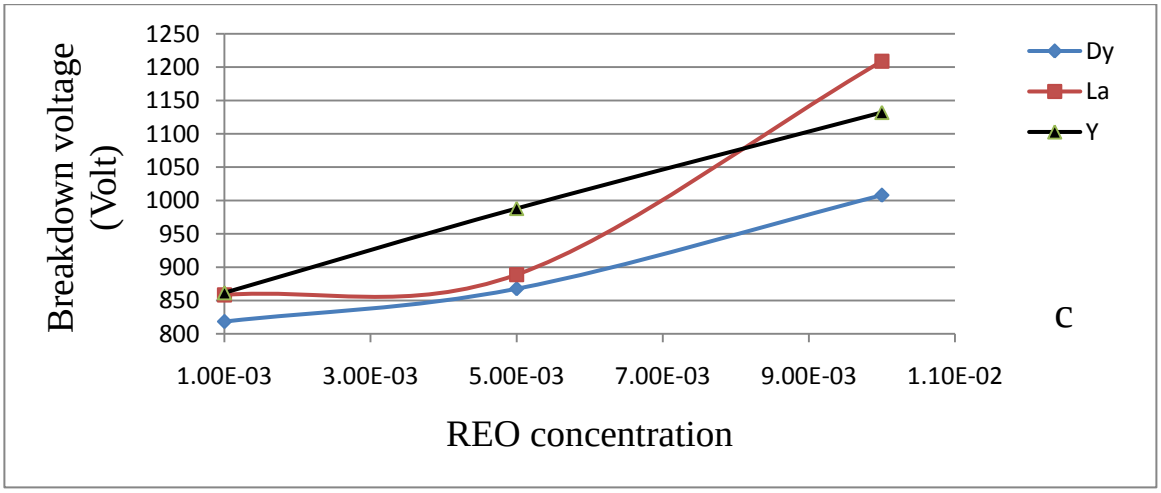

Fig (4.12). Breakdown voltage with respect to REO concentration at fixed sintering temperature, where (a) at 1050℃, (b) 1100℃, and (c) 1150℃, respectively.

4.5.4. Leakage Current

Table 4.6. figure (4.14), and figure (4.15) demonstrate the results of leakage current with respect to sintering temperature at fixed rare earth oxide concentrations and with respect to rare earth oxide concentrations at fixed sintering temperature .

Because of the thermal stresses and because of the DC electrical stresses which leads to thermal stresses too, these parameters leads to increasing the leakage current through the samples, decreasing of the depletion layer between ZnO grains which allow the current to moves through the grains, in addition to rapid volatilization (vaporization) of Bi_2O_3 and spinel phase ($Zn_7Sb_2O_{12}$) beyond (1100℃) [26,69]

Table (4.6). The leakage current with respect to sintering temperature at different rare earth oxide concentrations.

$I_L(\mu A)$					
Sintering Temperature ℃	$Concentration = 10^{-3}$			Zn	Bi
	Dy_2O_3	La_2O_3	Y_2O_3		
1050	44.4	42	48.4	trace	33
1100	13.1	24.7	40.2	trace	56.4
1150	31	73.9	61.5	trace	69.1

$I_L(\mu A)$			
Sintering Temperature ℃	$Concentration = 5 * 10^{-3}$		
	Dy_2O_3	La_2O_3	Y_2O_3
1050	46.3	45	51
1100	24.5	37	49.3
1150	53	85.5	75.3

$I_L(\mu A)$			
Sintering Temperature ℃	$Concentration = 10 * 10^{-3}$		
	Dy_2O_3	La_2O_3	Y_2O_3
1050	53.5	51	58
1100	30.5	43	51.4
1150	66.5	98.4	77.2

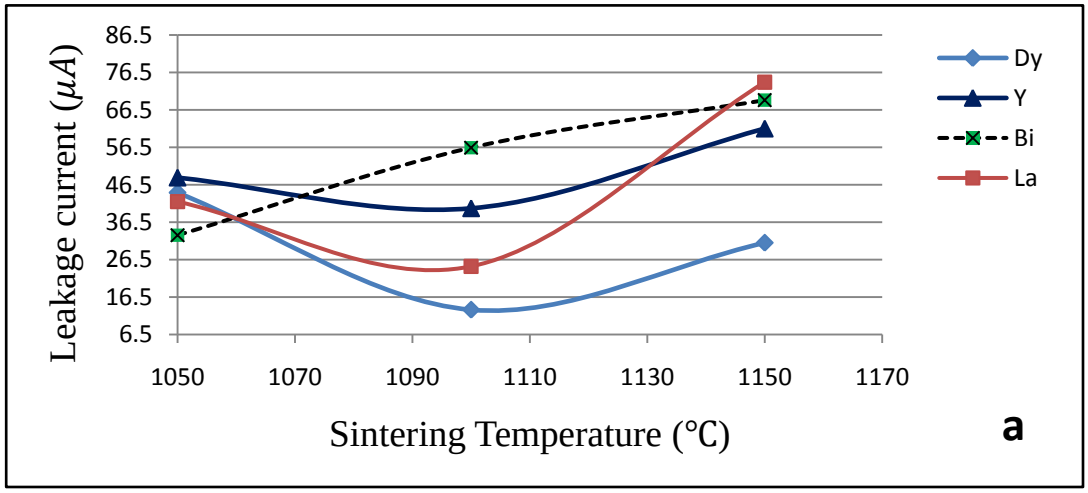

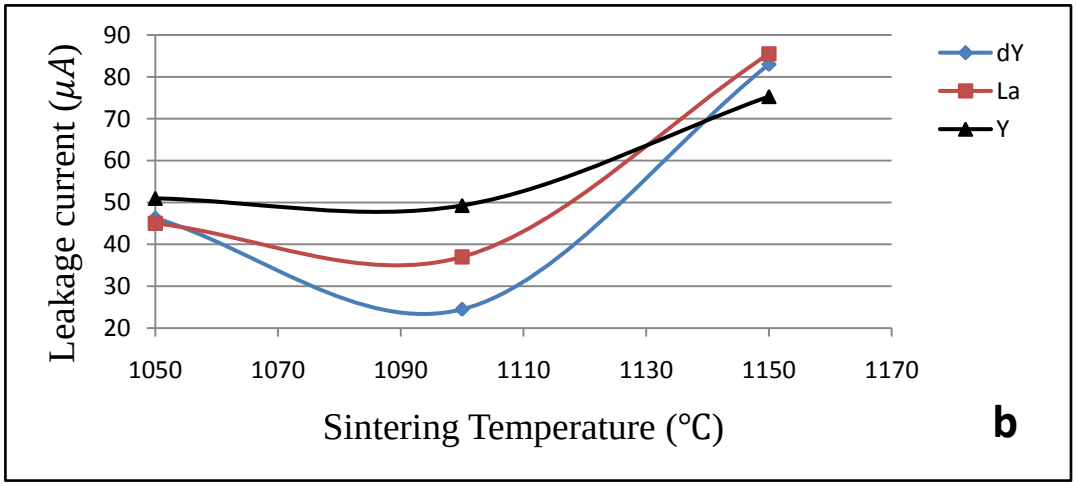

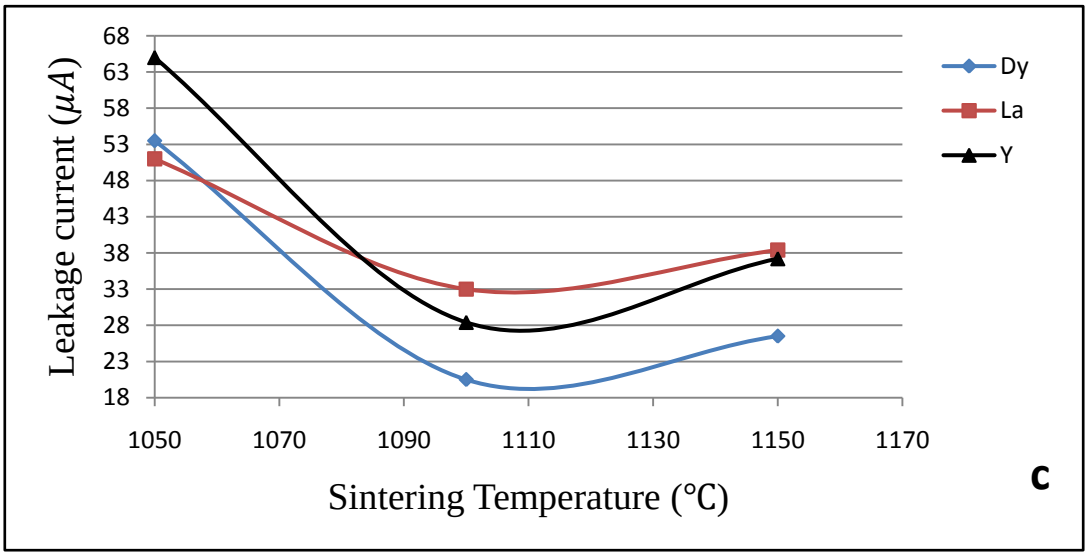

Fig (4.13). Leakage current with respect to sintering temperature, (a) ZnO + other oxides (without REO), ZnO + other oxides+ REO at 10^{-3}, (b) $5*10^{-3}$, and (c) $10*10^{-3}$.

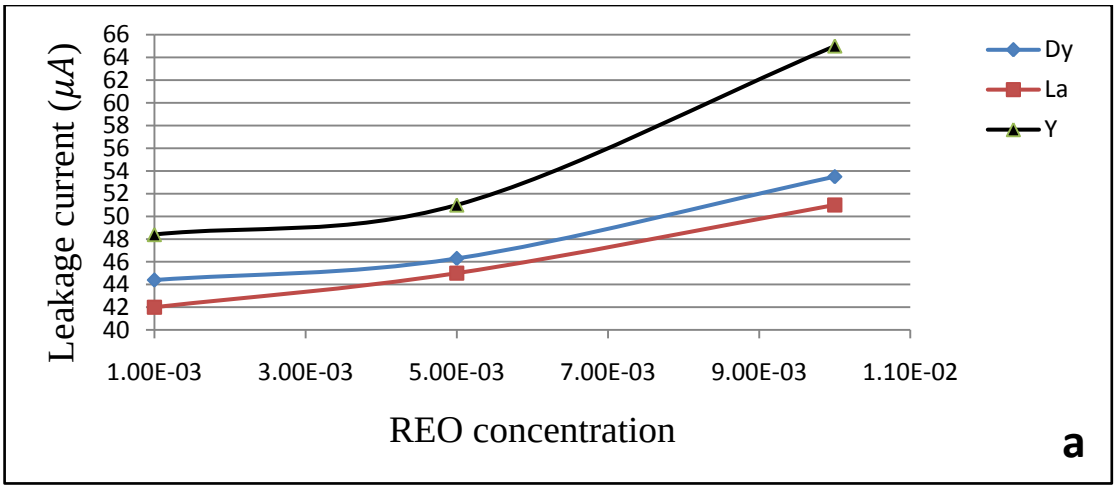

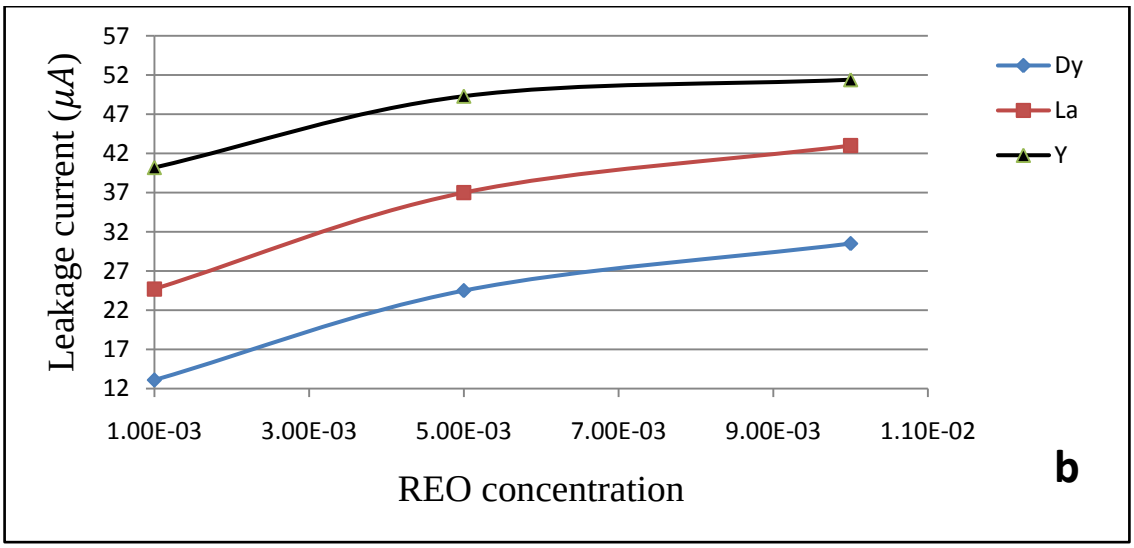

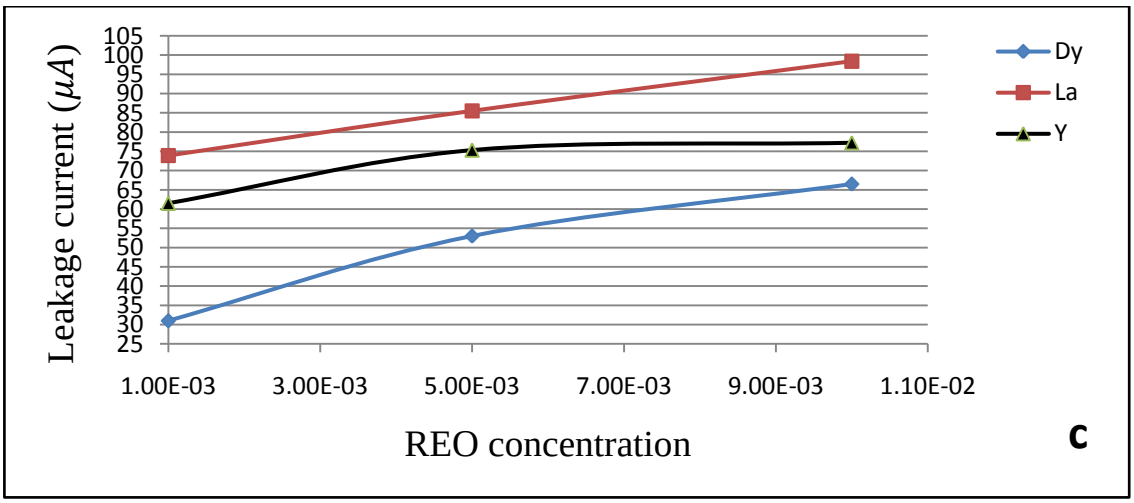

Fig (4.14). Leakage current with respect to REO concentration at fixed sintering temperature, where (a) at 1050℃, (b) 1100℃, and (c) 1150℃.

4.5.5. Energy Absorption Capability

Table (4.7), figure (4.16), and figure (4.17) demonstrate the results of energy absorption capability with respect to sintering temperature at fixed rare earth oxide concentrations and with respect to rare earth oxide concentrations at fixed sintering temperature.

The varistors degradation increased and efficiency decreased because of the leakage current which gradually increases with electrical stresses and time, therefore the electrical stability of the varistor is decreased during time and the energy absorption decreased with rising sintering temperature that means the losing in absorption energy decreased during time because of the continuous increasing in leakage current which leads to continuous losing in energy and so on, in addition to decreasing breakdown voltage will decreases the energy absorption capability [70].

While the rare earth oxides increase the energy absorption capability in a fixed sintering temperature because of the high melting point, and the high radius which enlarged the insulation layer (depletion layer) between ZnO grains.

Table (4.7). Energy absorption capability with respect to sintering temperature at different REO concentrations.

E (Joul)					
Sintering Temperature (℃)	$Concentration = 10^{-3}$			Zn	Bi
	Dy_2O_3	La_2O_3	Y_2O_3		
1050	2088	1290	1800	trace	1450
1100	737.5	861.6	710	trace	594
1150	511.5	708	538.5	trace	453

E (Joul)			
Sintering Temperature (℃)	$Concentration = 5 * 10^{-3}$		
	Dy_2O_3	La_2O_3	Y_2O_3
1050	2450	1380	2110
1100	826.5	1245	972.5
1150	411	555.5	617.5

E (Joul)			
Sintering Temperature (℃)	$Concentration = 10 * 10^{-3}$		
	Dy_2O_3	La_2O_3	Y_2O_3
1050	2570	1700	2525
1100	1193	1277	1695
1150	720	755.5	707.5

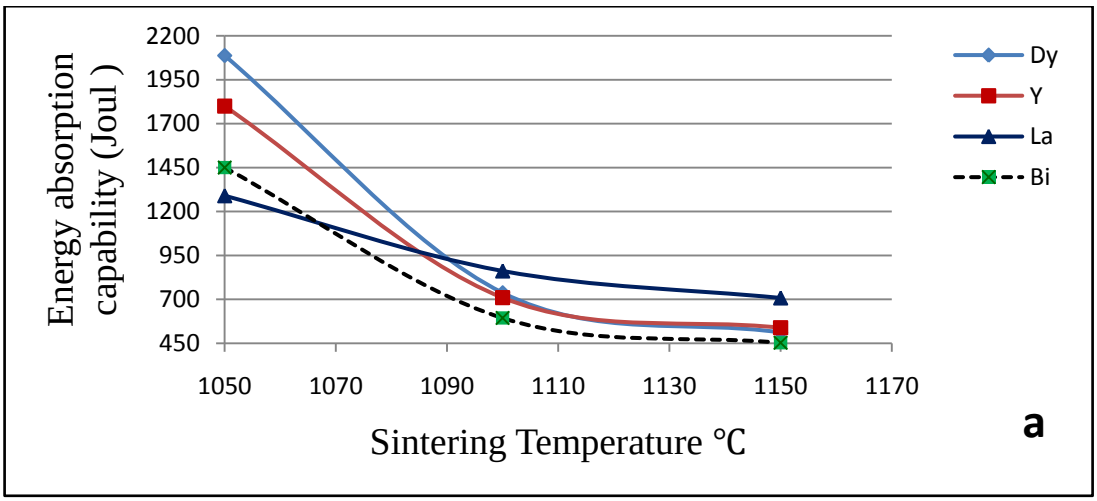

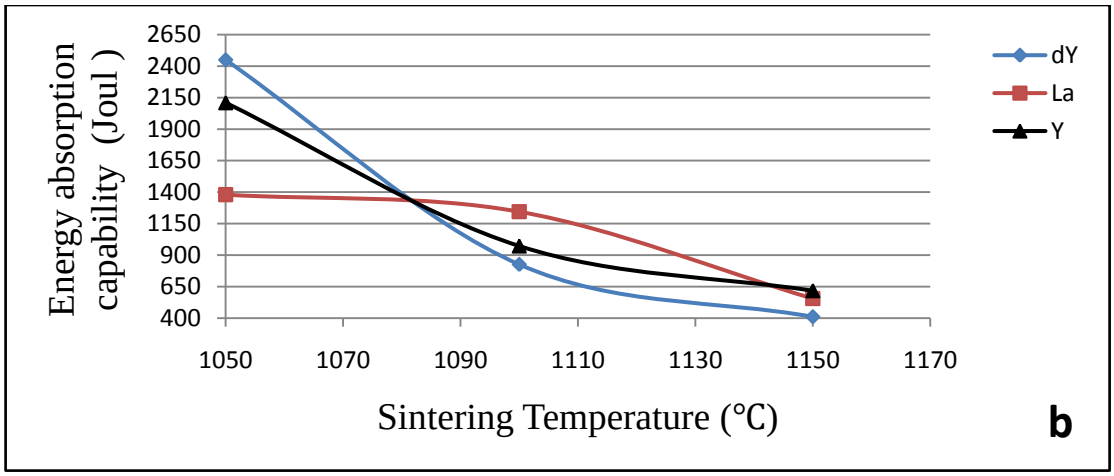

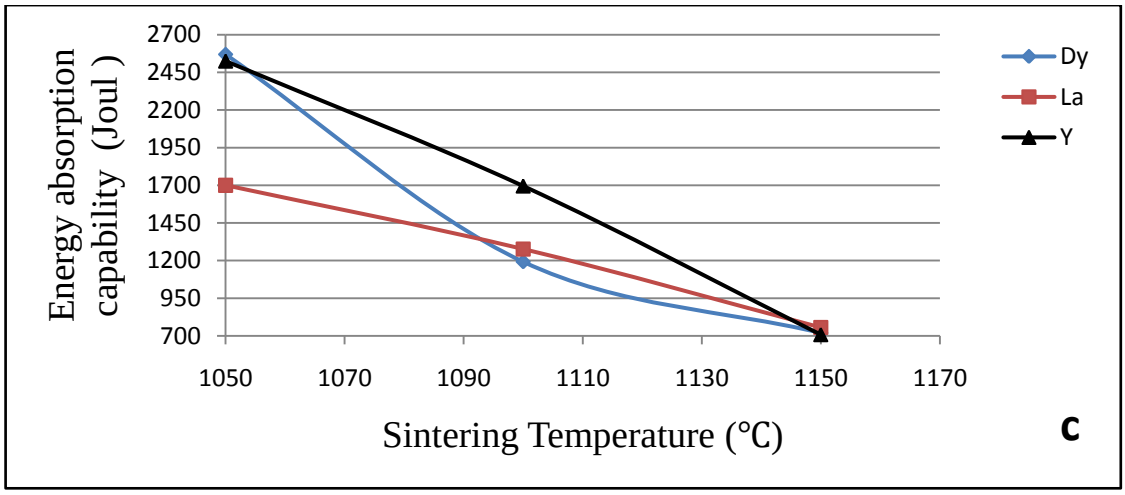

Fig (4.15). Energy absorption capability with respect to sintering temperature, (a) ZnO + other oxides (without REO), ZnO + other oxides+ REO at 10^{-3}, (b) $5*10^{-3}$, and (c) $10*10^{-3}$.

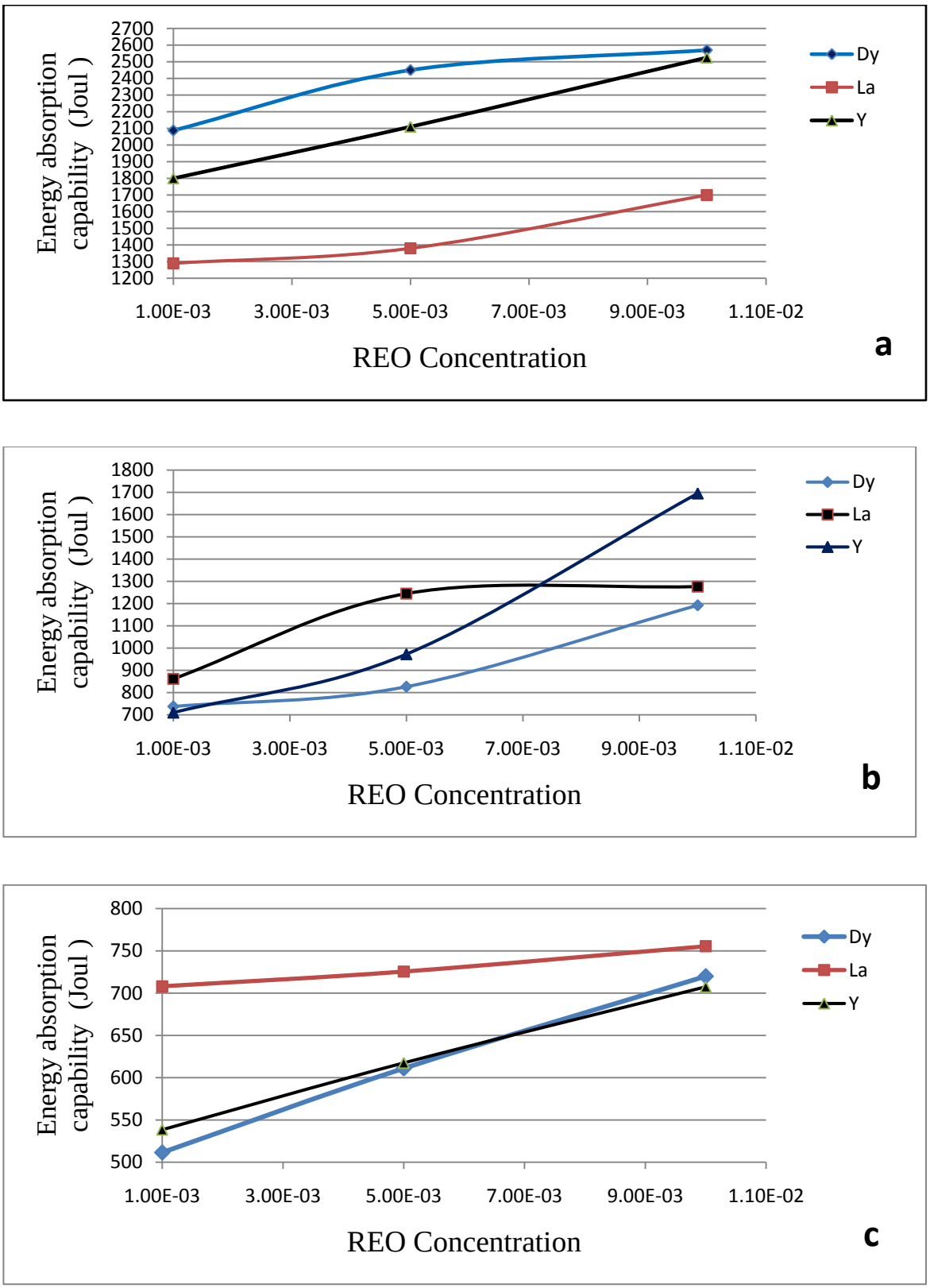

Fig (4.16). Energy absorption capability with respect to REO concentration at fixed sintering temperature, where (a) at 1050℃, (b) 1100℃, and (c) 1150℃, respectively.

4.5.6. Clamping Ratio

Table (4.8), figure (4.18), and figure (4.19), demonstrate the results of clamping ratio of ZnO varistors samples with respect to sintering temperature at fixed rare earth oxide concentrations, and with respect to rare earth oxide concentrations at sintering temperature.

Because of thermal and electrical stresses, the clamping ratio increases with increasing sintering temperature which increase the leakage current which decreases the clamping ratio, in addition to the defect in the crystal structure that results from the volatilization (vaporization) of Bi_2O_3 and spinel phase ($Zn_7Sb_2O_{12}$) which represents the insulation layer and that will weaken the Schottky barrier which represents the essential of the varistor work [70].

In other hand the pure ZnO has large clamping voltage ratio because of the non-linearity property.

The rare earth oxides concentration has a small effect on the clamping voltage ratio, but the increasing of rare earth oxides concentration more than $(5 * 10^{-3})$will increases the charge carrier which in turn decrease the efficiency of the varistor (clamping voltage ratio).

Table (4.8). Clamping ratio of ZnO varistors samples with respect to sintering temperature at different rare earth oxide concentrations.

C_r					
Sintering Temperature (℃)	$Concentration = 10^{-3}$			Zn	Bi
	Dy_2O_3	La_2O_3	Y_2O_3		
1050	1.014	1.035	1.016	3.30985	1.05
1100	1.038	1.046	1.037	10.333	1.099
1150	1.087	1.093	1.081	1.71E+04	1.193

C_r			
Sintering Temperature (℃)	$Concentration = 5 * 10^{-3}$		
	Dy_2O_3	La_2O_3	Y_2O_3
1050	1.011	1.01	1.007
1100	1.036	1.045	1.035
1150	1.076	1.075	1.076

C_r			
Sintering Temperature (℃)	$Concentration = 10 * 10^{-3}$		
	Dy_2O_3	La_2O_3	Y_2O_3
1050	1.02	1.031	1.032
1100	1.047	1.047	1.041
1150	1.089	1.083	1.093

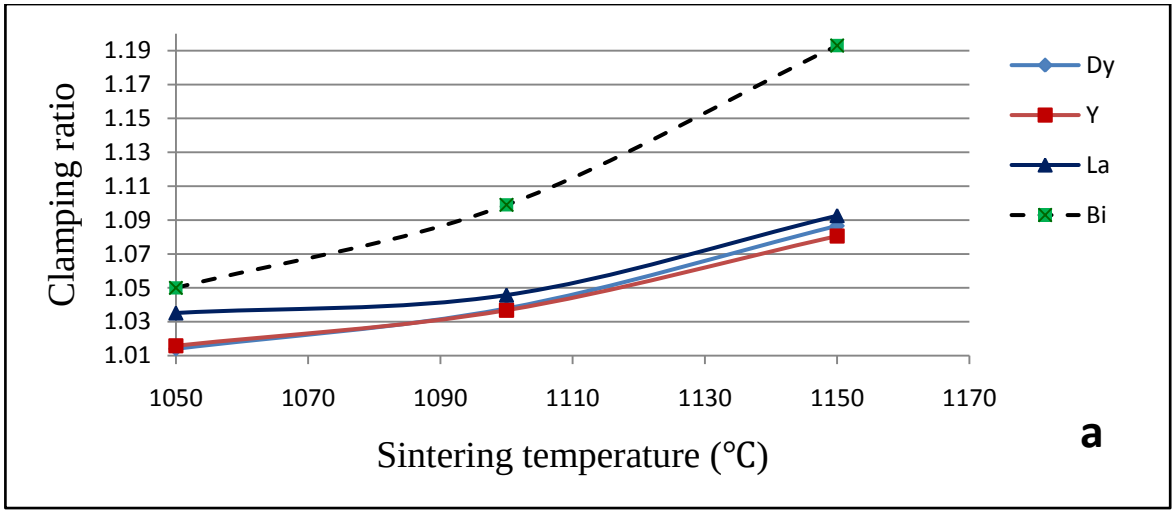

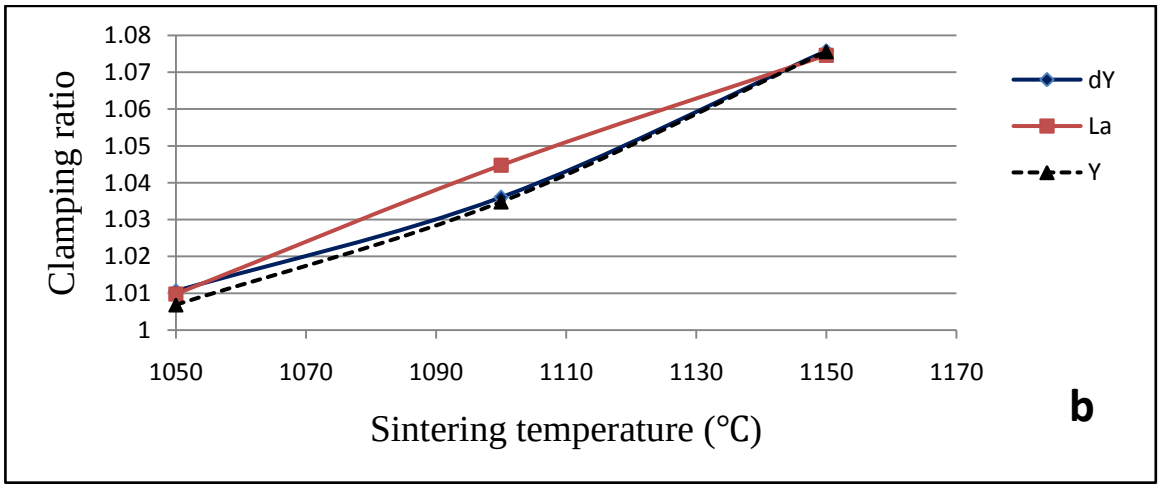

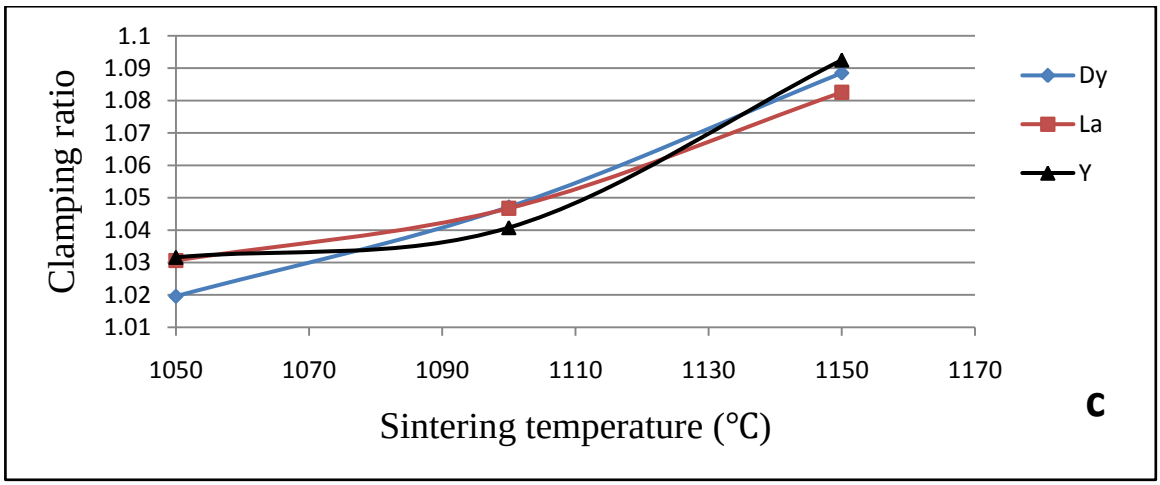

Fig (4.17). Clamping ratio with respect to sintering temperature, (a) ZnO + other oxides (without REO), ZnO + other oxides+ REO at 10^{-3}, (b) $5*10^{-3}$, and (c) $10*10^{-3}$.

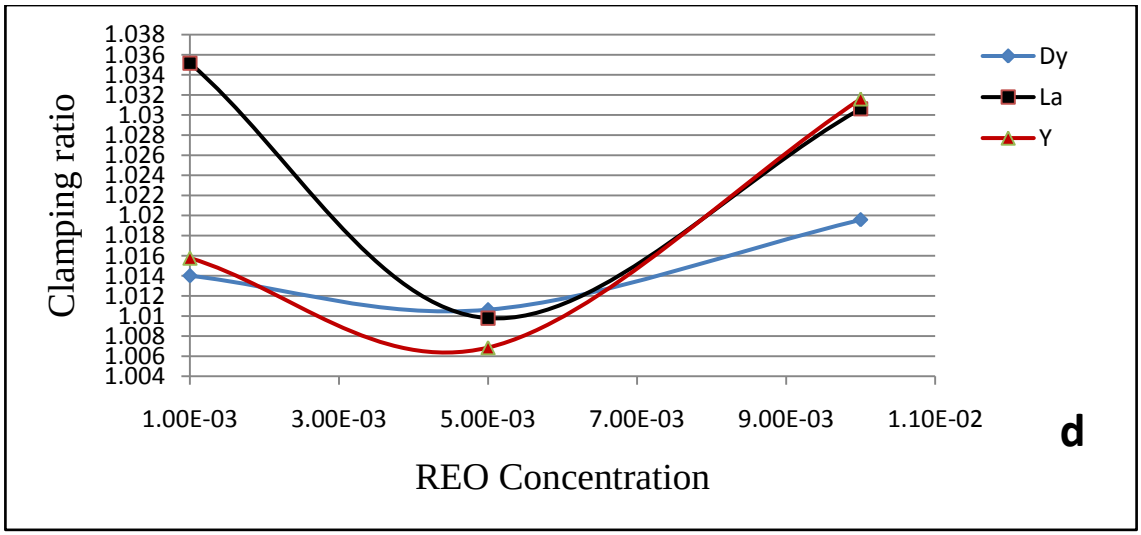

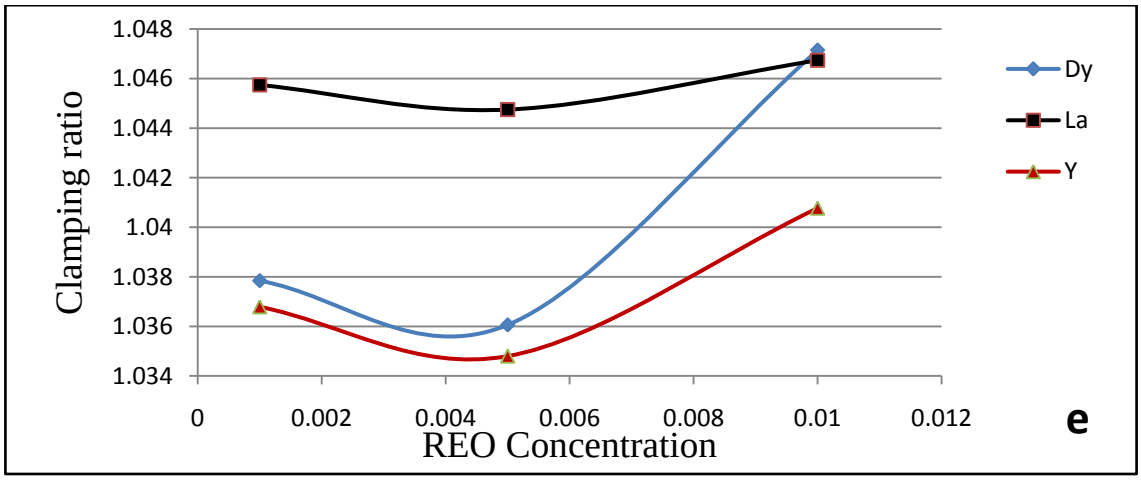

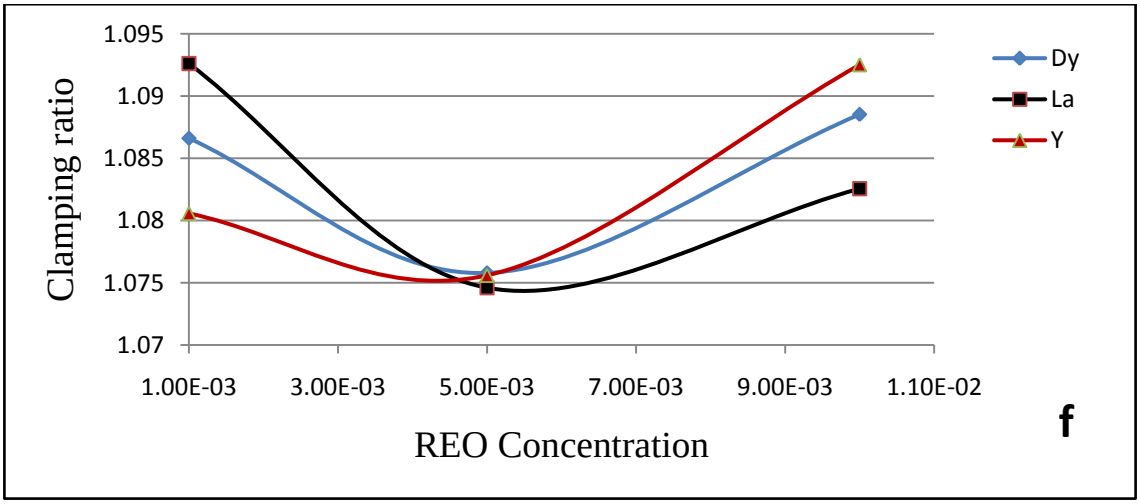

Fig (4.18). Clamping ratio with respect to REO concentration at fixed sintering temperature, where (a) at 1050℃, (b) 1100℃, and (c) 1150℃.

4.5.7. Potential Gradient

Table (4.9), figure (4.20), and figure (4.21), explain the results of potential gradient of ZnO varistors samples with respect to sintering temperature at fixed rare earth oxide concentrations, and with respect to rare earth oxide concentrations at sintering temperature.

The potential gradient (the voltage at current equals to $0.5mA$), which represents the voltage at the heart of the breakdown region (action region or the heart of varistor works), which depends on the breakdown voltages of the samples (as explained in section 4.5.3).

Table (4.9). Potential gradient (V/mm) with respect to sintering temperature at fixed rare earth oxide concentrations.

Potential gradient (V/mm)					
Sintering Temperature (℃)	$Concentration = 10^{-3}$			Zn	Bi
	Dy_2O_3	La_2O_3	Y_2O_3		
1050	1977	1558	2014	56.969	1532
1100	696.8	765.6	737.5	15.5	668.9
1150	402.3	509.9	485.7	4.036	505.6

Potential gradient (V/mm)			
Sintering Temperature (℃)	$Concentration = 5 * 10^{-3}$		
	Dy_2O_3	La_2O_3	Y_2O_3
1050	2565	1584	2438
1100	735.9	1122	975.6
1150	334.1	503.1	522.1

Potential gradient (V/mm)			
Sintering Temperature (℃)	$Concentration = 10 * 10^{-3}$		
	Dy_2O_3	La_2O_3	Y_2O_3
1050	2508	1759	3146
1100	935.8	1055	1557
1150	562.7	637	666.8

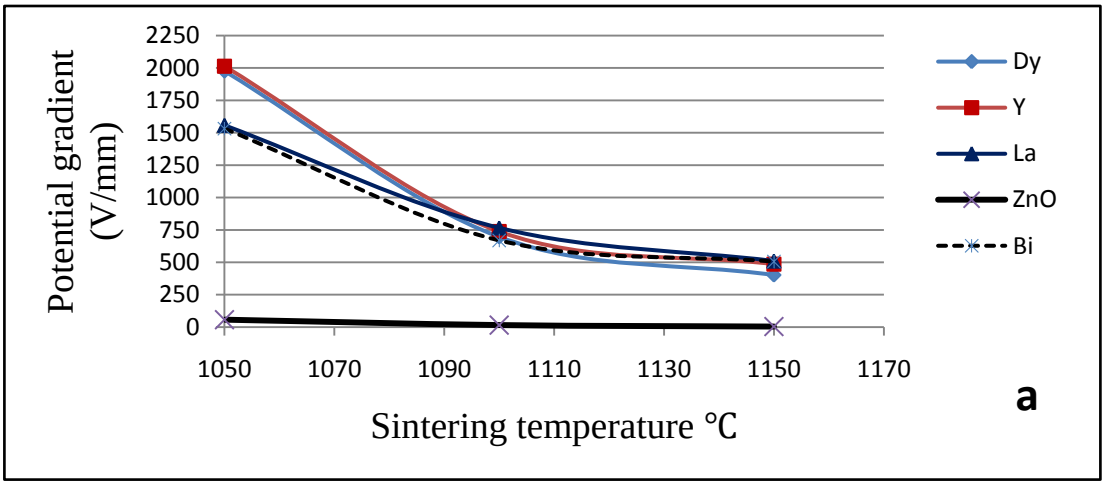

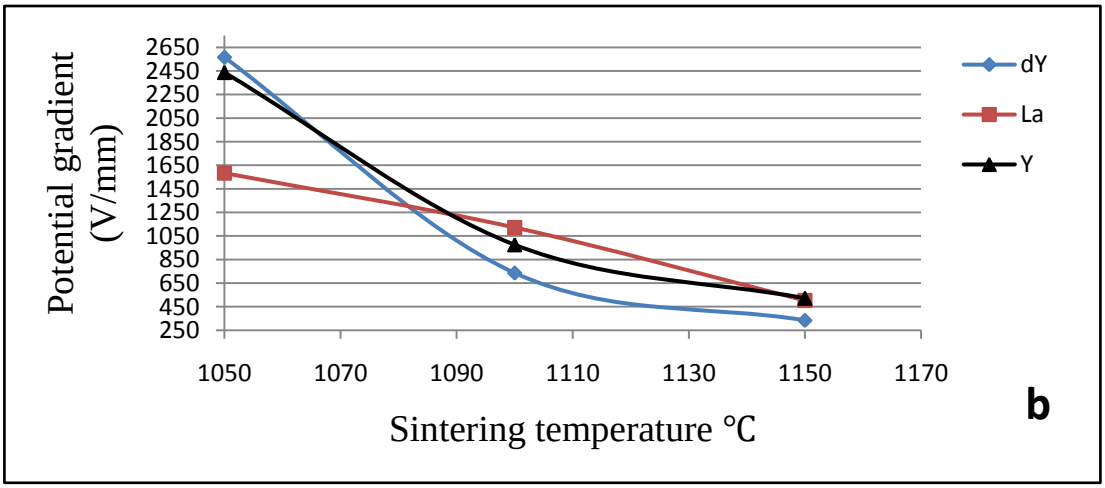

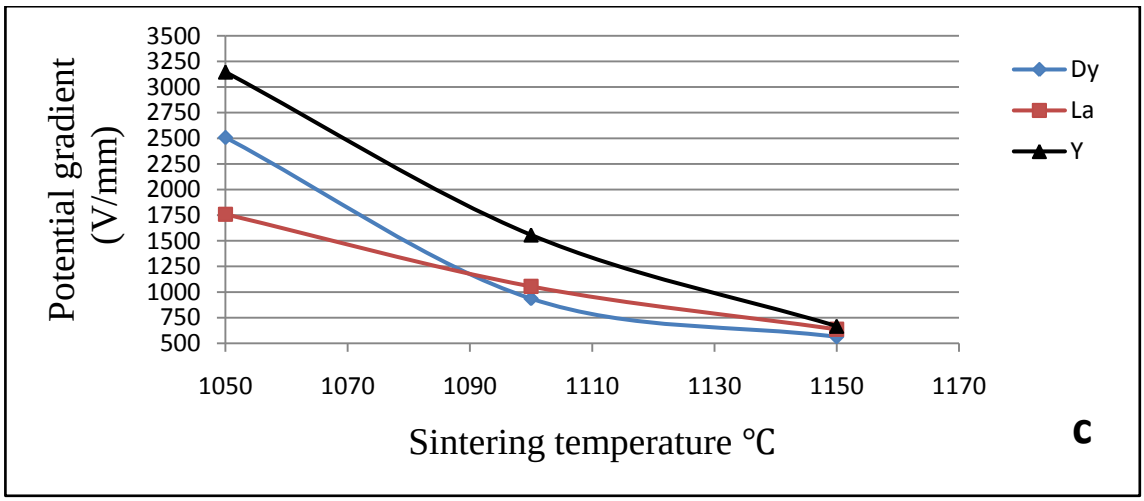

Fig (4.19). Potential gradient with respect to sintering temperature, (a) ZnO + other oxides (without REO), ZnO + other oxides+ REO at 10^{-3}, (b) $5*10^{-3}$, and (c) $10*10^{-3}$.

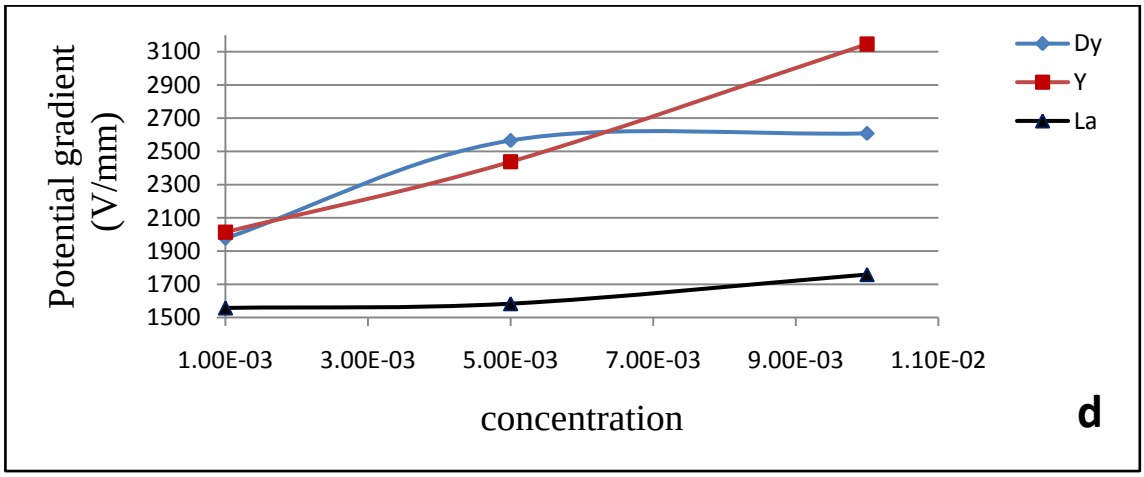

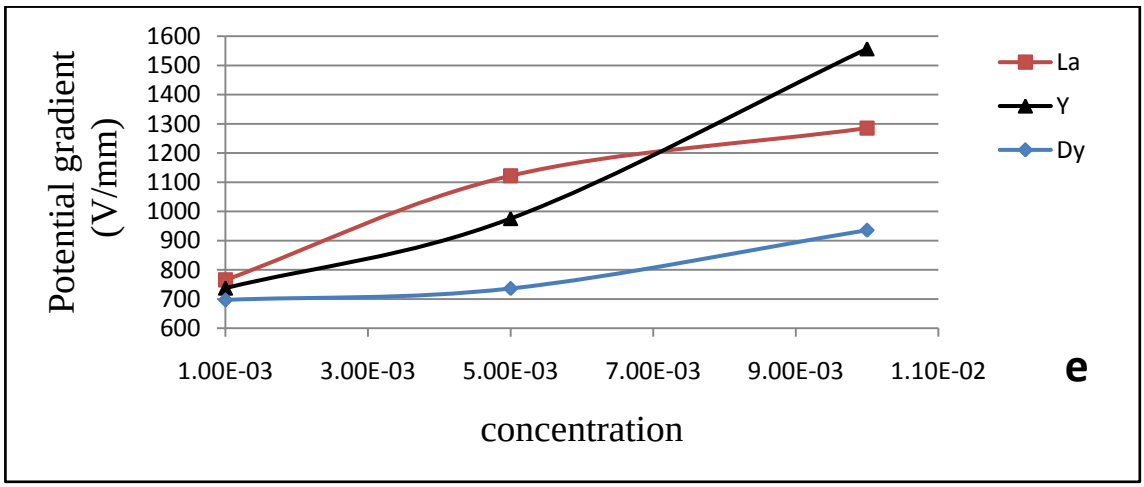

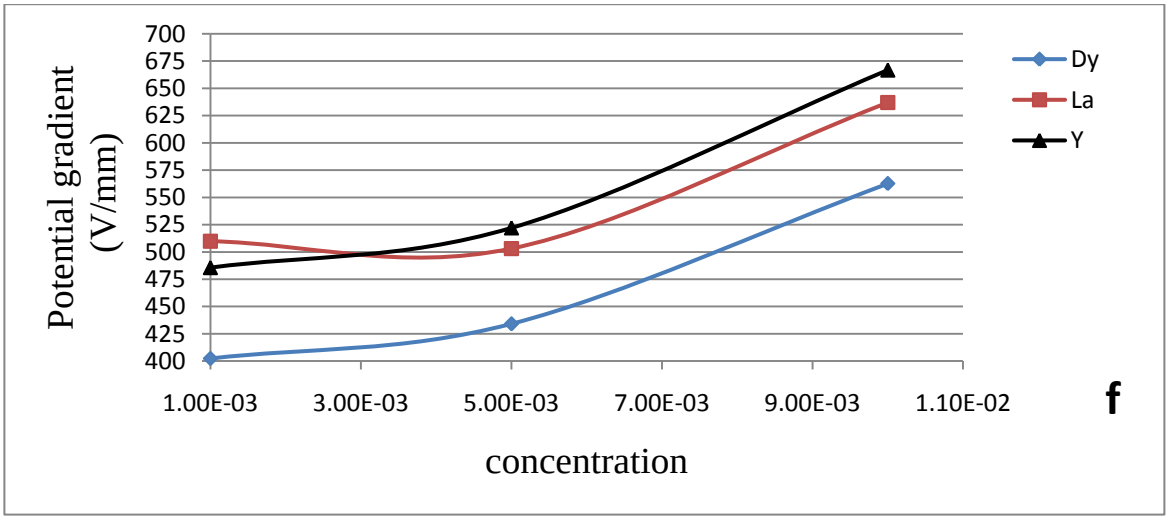

Fig (4.20). Potential gradient with respect to REO concentration at fixed sintering temperature, where (a) at 1050℃, (b) 1100℃, and (c) 1150℃.

4.5.8. Voltage Per Grain Boundary (V_{gb})

Table (4.10), and figure (4.22), demonstrate the results of voltage per grain boundary values of ZnO varistors samples with respect to sintering temperature at the same rare earth oxide concentration.

According to equation (2-22) $V_{gb} = V_b(\frac{d}{D})$, in view of the fact that the voltage per grain boundary directly proportional with grain size value, and as mentioned above the grain size increases with increasing sintering temperature there for the voltage per grain boundary increases with increasing sintering temperature too.

Table (4.10). Voltage per grain boundary with respect to sintering temperature at rare earth oxide concentrations (10^{-3}).

$V_{gb}(Volt)$					
Sintering Temperature (℃)	$Concentration = 10^{-3}$			Zn	Bi
	Dy_2O_3	La_2O_3	Y_2O_3		
1050	0.136	0.144	0.164	TRACE	0.092
1100	0.32	0.184	0.38	TRACE	0.155
1150	2.02	2.832	2.532	TRACE	0.296

.

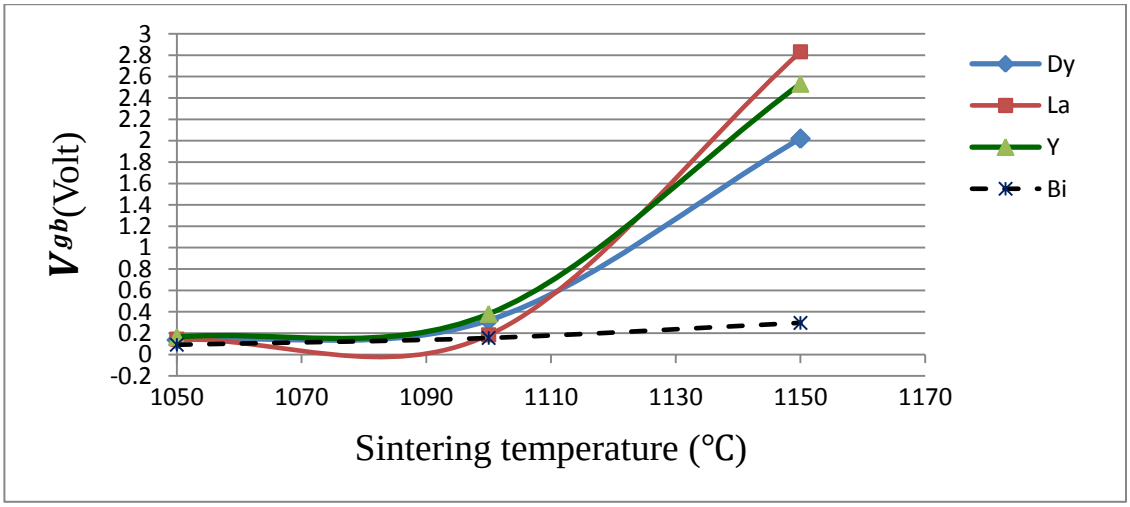

Fig (4.21). Voltage per grain boundary with respect to sintering temperature, pure ZnO, ZnO+ other oxides (without REO), ZnO + other oxides at REO (10^{-3}).

Conclusion And Suggestions For Future Work

5.1. Conclusion

From the obtained results we can conclude the following:

1- ZnO has ohmic (linear) behavior, non-linear electrical properties small, where its maximum non-linear coefficient of (1.54), breakdown voltage of (56.8V), the energy absorption capability is very trace, clamping voltage ratio of (3.30985), Potential gradient ($56.969\ V/mm$), and the voltage per grain boundary is very trace. But it has good basic properties enable it to be a base of varistor.

2- The doping of ZnO with some metal oxides (Bi_2O_3, Sb_2O_3, Co_3O_4, Cr_2O_3, and $MnO_{2)}$ changes the behavior of ZnO varistor from linear to non-linear, and enhances the electrical properties, where they will be, non-linear coefficient of (6.46), breakdown voltage of (2320V), the energy absorption capability (1450Joul), clamping voltage ratio of (1.05), Potential gradient ($1532\ V/mm$) and the voltage per grain boundary (0.296), and transform the phase of ZnO structure system from hexagonal close packed to Orthorhombic.

3- The doping of ZnO varistor with rare earth oxides elevates the magnitude of improvement, enhancement and efficiency of it, and improves the microstructure of the varistor, where non-linear coefficient of (46.566), breakdown voltage of (3340V), the energy absorption capability (2088 Joul), clamping voltage ratio of (1.014), Potential gradient ($2014\ V/mm$) and the voltage per grain boundary (2.832V).

4- The doping with REO increases the density of the samples from (3.763 gm/cm^3) to be (4.8035 gm/cm^3), while the porosity decreases from (33.75%) to be (15.42%).

5- The doping with metal oxides increases the grain size from (45.8050 nm) to be (50.4091nm), the doping with REO change the grain size, where Dy_2O_3 increases it from (50.4091nm) to be (51.5167 nm), Y_2O_3 (50.4091nm) to (55.8724nm), while La_2O_3 decreases it from (50.4091nm) to (47.1375nm).

5.2. Suggestions For Future Work

1- Usage Pr_6O_{11} Instead of Bi_2O_3 as a basic oxide in doping to avoid the volatilization at high temperature degrees.

2- Doping with two rare earth oxides in every process instead of doping with one rare earth oxide to enhance and efficiency of the varistor.

3- Increasing time sintering with decreasing sintering temperature to inhibit the grain growth at high sintering temperature.

4- Increase the magnitude of pressure of the pressing process and the time of pressing to decrease the porosity.

REFERENCES

[1] M. W. Allen, “Schottky Contact Formation to Bulk Zinc Oxide ”PhD thesis, University of Canterbury, Christchurch, New Zealand. 2008.

[2] A. Janotti and C. G. Van de Walle, “Fundamentals of zinc oxide as a semiconductor,” IOP Publishing, Reports Prog. Phys, vol. 72, no.12, 2008.

[3] U. Ö zgür, Y. I. Alivov, C. Liu, A. Teke, M. a. Reshchikov, S. Doğ an, V. Avrutin, S.-J. Cho, and H . Morkoç, “A comprehensive review of ZnO materials and devices,” *J. Appl. Phys.*, vol. 98, no. 4, 2005.

[4] Y.-S. Choi, J.-W. Kang, D.-K. Hwang, and S.-J. Park, “Recent Advances in ZnO-Based Light-Emitting Diodes,” IEEE Trans. Electron Devices, vol. 57, no. 1, 2010.

[5] N. Aggarwal, V. K. Anand, K. Walia, and S. C. Sood, “Structural and Optical Properties of Pure & Aluminium Doped ZnO Thin Films Prepared by Sol-Gel” .Tech. Int. J. Comput. Sci. Commun. Technol, vol. 4, no. 2, 2012.

[6] L. Hsiu- Yu, “Structure and properties of transparent conductive ZnO films grown by pulsed laser deposition (PLD)”,M.Sc, University of Birmingham, School of Metallurgy and Materials, 2009.

[7] H. Morkoc. and Ü. Özgür, “Zinc Oxide Fundamentals, Materials and Device Technology”. Federal Republic of Germany: WILEY-VCH Verlag GmbH & Co. KGaA, Weinheim All, 2009.

[8] M. Elfwing, “Nanoscale Characterisation of Barriers to Electron Conduction in ZnO Varistor Materials ”PhD thesis, Uppsala University, Department of Materials Science, 2002.

[9] X. Zheng. FU Jing, “Mechanism and Development of TiO_2 -Doped ZnO-Bi_2O_3-Based Varistors,” J. Electron. Sci. Technol. China, vol. 1, no. 1, 2003.

[10] P. R. Bueno, J. A. Varela, and E. Longo, “SnO_2, ZnO and related polycrystalline compound semiconductors: An overview and review on the voltage-dependent resistance (non-ohmic) feature” Journal of the European Ceramic Society, vol. 28, no. 3, 2008.

[11] M. a. Alim, S. Li, F. Liu, and P. Cheng, “Electrical barriers in the ZnO varistor grain boundaries,” Phys. Status Solidi, vol. 203, no. 2, 2006.

[12] J. Harloff, “In-Situ Quantitaive Measurment Of Electric Fields In Zinc Oxide Thin Films Using Electrostatic Force Microscopy”, MSc thesis, University Of Pennsylvania, school of engeneering and applied science, 1995.

[13] S. Begum, “Powder Processing Parameters and Their Influence on the Electrical Performance of ZnO Varistor”, Ph.D thesis, Dublin City University, 1996.
[14] S. C. Pillai, J. M. Kelly, R. Ramesh, and D. E. McCormack, “Advances in the synthesis of ZnO nanomaterials for varistor devices” J. Mater. Chem. *C*, vol. 1, no. 20, 2013.
[15] A. Sedky, E. El-Suheel “Nonlinear Conduction in Pure and Doped ZnO Varistors”, World Academy of Science, Engineering and Technology, vol. 65, 2012.
[16] Sahrom Mahmud, “The Effects Of Zinc Oxide Microstructure On The Electrical Properties Of Low-Voltage Ceramic Varistors”, M.Sc thesis University Sains Malaysia, 2004.
[17] S. Mahata, “Preparation And Electrical Characterization Of Zinc Oxide Varistor”, M.Sc thesis, Departement of instrumentation and electronics engeneering**,** Jadavpur University Salt Lake Campus, 2010.
[18] H. D. Alamdari, “Varistors Prepared from nanocrystalline powders obtained by high-energy ball milling”, Ph.D thesis, University of Laval Quebec, 2000.
[19] M. Kelleher, “Preparation of Metal Oxide Additive Particles via Mechanical Methods and their Influence on Subsequent Fabrication , Microstructural and Electrical Properties of Commercial ZnO Varistors”, Ph.D thesis, School of mechanical and manufacturing engineering, Dublin City University, 2003.
[20] J. Geraldo, M. Furtadoa, L. A. Saléha, E. T. Serrab, G. S. Gomes, M. C. Souza, “Microstructural Evaluation of Rare-Earth-Zinc Oxide-Based Varistor Ceramics”, Materials Research, vol. 8, no. 4, 2005.
[21] M. Hove, “Improvement Of The V-I Properties Of Zinc Oxide (ZnO) Based Metal Oxide Varistors(MOVs) Using Silicon Telluride ($SiTe_2$) And Lanthanum Hexaboride (LaB6) Materials”, Ph.D thesis, of Engineering and the Built Environment, University of Witwatersrand, 2006.
[22] J. Han, P. Mantas, and M. Senos, “Densification and grain growth of Al-doped ZnO,” J. Mater. Res., vol. 16, no. 4, 2001.
[23] S. Kuo, W. Tuan, Y. Lao, C. Wen, and H. Chen, “Grain Growth Behavior of Bi_2O_3 -Doped ZnO Grains in a Multilayer Varistor”, J. Am. Ceram. Soc, vol. 91, no. 5, 2008.

[24] J. He, J. Hu, and Y. Lin, “ZnO varistors with high voltage gradient and low leakage current by doping rare-earth oxide”, Science in China Series E: Technological Sciences, vol. 51, no. 6, 2008.

[25] J. Yoon, C. Lee, K. Lee, H. Lee, and S. Lee, “Voltage Enhancement of ZnO Oxide Varistors for Various Y_2O_3 Doping Compositions” Transition on Electrical and. Electronic Material, vol. 10, no. 5, 2009.

[26] M. Sabri, B. Azmi, Z. Rizwan, M. Halimah, M. Hashim, H. Sidek, and U. Serdang, “Application of Direct Current and Temperature Stresses of Low-Voltage ZnO Based Varistor Ceramics”, American Journal of Applied Sciences, vol. 6, no. 8, 2009.

[27] M. Arefin, F. Raether, D. Dolejs, and A. Klimera, “Phase formation during liquid phase sintering of ZnO ceramics”, Elsevier,Ceramics Int., vol. 35, no. 8, . 2009.

[28] D. Xu, X. Cheng, X. Yan, H. Xu, and L. Shi, “Sintering process as relevant parameter for Bi_2O_3 vaporization from ZnO-Bi_2O_3-based varistor ceramics”, Trans. Nonferrous Met. Soc. China, vol. 19, no. 6, 2009.

[29] Z. Malek, “A new Technique For Metal Oxide Surge Arresters Failure Diagonasitc using return voltage measurment”, Fakuliti Kejuruteraan Electric, University Teknologi Malaysia, M.Sc thesis, 2009.

[30] N. Yongvanich, P. Jivaganont, and F. Sakasuphalerk, “Densification and Grain Growth in BaO. Bi_2O_3. ZnO Varistor Ceramics” Journal of Metals, Materials and Minerals, vol. 20, no. 3, 2010.

[31] A. Sedky and E. El-Suheel, “A Comparative Study between the Effects of Magnetic and Nonmagnetic Dopants on the Properties of ZnO Varistors” Physics Research International, vol. 10, 2010.

[32] J. Zhao, G. Qi, and H. Yang. F.Wang, “Effect of composite additives on ZnO varistor ceramics”, Materials Science Forum, vol. 685, 2011.

[33] A. Sedghi and N. Riyahi, “Comparison of electrical properties of zinc oxide varistors manufactured from micro and nano ZnO powder,” Journal of Ceramic Processing Research, vol. 12, no. 6, 2011.

[34] A. Yaya, “The Influence Of Bi_2O_3 And Sb_2O_3 Doping On The Microstructure And Electrical Properties Of Sintered Zinc Oxide”, ARPN Journal of Engineering and Applied Sciences, vol. 7, no. 7, 2012.

[35] D. Xu, D. Tang, Y. Lin, L. Jiao, G. Zhao, and X. Cheng, “Influence of Yb_2O_3 doping on microstructural and electrical properties of ZnO-

Bi_2O_3-based varistor ceramics", J. Cent. South University, vol. 19, no. 6, 2012.

[36] K. Abdullah, and B. Bakour, "Semiconductors Elaboration / ZnO Based Varistors for Improving of Stability and Reliability of Electrical Systems Applications by Using the Rare-Earths", Elsevier Ltd, vol. 19, 2012.

[37] O. Desouky, S. Mansour, E. Negim, A. Najar, R. Rakhmetullayeva, P. Urkimbaeva, and W. Midlands, "Effect of MnO_2 on Electrical Properties of ZnO-V_2O_5 -Based Varistors", World Journal of Chemistry, vol. 8, no. 2, 2013.

[38] F. Jiang, Z. Peng, Y. Zang, and X. Fu, "Progress on rare-earth doped ZnO-based varistor materials", Journal of Advanced Ceramics, vol. 2, no. 3, 2013.

[39] L. Ke, M. Hu, and X. Ma, "Preparation of Ultrahigh Potential Gradient of ZnO Varistors by Rare-Earth Doping and Low-Temperature Sintering", Hindawi Publishing Corporation, Journal of Materials, vol. 2013, 2013.

[40] T. Kato and Y. Takada, "Correlation between electrical properties and crystalline phases for ZnO-Bi_2O_3 based varistor ceramics with rare earth additives", Journal of Electroceramics, vol. 31, 2013.

[41] Y. Hong, Y. Lee, S. Kim, J. Paik, and J. Kim, "Admittance spectroscopy and electrical properties of Co_3O_4-doped ZnO", Electron. Mater. Lett, vol. 10, no. 5, 2014.

[42] M. Mohammed, K. Abdullah, and F. Omar, "Studying The Optimal Performance Of The ZnO Based Varistors Using Artificial Intelligence Techniques", Journal of Electron devices, vol. 19, 2014.

[43] Akinnifesi, J. O; Erinfolami, F. B. and Akinwunmi, " Influence of microstructure on the non-ohmic behavior of zinc oxide varistor ceramics prepared by direct mixing of constituent phases", Ife Journal of Science, vol. 16, no. 1, 2014.

[44] S. Ioannou, "Comparative Study of Metal Oxide Varistors (Movs) for Failure Mode Identification", M.Sc thesis, Department of Electrical Engineering, College of Engineering, University of South Florida, 2004.

[45] E. Asa, "Novel Powder-Coating Solutions to Improved Micro-Structures of ZnO Based Varistors, WC–Co Cutting Tools, and Co/Ni Nano-Phase Films and Sponges", Ph.D thesis, Faculty of Science and Technology, Uppsala University, 2002.

[46] A. Karim, S. Begum, and M. Hashmi, “Performance And Failure During Energy Testing Of Zinc Oxide Varistor Processed From Different Powder Size Fraction And Passivation Thickness”, International Journal of Mechanical and Materials Engineering vol. 5, no. 2, 2010.

[47] C. Diao, S. Chien, C. Yang, H. Chan, Y. Chen, and H. Chung, “The Nonlinear Properties of Different Additives Added V_2O_5-ZnO Varistor” , Key Engineering Materials, vol. 372, 2008.

[48] W. Lihui, G. Guoyou, S. Jialin, and Y. Jikang, “Preparation and characterization of layered low-voltage ZnO varistors”, Journal of Semiconductors, vol. 30, no. 3, 2009.

[49] H. Debéda, S. Azzopardi, C. Lucat, M. P. Martin-Stempin, and P. Tardy, “Evaluation of insulated gate bipolar transistor protection with ZnO thick films varistors”, IET Power Electron, vol. 3, no. 1, 2010.

[50] J. Gubanski, W. Mielcarek, K. Prociow, J. Warycha, and J. Wrobel, “The effect of aluminium additive on the electrical properties of ZnO varistors”, Materials Science-Poland, vol. 27, no. 4, 2009.

[51] C. Nahm and S. Lee, “Microstructure and Electrical Properties of ZPCCYT Varistor Ceramics”, Transictions on Electrical and Electronic Materials, vol. 13, no. 5, 2012.

[52] C. Sikalidis, “Advances In Ceramics– Electric And Magnetic Ceramic And Enviroment”, Costas Sikalidis, First Publication. Rijeka,Croatia, Janeza Trade9, 2011.

[53] S. Dau, “Modelling of Lightning High voltages for the Protection of Transmission Lines by Means of Shielding Wires and Surge Arresters”, Ph.D. Thesis, Department of Electrical Engineering and Electrical Power, Faculty of Electrical Engineering, Automatics, Computer Science and Electronics, 2008.

[54] J. Carlsson, “A First-Principles Study of Interface Systems Electronic properties of Metal Quantum Wells and Varistor Materials ”, Ph.D. Thesis, School of Physics and Engineering Physics, Chalmers University of Technology and Goteborg University, 2002.

[55] K. Anm and S. Begum, “Enhanced Performance of Zinc Oxide Arrester by Simple Modification in Processing and Design” Material Science & Engineering, vol. 3, no. 1, 2014.

[56] M. Arefin, “In-situ measurements of the Liquid- Phase Sintering of Zinc Oxide”, M.Sc thesis, University of Bayreuth, Germany, 2009.

[57] R. Riedel and I. Chen, “Ceramics Science and Technology Thematische Gliederung”, First Edition., vol. 3. Wiley-VCH Verlag GmbH & Company. KGaA., 2012.

[58] S. Somiya, F. Aldinger, N. Claussen, R. Spriggs, K. Uchino, K. Koumoto, and M. Kaneno, “Handbook of Advanced Ceramics”, Elsevier Inc. San Diego, California, USA, 2003.

[59] R. Chaim, M. Levin, a. Shlayer, and C. Estournes, “Sintering and densification of nanocrystalline ceramic oxide powders: a review” Advances in Applied Ceramics, vol. 107, no. 3, 2008.

[60] J. Wessel, “Handbook Of Advanced Materials”. New Jersey: John Wiley & Sons, Inc., Hoboken, 2004.

[61] A. Tiwari, “Liquid phase sintering in microgravity”, Current Science, vol. 9, no. 3, 2000.

[62] A. Gusai, I. Teoreanu, and M. Barladeanu, “The Influence Of Sb_2O_3 Proportion On The ZnO Grains Growth During Sintering”, *U.P.B. Sci. Bull., Ser. B*, vol. 73, no. 2, 2011.

[63] Z. Nikolic and F. Wakai, “Computer study of liquid phase sintering - three-dimensional time dependent rearrangement,” IOP Conf. Materials Science and Engineering, vol. 18, no. 2, 2011.

[64] N. Yongvanich, P. Visuttipitukkul, and P. Leksuma, “Sinterability and Microstructure of Bi-Added SnO_2 Nanomaterials by Precipitation Method” Journal of Metals, Materials and Minerals, vol. 20, no. 3, 2010.

[65] M. A. De Rubia, M. Peiteado, J. Frutos, and T. Jardiel, “Solid state compatibility in the ZnO-rich region of ZnO-Bi_2O_3-Sb_2O_3 and ZnO-Bi_2O_3-Sb_2O_5 systems” Bol. Soc. Esp. Ceram, vol. 49, no. 2, 2010.

[66] C. Lin, Z. Xu, H. Peng, and D. Sun, “Densification and grain growth of microwave-sintered zinc oxide varistors”, Am. Ceram. Soc. Bull, vol. 86, no. 1, 2007.

[67] A. Swarnakar, L. Donzel, J. Vleugels, and O. Biest, “High temperature properties of ZnO ceramics studied by the impulse excitation technique”, Journal of the European Ceramic Society, vol. 29, no. 14, 2009.

[68] L. Ke, Y. Yuan, H. Zhao, and X. Ma, “Influence Of Rare-Earth Doping On The Electrical Properties Of High Voltage Gradient ZnO Varistors”, Ceramics,Silikáty, vol. 57, no. 1, 2013.

[69] D. Michael, "The Effects Of Powder Processing Parameters On The Microstructure And Energy Absorption Characteristics Of Low Voltage

ZnO Varistor", M.Sc thesis, Cathy, Darina, Colleen, Dublin City University, 1996.

[70] G. Nahm, “Clamping Voltage Properties and Accelerated Aging Behavior of CoCrTb-doped Zn/Pr-based Varistors with Sintering Temperature”, Transition on Electrical and Electronic Materal, vol. 10, no. 4, 2009.

[71] M. Bin Ahmad, A. Fatehi, A. Zakaria, S. Mahmud, and S. Mohammadi, “Fabrication of an electrically-resistive, varistor-polymer composite” International Journal of Molecular Sciences, vol. 13, no. 12, 2012.

[72] A. Monshi, M. Foroughi, and M. Monshi, “Modified Scherrer Equation to Estimate More Accurately Nano-Crystallite Size Using XRD”, World Journal of Nano Science and Engineering, vol. 2, no, 2012.

[73] T. Vishnuvardhan, V. Kulkarni, C. Basavaraja, and S. Raghavendra, “Synthesis, characterization and a. c. conductivity of polypyrrole/ Y_2O_3 composites”, Indian Academy of Sciences, vol. 29, no. 1, 2006.

[74] W. Abdullah, A. Zakaria, and M. Ghazali, “Synthesis mechanism of low-voltage praseodymium oxide doped zinc oxide varistor ceramics prepared through modified citrate gel coating”, International Journal of Molecular Sciences, vol. 13, no. 4, 2012.

[75] W. Mielcarek, K. Prociów, and J. Warycha, “Potentialities Of Modification Of Metal Oxide Varistor Microstructure”, in International Conference of IMAPS- CPMP IEEE, Poland, Pułtusk, 21-24.09.2008, 2009, no. 1,

[76] L. Petit. A. Svane, Z. Szotek, and W. Temmerman, “Electronic Structure of Rare Earth Oxides”, Springer-Verlag Berlin Heidelberg, Appl. Phys., vol. 343, 2007.

[77] K. Gschneidner, Jr. and L. Eyring, “Handbook on the Physics and Chemistry of Rare Earths”, volume 26, 26th edition. Elsevier Science B.V, 1999.

[78] D. Yu, C. Feng, J. Lei, X. Hong, T. Dong, W. Jie, Y. Ren, X. Dong, , “Effects of Eu_2O_3 doping on microstructural and electronic properties of $ZnO{-}Bi_2O_3$ based varistor ceramics prepared by high energy ball milling”, J. Cent. South Univ, vol. 20, 2013.

[79] L. Jun, H. Jun, H. Jinliang, L. Yuanhua, and L. Wangcheng, “Microstructures and properties of deep trap levels in ZnO varistors

doped with Y_2O_3", Science in China Series E: Technological Sciences, vol. 52, no. 12, 2009.

[80] R. Dinnebier, and S. Billinge, Powder Diffraction Theory and Practice", Edited by. The Royal Society of Chemistry, Thomas Graham House, Science Park, Milton Road, Cambridge, 2008.

[81] A. Mercy, R. Selvaraj, B. Boaz, A. Anandhi, and R. Kanagadurai, "Synthesis, structural and optical characterisation of cadmium sulphide nanoparticles", Indian J. Pure Appl. Phys, vol. 51, no. June, 2013.

[82] M. Berger, "The Importance And Testing Of Density/Porosity/ Permeability/Pore Size For Refractories", The Southern African Institute of Mining and Metallurgy, Refractories Conference, 2010.

[83] Y. Nakayama, "Introduction to Fluid Mechanics", UMIST, UK: Printed and bound in Great Britain by MPG, Bodmin, Cornwall, 1999.

[84] A. Akmukhopadhyay, M. Chaudhuri, "Mechanical characterization of microwave sintered zinc oxide Sintering Porosity Theoretical", Indian Acad. Sci. Mech., vol. 24, no. 2, 2001.

[85] D. Kosanovi, S. Filipović, N. Obradović, V. Pavlović, and M. Ristić, "Microstructure Evolution And Sintering Kinetics Of ZnO", Journal of Applied Engineering Science, vol. 9, 2011.

[86] I. Silva, A. Simoes, F. M. Filho, E. Longo, J. A. Varela, and L. Perazolli, "Dependence of La_2O_3 content on the nonlinear electrical behaviour of ZnO , CoO and Ta_2O_5 doped SnO_2 varistors", Elsevier,Materials Lett., vol. 61, 2007

[87] M. Houabes and R. Metz, "Rare earth oxides effects on both the threshold voltage and energy absorption capability of ZnO varistors", Ceram. Int., vol. 33, no. 7, 2007.

الخلاصة

يُعد أوكسيد الخارصين (ZnO) السيراميكي مادة شبه موصلة نوع -n، ويلعب دورا هاما في مدى واسع من العمليات الصناعية والمنتجات التجارية.

إنّ من أكثر الاستعم الات أهمية إستعماله لحماية الدوائر الكهربائية والمعدات الإلكترونية من الجهد الزائد المدمر نتيجة البرق أو الناتج من الارتفاع الكبير والمفاجيء في قيم الجهد الكهربائي، وتُسمّى المقاوم المتغير المعدني (Metal Oxide Varistor MOV) .

يُعد المقاوم المتغير نبيطة ذات سلوك غير أومي وخواصه الكهربائية تشبه تقريبا في عملها ثنائي زينر.

لغرض دراسة وتوصيف مركبات مقوّم أوكسيد الخارصين السيراميكي المتغير وتحسين خواصه الكهربائية ، تمّ تحضير مركباته بإضافة بعض الأكاسيد المعدنية وهي Bi_2O_3، Sb_2O_3، Co_3O_4، Cr_2O_3، وMnO_2، حيث تم اختبار تأثيرها لوحدها أولاً، وثانياً تمّ إضافة أكاسيد الأتربة النادرة (M_2O_3) مع الأكاسيد المذكورة أعلاه واختبار تأثيرها على المقاوم المتغير، حيث أنّ (M=Dy, La,Y) وبتراكيز موليّة (10^{-3}*(1,5,10)).

تمّت عمليات التحضير والسيطرة على التركيب الدقيق عن طريق التحكّم بظروف عمليات الحرق بدءًا من عملية إلاعداد بخلط أوكسيد الزنك مع الأ كاسيد المضافة و من ثمّ الحرق في درجة حرارة $600℃$ وبمعدل $5\ ℃/min$ في الفرن ولمدة ساعتين للعينات جميعها وذلك لإزالة الغازات والرطوبة من المساحيق.

بعد عملية الحرق تم كبس المساحيق بشكل اقراص بقطر $15mm$ وسمك $2mm$ تقريباً تحت ضغط يساوي $25MP$.

بعد عملية الكبس أجريت عملية التلبيد (تفاعلات الأطوار الصلبة والأطوار السائلة) بدرجات حرارة مختلفة (℃ 1050, 1100, 1150) وزمن ثابت للعينات جميعها مقداره ساعتين للحصول على الأشكال النهائية والوصول إلى الخصائص المطلوبة.

تمّت دراسة بعض الخواص الفيزيائية للعين ات المحضَّرة وهي الكثافة والمسامية والخواص التركيبية وذلك لغرض تقييم تأثير الأكاسيد المضافة وظروف التحضير على سلوك التطبيق الصناعي للعينات.

وقد تبيّن أنّ مقدار الكثافة النسبية والمساميّة تتأثر بدرجة حرارة التلبيد وبنسب تراكيز أكاسيد الاتربة النادرة المضافة ونوعها ،فقد أزداد مقدار الكثافة بازدياد درجة حرارة التلبيد ونسبة أو تركيز أكاسيد الاتربة النادرة المضافة ونتيجة لذلك فقد نقص مقدار المساميّة.

لقد أعطى إختبار التركيب المجهري للمادة المحضّرة رؤية واضحة عن الانتشار والنمو الحبيبي ، وإنّ نتائج إختبار ا لاشعة السينية (XRD) أوضحت أن التركيب البلوري لها معيني قائم كما أنّ قيم (a, b, c) وحجم خلية الوحد قد إزداد بزيادة درجة حرارة التلبيد ونسب تراكيز الأكاسيد المضافة ونوعها.

أظهرت الحبيبات النانوية والميكروية ضمن البحث الحالي تأثيراً كبيراً على الخصائص الكهربائية المدروسة والتي صُمّمت لها أداة في المختبر لقياس معامل السلوك اللاخطي ، مقدار جهد الانهيار ، تيار التسرّب، قابلية إمتصاص الطاقة ، إنحدار الجهد وجهد الحدود الحبيبيةِ.

حيث تبيّن أن معامل السلوك اللاخطي يزداد بازدياد تركيز الأكاسيد المضافة وارتفاع درجة حرارة التلبيد ومن ثمّ يبدا بالنقصان بعد درجة (1100°C) بسبب تطاير وتبخر أوكسيد البزموث وطور ($Zn_7Sb_2O_{12}$) .

بينما نقص مقدار جهد الانهيار وقابلية إمتصاص الطاقة وإنحدار الجهد بازدياد درجة حرارة التلبيد،أمّا تيار التسرب فقد إزداد مقداره بازدياد درجة حرارة التلبيد ، وكذلك بالنسبة لجهد الحدود الحبيبية فقد ازدادت قيمها بازدياد درجة حرارة التلبيد.

جمهورية العراق
وزارة التعليم العالي والبحث العلمي
جامعة بغداد
كلية التربية للعلوم الصرفة (ابن الهيثم)

الخواص الكهربائية والتركيب الدقيق لمقاوم أوكسيد الخارصين السيراميكي المتغير المطعّم بالأتربة النادرة

أطروحة قدمها

عادل إسماعيل كاظم

إلى

مجلس كلية التربية للعلوم الصرفة (ابن الهيثم)– جامعة بغداد

كجزء من متطلبات نيل درجة الدكتوراه في الفيزياء

بأشراف

أ.م. د. أيسر جمعة إبراهيم **أ.م. د. عبد الحميد رحيم مهدي**

ربيع الثاني 1436 هـ كانون الثاني 2015 م